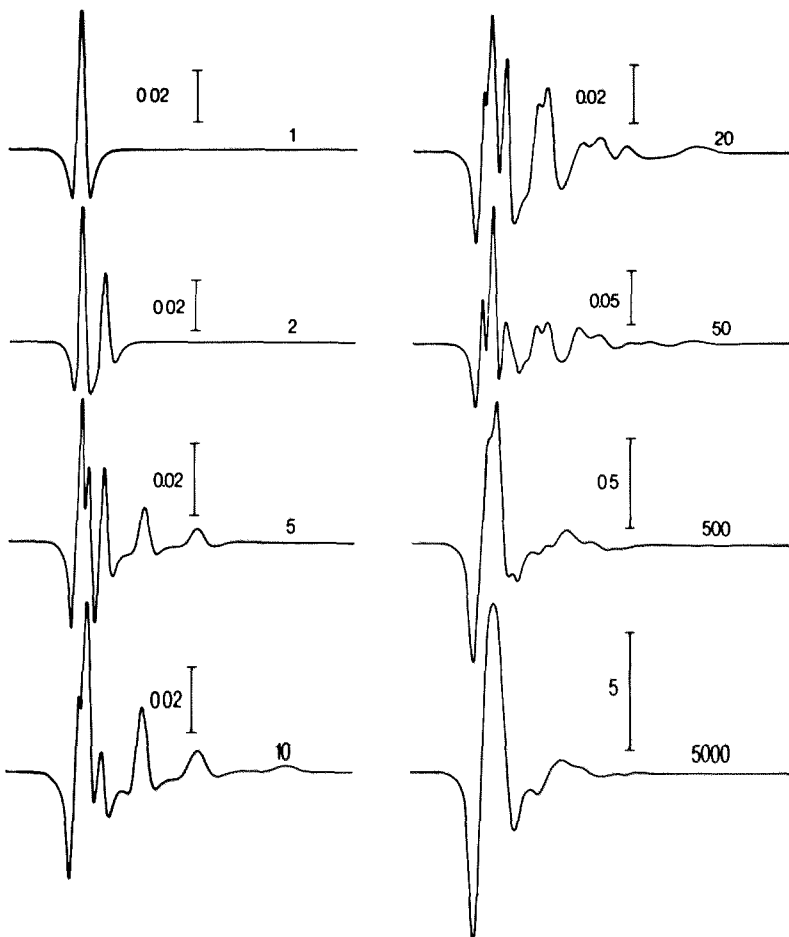


COMPOUND NERVE ACTION POTENTIALS

an electrophysiological model study
of human peripheral nerves *in situ*



DICK STEGEMAN

COMPOUND NERVE ACTION POTENTIALS

Promotores: Prof. dr. ir. E. G. J. Eijkman
Prof. dr. S. L. H. Notermans

Co-referent: dr. ir. J. P. C. M. de Weerd

COMPOUND NERVE ACTION POTENTIALS

an electrophysiological model study of human peripheral nerves *in situ*

PROEFSCHRIFT

ter verkrijging van de graad van
doctor in de Geneeskunde aan de
Katholieke Universiteit te Nijmegen, op gezag
van de Rector Magnificus Prof dr P G A B Wijdeveld
volgens het besluit van het College van Decanen
in het openbaar te verdedigen op
dinsdag 23 juni 1981
des namiddags om 2 00 uur precies,

door

Derk Frederik Stegeman

geboren te Enschede

juni 1981



krips repro meppel

Dit onderzoek werd uitgevoerd als samenwerkingsproject van het laboratorium voor Medische Fysica en Biofysica en de afdeling Klinische Neurofysiologie aan de Katholieke Universiteit van Nijmegen.

Met dank aan:

- Alle proefpersonen.
- Dick Vingerhoets voor hulp bij de neurofysiologische experimenten.
- Jaap Kap, Jan Moleman en Eric van de Velden voor ondersteuning op het technische vlak en bij programmeeractiviteiten.
- Anco Heringa en Gérard Uijen voor de onmisbare discussies, vooral op het terrein van de volumegeleiding en de signaaltheorie.
- Ton Vos voor de becommentariëring van een deel van het manuscript.
- De mensen van de foto-, film- en tekenafdeling van het Instituut voor Neurologie voor hun hulp en het in goed vertrouwen beschikbaar stellen van faciliteiten.
- De mensen van de centrale medische fotografie voor de verzorging van een deel van het fotografische werk.
- Dennis Cotton en Ria Kroon voor de korrekties op het gebruik van de engelse taal.
- Marianne de Leng voor het zeer zorgvuldige typewerk voor het proëfschrift.

ter nagedachtenis aan opa

CONTENTS

PART I: BACKGROUND

1. Electrical activity of human peripheral nerves <i>in situ</i> .	
1.1 Introduction	3
1.2 The forward and the inverse problem in electroneurography	4
1.3 Methods to measure activity from human nerves	5
1.4 The relation between neurographical and histometrical parameters	6
1.5 Prerequisites for a reconstruction procedure, based on volume conduction theory	7
1.6 Structure of this investigation	7
1.7 References	8

PART II: MATHEMATICAL FORMULATION

2. A volume conductor study of compound action potentials. (Biol. Cybernetics, 1979, 33: 97-111. D.F. Stegeman, J.P.C. de Weerd and E.G.J. Eijkman)	
Abstract	15
2.1 Introduction	16
2.2 A model of the single fibre action potential	17
2.2.1 Poisson's equation	18
2.2.2 Cylindrical coordinates	19
2.2.3 Constant propagation velocity	19
2.2.4 The fibre as a circular cylinder	21
2.2.5 Core conductor model	22
2.2.6 Nerve trunk properties	24
2.2.7 The surface of the skin	27
2.3 Modelling the compound action potential	28
2.3.1 Linear superposition	28
2.3.2 Aspects of stimulation	29
2.3.3 Fibre radius versus propagation velocity	30
2.3.4 Distribution of diameters and arrival times	30
2.4 Discussion	32
2.4.1 The intracellular fibre potential	33
2.4.2 The diameter distribution	36

2.4.3	Conductivity parameters	36
2.4.4	Propagation velocity and fibre diameter and wave shape	39
2.5	Conclusions	42
2.6	References	44

PART III: MODEL RECONSTRUCTIONS OF EXPERIMENTAL DATA FROM NORMAL HUMAN SURAL NERVES.

3.	Model description; the relation between diameter and velocity. (submitted for publication to Electroenceph. clin. Neurophysiol., 1981. D.F. Stegeman and J.P.C. de Weerd)	
	Abstract	49
3.1	General introduction	50
3.2	Introduction to the model	51
3.3	The compound nerve action potential	52
3.4	Experimental methods	55
3.5	Experimental results	56
3.6	A first model approach	58
3.7	Parameter inspection	61
3.8	Fibre diameter and propagation velocity	63
3.9	Discussion and conclusions	66
3.10	References	68
4.	A study of the influence of temperature. (submitted for publication to Electroenceph. clin. Neurophysiol., 1981. D.F. Stegeman and J.P.C. de Weerd)	
	Abstract	73
4.1	Introduction	74
4.2	Experimental methods	75
4.3	Experimental results	76
4.4	Temperature and single fibre characteristics	80
4.5	Model approaches	82
4.6	Discussion and conclusions	86
4.7	Appendix	90
4.8	References	92

5. Nerve propagation in the refractory period.	
(submitted for publication to Electroenceph. clin. Neurophysiol., 1981.	
D.F. Stegeman, J.P.C. de Weerd and S.L.H. Notermans)	
Abstract	95
5.1 Introduction	96
5.2 Methods	97
5.3 Experimental results	98
5.4 Single fibre propagation in the relative refractory period	99
5.5 Estimation of single fibre recovery functions	101
5.6 Relative block of fibres	105
5.7 Discussion and conclusions	107
5.8 Appendix	109
5.9 References	112

PART IV: SURVEY AND SUMMARY

6. A survey of some essential aspects in modelling compound nerve activity.	
6.1 Introduction	117
6.2 Dispersion of arrival times	119
6.3 The stochastic process of arrival times	121
6.4 The 'frozen noise' in compound action potentials	121
6.5 The passive electrical properties of the nerve trunk	123
6.6 Diameter and propagation velocity	124
6.7 Parameter variation	124
6.8 In conclusion	126
6.9 References	126
7. Summary of results	129
Samenvatting	133
Curriculum vitae	136

PART I

BACKGROUND

C H A P T E R 1
ELECTRICAL ACTIVITY OF HUMAN PERIPHERAL
NERVES *IN SITU*

1.1 INTRODUCTION

When a peripheral nerve is stimulated strongly enough with a short current pulse each of many fibres in the current field starts propagating an action potential. By means of a recording electrode, usually placed at a certain distance (10 - 50 cm) from the site of stimulation, a *compound* action potential can be measured, which is the summated activity originating from individual fibres. This method of stimulation and recording from a peripheral nerve is common practice in clinical neurophysiology.

It is known that the external diameter of a myelinated nerve fibre and the propagation velocity of its action potential are approximately proportionally related. The 'whole nerve' propagation velocity, which is the usual parameter to be derived from the recorded signal, refers to the earliest component in the compound action potential and thus corresponds to the velocity of the fastest, and hence the thickest, fibres.

The presumption underlying the present study is that, beside the whole nerve propagation velocity, additional information about the nerve fibres is comprised in a compound nerve action potential. This idea is not new as will appear in the following sections. Most of the studies reported in the literature, however, depart from assumptions that do not really concern the single fibre activity at a basic level. Studies which explain compound action potentials of human nerves on the basis of the structure of the nerve including neurophysiological data of single fibre activity have, to our knowledge, not been reported in the literature thusfar.

Soon after Gasser and Erlanger (1922) made their first recordings of evoked electrical activity from prepared nerves *in vitro* by means of a cathode ray oscillograph the compound character of these signals was recognized (Erlanger and Gasser 1924). In those days relationships between nerve morphology and whole nerve action potentials were extensively discussed. The first attempts to make so-called 'reconstructions' of the compound action potential (CAP) of a nerve on the basis of the nerve structure were described a few years later (Gasser and Erlanger 1927). These reconstructions were based on the fibre diameter histogram and on a number of assumptions, among which was the proportionality between the fibre diameter and the propagation velocity of the single fibre action potential. Such predictions of electrical potential fields, due to presupposed source configurations are denoted by *forward* calculations.

The *inverse* procedure of estimating the sources on the basis of the recorded signal was first applied by Gasser and Grundfest (1939) when they predicted the relation between fibre diameter and velocity (cf. chapter 3). Since then little attention has been paid to the analysis of monophasic compound action potentials of dissected nerves. A computerized version of the tedious graphical constructions of monophasic CAP wave shapes has been used by Olson (1973).

Reconstructions of compound action potentials of nerves *in situ* were described for the first time by Buchthal and Rosenfalck (1966, 1971). They assumed simple triphasic single fibre action potential wave shapes and used the original assumptions of Gasser and Erlanger (1927). Although with this forward approach, a number of basic questions could be answered, the correspondence with measured CAPs was not very impressive.

In electrocardiography the notions 'forward and inverse problem' are immediately connected with the theory of *volume conduction* of currents in the extracellular medium (e.g. Swihart 1976, Barr and Spach 1976). This three-dimensional outward spread of current also governs the potential field of peripheral nerve fibres *in situ*. The effect of volume conduction in electro-neurography is illustrated when near-nerve recordings of compound action potentials, obtained with subcutaneous needle electrodes, are compared to the registrations with surface electrodes on the skin. It is clear at first sight that the former wave shapes contain more (high frequency) details (e.g. Ludin and Tackmann 1979) than the latter (e.g. Smorto and Basmajian

1972). Since nerve recordings are always made at some distance from the nerve trunk volume conduction always plays a part.

Volume conduction of currents from cylindrical fibres was described theoretically by Lorente de N6 (1947), by Clark and Plonsey (1966, 1968) and by Rosenfalck (1969). Application of this theory to the solution of the inverse problem of electrical nerve activity was suggested by Clark et al. (1978).

A forward reconstruction of monophasic compound action potentials from human sural nerve biopsies for *clinical use* has been used by Lambert and Dyck (1968). Recently clinical practice has also induced studies of the inverse problem. Barker et al. (1979), Cummins et al. (1979) and Cummins and Dorfman (1981) use techniques of recording compound action potentials from two sites along the nerve simultaneously. These methods predict the distribution of velocities, present in a nerve, without any *a priori* assumptions about the (volume conducted) single fibre action potential. Kovacs et al. (1979) use the nerve response to a very weak stimulus as an estimate of the single fibre action potential.

1.3 METHODS TO MEASURE ACTIVITY FROM HUMAN NERVES

The first recordings of compound nerve action potentials from human nerves *in situ* were reported in 1938 (see Buchthal and Rosenfalck 1966). The quality of such recordings improved substantially with the application of the photographic superimposition technique (Dawson and Scott 1949). Dawson (1956) was the first to record purely sensory nerve activity from human nerves. Sensory nerve recordings were used by Gilliatt and Sears (1958) in a clinical study of peripheral nerve lesions. The application of the principle of signal averaging, which was introduced in neurophysiology by Dawson in 1951, was initially limited to the recording of evoked potentials from the human scalp. Buchthal and Rosenfalck (1966) presented this technique in the measurement of sensory peripheral nerve action potentials. In their extensive study on this subject they also recommend the use of subcutaneous needles as recording electrodes. When several hundreds or even thousands of sweeps are averaged, even the activity from very slow nerve fibres can be obtained. In current clinical practice averages of 10 to 100 sweeps are usually made. In the following chapters we shall always refer to experimental data from the *sural nerve* of healthy volunteers. This nerve has been chosen because of its accessibility for experimentation on the one hand and because of the wide availability of histological data from this human nerve in literature on the

other hand. Orthodromic CAPs were obtained with needle electrodes according to a 'standard' procedure, which is described in a recent paper by Mamoli et al. (1980). Averages of 64 sweeps were made.

Inspired by the notion 'micro-neurography', introduced by Hagbarth and coworkers (e.g. Hagbarth 1979) to describe an intraneural recording technique for human single nerve fibres, the subject of the present study could be denoted by 'macro-neurography', since an overall picture of the nerve is obtained. Unlike intraneural recordings, the latter measurements suffer from the unfavourable electrical properties of the nerve trunk (see Sect. 1.5).

1.4 THE RELATION BETWEEN NEUROGRAPHICAL AND HISTOMETRICAL PARAMETERS

The proportionality between fibre diameter and action potential propagation velocity has already been mentioned. The whole nerve propagation velocity is defined on the base of the initial positive component in the compound nerve action potential which is due to the activity of the fastest fibres. The improvement of the signal quality of compound action potentials after averaging gave rise to studies relating a broader range of velocities to histometrical findings (Buchthal 1973, Buchthal et al. 1975, Tackmann et al. 1976). Beside the fibre diameter distribution, the quantification of nerve biopsy findings encloses additional determinations like the thickness of the myelin, the internodal lengths and the nodal widths (e.g. Thomas 1970). A 'disproportional slowing' after segmental demyelination has been described by Behse and Buchthal (1978) but not nearly all electrophysiological implications of specific pathological deviations from the normal fibre structure are known. Important in this respect are the recent model studies based on the Hodgkin-Huxley model for the fibre membrane, modified to describe propagation in myelinated fibres (e.g. Frankenhaeuser 1973, Waxman 1980).

An additional and much less studied problem is the translation of findings on a basic level of the fibre membrane to the characteristics of compound action potentials, measured *in situ*.

Of course a one to one representation toward histological findings cannot be pursued. Both ways of investigating a nerve will always be supplementary and not equivalent. The development of a nondestructive method for the analysis of (pathological) nerve structure will nevertheless be a challenging perspective for the future applications of the present and related studies.

1.5 PREREQUISITES FOR A RECONSTRUCTION PROCEDURE, BASED ON VOLUME CONDUCTION THEORY

The outward spread of transmembrane current determines the transfer function from the fibre membrane to the site of recording. A description of the passive electrical conductivities of the surrounding tissues must be available when an 'electrophysiological counterpart' to histological determinations has to be developed. This is certainly a complicating factor. It appears that the usual assumptions of homogeneity and isotropy of the extracellular medium (e.g. Lorente de N6 1947) cannot be maintained for a peripheral nerve fibre. The nerve trunk, the subcutaneous fat layer and the surface of the skin must all be taken into account. As mentioned before already, several volume conduction studies, based on cylindrical single fibre configurations have been presented in the literature. The combination of the, volume conducted, extracellular potential fields of several fibres to a compound signal has been reported in studies on the motor unit action potential in muscles (Broman and Lindstr6m 1974, Boyd et al. 1978, Griep et al. 1978), but not yet in the reconstruction of compound nerve action potentials. In conformity with these studies we have to included the statistics of an essentially finite number of fibres in the calculations. The resulting model is adapted to the structure, the number of fibres and the surroundings of the human sural nerve. The choice of this particular nerve is arbitrary with respect to the modelling procedure but we believe that most results will be valid for normal peripheral nerves in general.

A model test in the strict sense cannot be found in this thesis since biopsy data from the particular nerves, studied electrophysiologically, were not available. Biopsy data from normal human sural nerves in the literature, however, give sufficient quantitative histological information for the scope of the present study.

1.6 STRUCTURE OF THIS INVESTIGATION

The mathematical formulation of the model is stepwise built up in chapter 2, which contains a number of subsections each containing a separate, circumscribed, aspect. The model as a whole is recapitulated in the first sections of chapter 3, so that readers, who are not familiar with the mathematical material, may be recommended to skip the central part of chapter 2.

In evaluating the model, three aspects of nerve propagation are studied, mainly as a 'validity test' for the model, namely:

- the relation between fibre diameter and velocity (chapter 3),
- the influence of the temperature (chapter 4), and
- the influence of the relative refractory state (chapter 5).

The first aspect needs no further clarification for the moment. The temperature and the refractory state of a nerve *in situ* can be influenced easily and in a well-defined manner. The implications of such interferences at the fibre membrane level have been extensively studied and the relevant literature on this subject has been evaluated. A number of unclarified questions or controversial statements in literature are discussed with the help of reconstructed CAPs. It will be illustrated that a quantitative model is an indispensable tool in understanding the generation of CAPs under various conditions.

The results are discussed for each of the chapters 2 to 5 separately. The most notable aspects of the model have been summarized in chapter 6 in a tutorial way explaining the main principles of the modelling procedure. In chapter 7 the main results are summarized. Some results may have certain implications for CAP measurements in clinical practice, or may broaden the usual interpretation of CAPs. The main scope of the present study, however, has been the development of a model for the main complex of compound action potentials from normal sural nerve in order to gain insight in the factors determining its appearance. Pathological nerve propagation and a more detailed analysis of the contributions of slower fibres will be the subject of future investigations.

1.7 REFERENCES

- Barker, A.T., Brown, B.H. and Freeston, I.L. Determination of the distribution of conduction velocities in human nerve trunks. IEEE Trans. biomed. Engng, 1979, BME-26: 76-81.
- Barr, R.C. and Spach, M.S. Inverse solutions directly in terms of potentials. In: C.V. Nelson and D.B. Geselowitz (Eds.), The theoretical basis of electrocardiology. Clarendon Press, Oxford, 1976: 294-322.
- Behse, F. and Buchthal, F. Sensory action potentials and biopsy of the sural nerve in neuropathy. Brain, 1978, 101: 473-494.
- Boyd, D.C., Lawrence, P.D. and Bratty, P.J.A. On modeling the single motor unit action potential. IEEE Trans. biomed. Engng., 1978, BME-25: 236-242.

- Broman, H. and Lindström, L. A model describing the power spectrum of myoelectric signals. part II: motor unit signal. Chalmers Univ. of Technology, Göteborg, 1974.
- Buchthal, F. Sensory and motor conduction in polyneuropathies. In: J.E. Desmedt (Ed.), New developments in electromyography and clinical neurophysiology, Vol. 2. Karger, Basel, 1973: 259-271.
- Buchthal, F. and Rosenfalck, A. Evoked action potentials and conduction velocity in human sensory nerves. Brain Res., 1966, 3: 1-122.
- Buchthal, F. and Rosenfalck, A. Sensory potentials in polyneuropathy. Brain, 1971, 94: 241-262.
- Buchthal, F., Rosenfalck, A. and Behse, F. Sensory potentials of normal and diseased nerve. In: P.J. Dyck, P.K. Thomas and E.H. Lambert (Eds.), Peripheral neuropathy, Vol. 1. Saunders, Philadelphia, 1975: 442-464.
- Clark, J.W., Greco, E.C. and Harman, T.L. Experience with a Fourier method for determining the extracellular potential field of excitable cells with cylindrical geometry. CRC crit. Rev. Bioengng., 1978, 3: 1-22.
- Clark, J.W. and Plonsey, R. A mathematical evaluation of the core conductor model. Biophys. J., 1966, 6: 95-112.
- Clark, J.W. and Plonsey, R. The extracellular potential field of the single active nerve fiber in a volume conductor. Biophys. J., 1968, 8: 842-864.
- Cummins, K.L., Dorfman, L.J. and Perkel, D.H. Nerve fibre conduction velocity distributions. II. Estimation based on two compound action potentials. Electroenceph. clin. Neurophysiol., 1979, 46: 647-658.
- Cummins, K.L. and Dorfman, L.J. Nerve fiber conduction velocity distributions: Studies of normal and diabetic human nerves. Ann. Neurol., 1981, 9: 67-74.
- Dawson, G.D. A summation technique for detecting small signals in a large irregular background. J. Physiol., 1951, 115: P2-P3.
- Dawson, G.D. The relative excitability and conduction velocity of sensory and motor nerve fibres in man. J. Physiol., 1956, 131: 436-451.
- Dawson, G.D. and Scott, J.W. The recording of nerve action potentials through skin in man. J. Neurol. Neurosurg. Psychiat., 1949, 12: 259-267.
- Erlanger, J. and Gasser, H.S. The compound nature of the action current of nerve as disclosed by the cathode ray oscillograph. Amer. J. Physiol., 1924, 70: 624-666.
- Frankenhaeuser, B. The nerve impulse. In: J.E. Desmedt (Ed.), New developments in electromyography and clinical neurophysiology, Vol. 2. Karger, Basel, 1973: 42-44.

- Gasser, H.S. and Erlanger, J. A study of the action currents of nerve with the cathode ray oscillograph. *Amer. J. Physiol.*, 1922, 62: 496-524.
- Gasser, H.S. and Erlanger, J. The role played by the sizes of the constituent fibers of a nerve trunk in determining the form of its action potential wave. *Amer. J. Physiol.*, 1927, 80: 522-547.
- Gasser, H.S. and Grundfest, H. Axon diameters in relation to the spike dimensions and the conduction velocity in mammalian A fibers. *Amer. J. Physiol.*, 1939, 127: 393-414.
- Gilliatt, R.W. and Sears, T.A. Sensory nerve action potentials in patients with peripheral nerve lesions. *J. Neurol. Neurosurg. Psychiat.*, 1958, 21: 109-118.
- Griep, P.A.M., Boon, K.L. and Stegeman, D.F. A study of the motor unit action potential by means of computer simulation. *Biol. Cybernetics*, 1978, 30: 221-230.
- Hagbarth, K.E. Microneurography technique. In: E. Persson (Ed.), *Symposia 6th international congress of electromyography in Stockholm, 1979*: 11-13.
- Kovacs, Z.L., Johnson, T.L. and Sax, D.S. Estimation of the distribution of conduction velocities in peripheral nerves. *Comp. Biol. Med.*, 1979, 9: 281-293.
- Lambert, E.H. and Dyck, P.J. Compound action potentials of human sural nerve biopsies. (abstract). *Electroenceph. clin. Neurophysiol.*, 1968, 25: 399-400.
- Lorente de N6, R. A study of nerve physiology. *Studies from the Rockefeller Institute for Medical Research*, 1947, 132: 384-482.
- Ludin, H.P. and Tackmann, W. *Sensible neurographie*. Georg Thieme, Stuttgart, 1979.
- Mamoli, B., Mayr, M., Gruber, H. and Maida, E. *Elektroneurographische Untersuchungen am N. Suralis. Methodische Probleme und Normwerte*. *Z. EEG-EMG*, 1980, 11: 119-127.
- Olson, W.H. *Peripheral nerve compound action potentials and fiber diameter histograms*. (Ph.D. dissertation). Univ. of Michigan, Ann Arbor, Mich. 1973.
- Rosenfalck, P. Intra- and extracellular potential fields of active nerve and muscle fibres. *Acta Physiol. Scand.*, 1969, Suppl. 321.
- Smorto, M.P. and Basmajian, J.V. *Clinical electroneurography*. Williams and Wilkins, Baltimore, 1972.
- Swhihart, J.C. Numerical methods for solving the forward problem in electrocardiography. In: C.V. Nelson and D.B. Geselowitz (Eds.), *The theoretical basis of electrocardiology*. Clarendon Press, Oxford, 1976: 257-293.

- Tackmann, W., Spalke, H.J. and Oginzus, H.J. Quantitative histometric studies and relation of number and diameter of myelinated fibres to electrophysiological parameters in normal sensory nerves in man. *J. Neurol.* 1976, 212: 71-84.
- Thomas, P.K. The quantitation of nerve biopsy findings. *J. Neurol. Sci.*, 1970, 11: 285-295.
- Waxman, S.G. Determinants of conduction velocity in myelinated nerve fibers. *Muscle Nerve*, 1980, 3: 141-150.

PART II

MATHEMATICAL FORMULATION

A volume conductor study of compound action potentials of nerves *in situ*: the forward problem.

D.F. Stegeman, J.P.C. de Weerd, E.G.J. Eijkman
Biol. Cybernetics, 1979, 33: 97-111.

C H A P T E R 2
A VOLUME CONDUCTOR STUDY OF COMPOUND
ACTION POTENTIALS

ABSTRACT

A computer model for the simulation of compound nerve action potentials, based on superposition of volume conducted single nerve fibre potentials, is presented. The model assumes that the intracellular fibre potential, the fibre diameter distribution and the electrical conductivities of different tissues are known. Volume conductor fields are calculated in the spatial frequency domain. The influence of important parameters in the model is evaluated numerically. It is shown that it is necessary to give up the usual assumption of homogeneity and isotropy in the extracellular medium. In the present model parameters are introduced which allow an overall description of the complex morphological and physiological structure of the nerve trunk. Simulation results indicate that the model is a rather promising tool in studying the main properties of compound action potentials which up till now have not been sufficiently well understood.

2.1 INTRODUCTION

The compound action potential (CAP) of human sensory nerves has been the subject of clinical investigations for more than 20 years (e.g. Dawson 1956, Buchthal and Rosenfalck 1966). In particular the determination of the maximum sensory conduction velocity, which can be deduced easily from the arrival time of the compound potential, has proven to be a powerful diagnostic tool in peripheral nerve diseases. Other features of a CAP, such as its wave shape and its amplitude have appeared to be of less diagnostic significance, probably because they cannot as easily be interpreted in terms of underlying properties of the nerve under consideration. Nevertheless it is obvious that morphological information about the nerve must also be present in a CAP.

A compound potential can be interpreted as a linear summation of the action potentials of those single fibres that are activated by the stimulus. However, the spread in propagation velocities between these fibres, together with the triphasic character of single fibre action potentials (SFAPs) of a nerve in situ, causes extinction of SFAPs of different fibres and therefore the interpretation of the resulting CAP is seriously hindered. To some extent this has already been demonstrated by Buchthal and Rosenfalck (1966) and Barker (1976) but the essential anisotropy and inhomogeneity of the nerve trunk have not been included in their reconstruction studies. Nerve recordings done in a prepared situation show monophasic SFAP-shapes, causing a CAP-wave shape that can be more easily interpreted (Gasser and Erlanger 1927, Olson 1973). The properties of a nerve in situ can be handled with theories of volume conduction (e.g. Lorente de N6 1947, Clark and Plonsey 1966, Rosenfalck 1969). Therefore in this chapter a reconstruction model is presented which incorporates the volume conduction properties of the nerve bundle and its surroundings. The model description starts at the level of the intracellular single fibre potentials, and assumes knowledge of the distribution of fibre diameters. With this model it appears to be possible to reconstruct CAPs that closely resemble potentials which can be measured in practice.

Many factors can influence the CAP appearance. The effects of most of these factors such as temperature (Ludin and Beyeler 1977, Lowitzsch et al. 1977), refractoriness of fibre membranes (Buchthal and Rosenfalck 1966, Tackmann and Lehmann 1974, de Weerd et al. 1979), loss of active fibres or changes in the diameter histogram are not very well understood quantitatively. The development of our model has been inspired mainly by this lack of quanti-

tative data. As the model appears to be able to predict CAPs from the underlying fibre configurations (diameter distribution) in a satisfactory way, an obvious question is whether it is possible to follow the opposite approach i.e. to construct a diameter distribution when an accurate recording of a CAP is available. In order to distinguish between these two procedures we propose to adopt a custom from modelling heart activity and indicate the latter as the *inverse problem*, while the subject of this paper can then be denoted as the *forward problem*.

The linear summation properties of a volume conductor allow a clear distinction to be made between the two main aspects of the present model. First the activity of a single fibre is modelled in Sect. 2.2 on the basis of seven assumptions, each of which is worked out in a separate subsection. In Sect. 2.3 the superposition phenomenon is described in terms of a statistical process. In the discussion (Sect. 2.4) some relevant parameters of the model are evaluated. Special attention is paid to the choice of the intracellular potential, the use of the diameter distribution of a nerve, the conductivity parameters inside and outside the nerve trunk and the important role of the propagation velocity in all results. The inverse problem i.e. the construction of diameter histograms from a known CAP is also touched on in that section. Finally our conclusions are summarized in Sect. 2.5.

2.2 A MODEL OF THE SINGLE FIBRE ACTION POTENTIAL

The analytical equations which will be derived in this section relate the extracellular potential of a single nerve fibre at any point outside the nerve trunk to the intracellular single fibre potential. The final result is based on seven assumptions which will be worked out in as many subsections. The assumptions are:

- 2.1 The potential field caused by physiological current sources in a physiological volume conductor is a *quasi-static* one.
- 2.2 All the boundaries in the volume conductor e.g. the active fibre membrane and separation between areas of different *non zero* conductivities, have *cylinder symmetry* around the same axis and are of infinite length.
- 2.3 Each fibre has its *constant propagation velocity* by which the active process travels along the fibre membrane.
- 2.4 A nerve fibre can be conceived of as a circular cylinder. It contains an *axoplasm* and is bounded by the thin *membrane* layer.

- 2.5 Potential differences inside the nerve fibre only appear in the axial direction for which the *core conductor model* applies.
- 2.6 A nerve trunk acts as a tube around each fibre consisting of a medium with an electrical *anisotropy*. The conductivity in the axial direction is different from that in the radial direction.
- 2.7 The surface of the skin close to the nerve trunk can be modelled by an *insulating flat sheet*. The method of images can be applied.

The Assumptions 2.1-2.5 have also been made by other authors. Assumption 2.6 is based on the observation that each fascicle in a nerve, as well as the nerve as a whole, is surrounded by electrically relatively insulating tissues (Burke et al. 1975, Clark and Plonsey 1968, Patlak 1955). Assumption 2.7 arises from the fact that the influence of the skin cannot be neglected.

2.2.1 Poisson's equation

The validity of the first assumption has been discussed by many authors and is commonly accepted (e.g. Clark and Plonsey 1966, Rosenfalck 1969). When the volume conductor is homogeneous and isotropic the potential field satisfies Poisson's equation:

$$\nabla^2 \phi = \frac{\nabla \cdot \vec{J}_i}{\sigma + j\omega\epsilon} \quad (1)$$

where ϕ is the potential at any point of the conductor, \vec{J}_i is an impressed current, σ and ϵ are the conductivity and the dielectric permittivity of the medium respectively and $j\omega$ is the representation of d/dt in the frequency domain.

$\nabla \cdot \vec{J}_i = -i_v$ is a volume current source density with dimension $A \cdot m^{-3}$ and forms the analogue to the charge density in electrostatics. The contribution of $j\omega\epsilon$ to the denominator of (1) depends on the upper frequency in physiological processes and the ratio between ϵ and σ in biological tissue ($\approx 5 \cdot 10^{-6} \text{ Hz}^{-1}$). Normally it is neglected (Plonsey 1971).

A well known solution of (1) is obtained assuming an infinite medium containing current sources within volume V . By choosing zero potential at a point at infinite distance from volume V it follows (Jackson 1962):

$$\phi(\vec{r}') = \frac{1}{4\pi\sigma} \int_V \frac{i_v(\vec{r})}{R} dV \quad (2)$$

where \vec{r}' is the field point under consideration, \vec{r} is a point with nonzero current source density and $R = |\vec{r} - \vec{r}'|$ is the distance between these points.

2.2.2 Cylindrical coordinates

A mathematical model of the potential field of a nerve requires some simplifying assumptions such as 2.2 and 2.7. The simplest model configuration that can be based on Assumption 2.2 is a line current source density $i_r(z)$ per unit of length along the z -axis (see Fig. 2.1). The integration

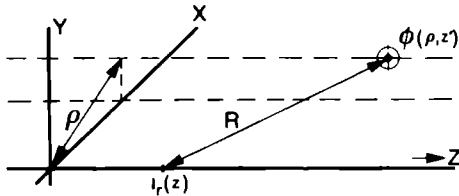


Fig. 2.1

The line source model

$$R = \sqrt{\rho^2 + |z - z'|^2}$$

of $i_v(\vec{r})$ along x - and y -direction is performed and the limit $x \rightarrow 0$ and $y \rightarrow 0$ is taken. This line source is still surrounded by an infinite homogeneous and isotropic volume conductor.

Since the source does not take up a part of the volume the medium is still homogeneous and (2) can be used.

$$\phi^S(\rho, z') = \frac{1}{4\pi\sigma} \int_{-\infty}^{\infty} dz \frac{i_r^S(z)}{R} = \frac{1}{4\pi\sigma} \int_{-\infty}^{\infty} dz \frac{i_r^S(z)}{(\rho^2 + |z - z'|^2)^{1/2}} \quad (3).$$

This model should be looked upon as an introduction to more complicated configurations that will be developed in subsequent subsections. The symbol S denotes that ϕ and i_r are expressed in spatial terms in contrast to their expression in temporal terms (indexed T).

2.2.3 Constant propagation velocity

A realistic model for an *active* fibre requires incorporation of the travelling character of the active process, which therefore leads to Assumption 2.3. In medullated fibres the propagation has a saltatory character. Deviations from Assumption 2.3 caused by this property can be neglected as can be justified with Subsect. 2.4.1 and Fig. 2.8. In general, Assumption 2.3 leads to the transformation $z = U \cdot t + z_0$ which, without loss of generality, can be reduced to

$$z = U.t \quad (4)$$

where U is the propagation velocity.

With (4), (3) can be rewritten:

$$\phi^T(\rho, t') = \frac{1}{4\pi\sigma} \int_{-\infty}^{\infty} dt \frac{i_{\mathbf{r}}^T(t)}{((\rho/U)^2 + (t-t')^2)^{1/2}} \quad (5)$$

where $\phi^T(\rho, t') = \phi^S(\rho, U.t')$ and $i_{\mathbf{r}}^T(t) = i_{\mathbf{r}}^S(U.t)$, a general relation between T- and S-denoted functions using Assumption 2.3.

Equation (5) is a convolution integral which often reduce in complexity after transformation to the frequency domain.

Although the necessity to do so in this case is not self-evident, we show the result in order to be able to refer to it later on.

By defining the Fourier transforms:

$$\mathbf{F}\{f(t)\} = F(\omega) = \int_{-\infty}^{\infty} f(t)e^{-j\omega t} dt \quad (6)$$

and:

$$\mathbf{F}^{-1}\{F(\omega)\} = f(t) = \frac{1}{2\pi} \int_{-\infty}^{\infty} F(\omega)e^{j\omega t} d\omega \quad (7)$$

and by substitution of (Jackson 1962)

$$\mathbf{F} \left\{ \frac{1}{(q^2+t^2)^{1/2}} \right\} = 2 K_0(|q\omega|) \quad (8)$$

where $K_0(\xi)$ is the modified Bessel function of the second kind and order zero, we find

$$\phi^T(\rho, \omega) = \frac{1}{2\pi\sigma} I_{\mathbf{r}}^T(\omega) H_0(\omega/U; \rho) \quad (9)$$

where $H_0(\omega/U; \rho) = K_0(|\omega/U| \rho)$ and $\phi^T(\rho, \omega)$ and $I_{\mathbf{r}}^T(\omega)$ are the Fourier transforms of $\phi^T(\rho, t')$ and $i_{\mathbf{r}}^T(t)$ respectively.

Equation (9) is the first presentation of the extracellular potential field of a nerve fibre in the frequency domain. $H_0(\omega/U; \rho)$ is introduced for reasons of similarity with future notation. From now on all the potential fields will be expressed in the temporal or the spatial frequency domain.

2.2.4 The fibre as a circular cylinder

Assumption 2.4 is visualized in Fig. 2.2. By defining the membrane current per unit area of the membrane, maintaining cylinder symmetry, it follows:

$$i_m^S(z) = i_r^S(z)/2\pi a \quad (10).$$

For $\rho > a$ (9) can be rewritten:

$$\phi_e^T(\rho, \omega, a) = \frac{a}{\sigma_e} I_m^T(\omega) H_0(\omega/U; \rho) \quad (11)$$

where σ has been replaced by σ_e and ϕ^T by ϕ_e^T .

Considering Fig. 2.2 (11) is an approximation for two reasons:

1. The current is no longer set free in a point on the z-axis but rather along a circumference.
2. The interior of the fibre does not "take part" in the volume conduction of current set free outside the fibre, i.e. an inhomogeneity is introduced.

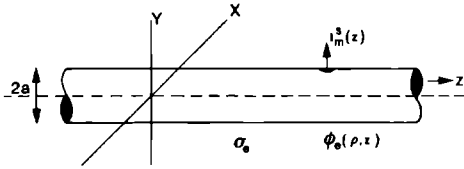


Fig. 2.2
The cylinder source model

An exact solution for $\phi_e^T(\rho, \omega, a)$ can be found using Laplace's equation which is applicable in the local absence of current sources. In cylinder symmetry we have:

$$\frac{\partial^2 \phi}{\partial \rho^2} + \frac{1}{\rho} \frac{\partial \phi}{\partial \rho} + \frac{\partial^2 \phi}{\partial z^2} = 0 \quad (12).$$

A general solution, which is physically possible, can be found after separation of variables (Clark and Plonsey 1966):

$$\phi_e^S(\rho, z, a) = \frac{1}{2\pi} \int_{-\infty}^{\infty} A(k) K_0(|k|\rho) e^{jkz} dk \quad (13)$$

where k will be called the spatial frequency. It is related to z by Fourier-

transformation. The dimension of k is cycles per unit of length and with Assumption 2.3 it equals ω/U which is analogous to $z = U.t$.

$A(k)$ can be found by substitution of the known boundary condition at the membrane surface (Rosenfalck 1969, Clark and Plonsey 1968)

$$\sigma_e \frac{\partial \phi_e^S(\rho, z, a)}{\partial \rho} \Big|_{\rho=a} = -i_m^S(z) \quad (14).$$

Consequently in (13) we obtain:

$$A(k) = \frac{1}{\sigma_e} \frac{I_m^S(k)}{|k|K_1(|k|a)} \quad (15)$$

where $I_m^S(k) = \mathcal{F}\{i_m^S(z)\}$ and $K_1(\xi)$ is the modified Bessel function of the second kind and order one.

Analogous to (11) we get:

$$\phi_e^T(\rho, \omega, a) = \frac{a}{\sigma_e} I_m^T(\omega) \cdot H_1(\omega/U; \rho; a) \quad (16)$$

$$\text{where } H_1(\omega/U; \rho; a) = \frac{K_0(|\omega/U|\rho)}{|\omega/U|aK_1(|\omega/U|a)}$$

The denominator in H_1 describes the deviation from the previous result (11). This deviation increases with increasing $|\omega/U|a = |k|a$ and makes $H_1(\omega/U; \rho; a) > H_0(\omega/U; \rho)$.

An estimation of the deviation can be obtained by taking a high value for $a (= 10 \mu\text{m})$ and for k a value which can be approximated considering the normal extensiveness of the active process along the membrane ($\approx 10 \text{mm}$) in which case the deviation is less than 2%. Note that $H_1(\omega/U; \rho; 0) = H_0(\omega/U; \rho)$.

2.2.5 Core conductor model

Assumption 2.5 can be evaluated by setting up an equation like (16) but now for the intracellular medium (Rosenfalck 1969). The radial potential differences in this region appear to be extremely small relative to the differences in the axial direction. In the core-conductor-model they are assumed to be zero. Figure 2.3 shows the parameters in the core-conductor-model.

Combination of:

$$i_m^S(z) = i_r^S(z)/2\pi a$$

$$i_1^S(z) = -\pi a^2 \sigma_i \frac{d\phi_i^S(z)}{dz}$$

and:

$$i_r^S(z) = -di_1^S(z)/dz$$

yields:

$$i_m^S(z) = \frac{\sigma_i a}{2} \frac{d^2 \phi_i^S(z)}{dz^2} \quad (17)$$

or

$$i_m^T(t) = \frac{\sigma_i a}{2U^2} \frac{d^2 \phi_i^T(t)}{dt^2} \quad (18)$$

or

$$I_m^T(\omega) = \frac{\sigma_i a}{2U^2} [-\omega^2 \phi_i^T(\omega)] \quad (19)$$

where $\phi_i^T(\omega)$ is the Fourier transform of $\phi_i^T(t)$.

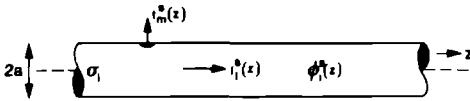


Fig. 2.3

Parameters in the core conductor equations

Inserting (19) in (16) yields:

$$\phi_e^T(\rho, \omega, a) = \frac{\sigma_i a^2}{2\sigma_e U^2} [-\omega^2 \phi_i^T(\omega)] H_1(\omega/U; \rho; a) \quad (20).$$

Equation (20) is the final solution for a nerve fibre in an isotropic and homogeneous extracellular medium with conductivity σ_e . Before introducing a more complicated configuration we formulate a general expression of which (11) and (20) are special cases.

The graphs of $K_0(\xi)$ and $K_1(\xi)$ (Abramowitz and Stegun 1972) show that $H_0(\omega/U; \rho)$ and $H_1(\omega/U; \rho; a)$ can be interpreted as low-pass filters acting upon the second derivative of the intracellular potential. Although the results in the following sections look quite complex we will be able to relate $\phi_i^T(\omega)$ and $\phi_e^T(\rho, \omega, a)$ by virtue of the Assumptions 2.1-2.5 in the *general expression*:

$$\phi_e^T(\rho, \omega, a) = \left[\frac{\sigma_i a^2}{2\sigma_e U^2} \right] \left[-\omega^2 \phi_i^T(\omega) \right] \left[H_v(\omega/U; \rho, \dots; a, \dots; \frac{\sigma_g}{\sigma_h}, \dots) \right] \quad (21).$$

The first term is a constant, the next one represents the second derivative of the intracellular potential and the third term always describes a low-pass filter with zero phase shift. The parameters indexed by e are related to the most outward region which will be defined as the e-region. It stretches out to infinity. The parameter list of H_v contains four types of parameters: spatial frequency; observation distance(s); boundary radii and ratio(s) between successive conductivities (except σ_i). We derived two examples (H_0 and H_1) and will derive another two (H_2 and H_3).

2.2.6 Nerve trunk properties

Assumption 2.6 has been chosen as a simplification of the nerve trunk geometry and conductivity within the possibilities of cylinder symmetry. It is based on observations of insulating tissues around fascicles and the trunk as a whole. Beside this there is also evidence for a contribution to the anisotropy caused by the small conductivity of the nerve membrane in the passive state. An anisotropy of the latter type is found for instance in muscle tissue (Geddes and Baker 1967). The current set free by an active piece of membrane, belonging to the fibre under consideration, encounters more "barriers" when flowing in the radial direction to the outside of the trunk than when flowing in the fibre direction. We represent these "barriers" by assuming an equally distributed anisotropy in the nerve trunk as a whole (Fig. 2.4).

Two different extracellular media are introduced, the o-(outer) and the e-(external) region which stands for a second inhomogeneity. Both media are in general thought to be anisotropic with conductivities $\sigma_{o\rho}$, σ_{oz} and $\sigma_{e\rho}$ and σ_{ez} respectively. The anisotropies can be handled with the introduction of the coordinate transforms in ρ -direction in the o- and e-region (Plonsey 1974):

$$\rho_m = \rho (\sigma_{mz} / \sigma_{m\rho})^{1/2} \quad m = o, e \quad (22).$$

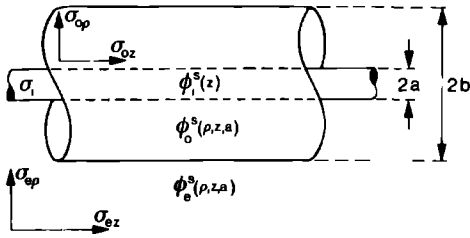


Fig. 2.4

Model configuration based on a cylinder source surrounded by anisotropic media. Three regions are distinguished: *i* (intracellular) with conductivity σ_i , *o* (outer) with anisotropic conductivity (σ_{op} , σ_{oz}) and *e* (external) with (σ_{ep} , σ_{ez}), where *o* and *z* indicate the radial and the axial direction respectively

Laplace's equation is satisfied in the new coordinate system (ρ_m, z):

$$\frac{\partial^2 \phi_m}{\partial \rho_m^2} + \frac{1}{\rho_m} \frac{\partial \phi_m}{\partial \rho_m} + \frac{\partial^2 \phi_m}{\partial z^2} = 0 \quad m = o, e \quad (23).$$

In the configuration of Fig. 2.4 a general solution for $\phi_o^S(\rho, z, a)$ and $\phi_e^S(\rho, z, a)$ is given by (e.g. Clark and Plonsey 1966):

$$\phi_o^S(\rho, z, a) = \frac{1}{2\pi} \int_{-\infty}^{\infty} \{A_1(k)K_0(|k|\rho_o) + A_2(k)I_0(|k|\rho_o)\} e^{jkz} dk \quad (24)$$

and

$$\phi_e^S(\rho, z, a) = \frac{1}{2\pi} \int_{-\infty}^{\infty} B(k)K_0(|k|\rho_e) e^{jkz} dk \quad (25)$$

with $I_0(\xi)$ the modified Bessel function of the first kind and order zero. In (13) and (25) $I_0(\xi)$ does not appear in the expression because it gives rise to physically impossible solutions in the *e*-region for $\xi \rightarrow \infty$. Three boundary conditions have to be fulfilled:

$$\phi_o^S(\rho, z, a) \Big|_{\rho=b} = \phi_e^S(\rho, z, a) \Big|_{\rho=b} \quad (26)$$

$$\sigma_{o\rho} \left. \frac{\partial \phi_o^S(\rho, z, a)}{\partial \rho} \right|_{\rho=b} = \sigma_{e\rho} \left. \frac{\partial \phi_e^S(\rho, z, a)}{\partial \rho} \right|_{\rho=b} \quad (27)$$

$$\sigma_{o\rho} \left. \frac{\partial \phi_o^S(\rho, z, a)}{\partial \rho} \right|_{\rho=a} = -i_m^S(z) \quad (28).$$

Equations (26) and (27) describe the continuity of potential and current across the boundary $\rho=b$, while (28) is equivalent to (14).

The solution in the e-region is important in view of our study. After substitution of (26)-(28) into (24) and (25) it follows in the notation of (21) after some straightforward but lengthy manipulations and substitution of $\nu = 2$; $k = \frac{\omega}{U}$; $\sigma_e = \sigma_{e\rho}$:

$$H_2\left(\frac{\omega}{U}; \rho; a, b; \frac{\sigma_{oz}}{\sigma_{o\rho}}, \frac{\sigma_{ez}}{\sigma_{e\rho}}, \frac{\sigma_{o\rho}}{\sigma_{e\rho}}\right) = \quad (29)$$

$$K_0\left(\left|\frac{\omega}{U}\right| \rho_e\right) \left[N\left(\frac{\omega}{U}; b_o, b_e\right) / D\left(\frac{\omega}{U}; a_o, a_e, b_o, b_e; \frac{\sigma_{o\rho}}{\sigma_{e\rho}}\right) \right]$$

where b_o , b_e , a_o and a_e are defined in the same manner as ρ_o and ρ_e in (22),

$$N(k; b_o, b_e) = \frac{I_0(|k|b_o)K_1(|k|b_o) + I_1(|k|b_o)K_0(|k|b_o)}{K_1(|k|b_e)K_0(|k|b_e)}$$

and

$$D(k; a_o, a_e, b_o, b_e; \frac{\sigma_{o\rho}}{\sigma_{e\rho}}) = \frac{a_e}{a_o} \left[\frac{|k|a_o K_1(|k|a_o) I_0(|k|b_o)}{K_0(|k|b_e)} + |k|a_o I_1(|k|a_o) \frac{K_0(|k|b_o)}{K_0(|k|b_e)} \right]$$

$$+ \frac{\sigma_{o\rho}}{\sigma_{e\rho}} \left[\frac{|k|a_o K_1(|k|a_o) I_1(|k|b_o)}{K_1(|k|b_e)} - |k|a_o I_1(|k|a_o) \frac{K_1(|k|b_o)}{K_1(|k|b_e)} \right]$$

$I_0(\xi)$, $I_1(\xi)$, $K_0(\xi)$ and $K_1(\xi)$ are the modified Bessel functions of order zero and one.

Note that: $H_2\left(\frac{\omega}{U}; \rho; a, b; 1, 1, 1\right) = H_1\left(\frac{\omega}{U}; \rho; a\right)$.

2.2.7 The surface of the skin

The final model configuration describing the potential field of a single fibre is drawn in Fig. 2.5a in the $x - y$ plane. The method of images, a well known principal in electrostatics (e.g. Jackson 1962), leads to an accurate solution in a simple way.

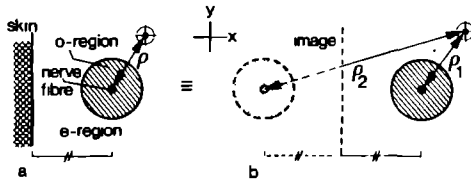


Fig. 2.5 a and b

Two equivalent representations of the surface of the skin as a perfectly insulating flat sheet in the $x - y$ plane. In both cases the boundary condition

$$\left. \frac{\partial \phi_e}{\partial x} \right|_{\text{skin level}} = 0 \text{ is fulfilled}$$

To the configuration of Fig. 2.5b a filter function H_3 applies. The ultimate model for the SFAP is obtained by inserting H_3 in Eq. (21).

$$H_3\left(\frac{\omega}{U}; \rho_1, \rho_2; a, b; \frac{\sigma_{oz}}{\sigma_{op}}, \frac{\sigma_{ez}}{\sigma_{ep}}, \frac{\sigma_{op}}{\sigma_{ep}}\right) = H_2\left(\frac{\omega}{U}; \rho_1; \dots; \dots\right) + H_2\left(\frac{\omega}{U}; \rho_2; \dots; \dots\right) \quad (30).$$

Two outermost situations in the influence of the image configuration are given by $\rho_1 = \rho_2$ and $\rho_2 \rightarrow \infty$, namely

$$H_3\left(\frac{\omega}{U}; \rho, \rho; \dots; \dots\right) = 2 H_2\left(\frac{\omega}{U}; \rho; \dots; \dots\right)$$

$$H_3\left(\frac{\omega}{U}; \rho, \infty; \dots; \dots\right) = H_2\left(\frac{\omega}{U}; \rho; \dots; \dots\right)$$

which are well-known reductions when leading-off on the skin surface and with the skin surface very far away respectively. In the calculations, presented in the chapters 3, 4 and 5, a second boundary was involved (Fig. 3.1).

2.3 MODELLING THE COMPOUND ACTION POTENTIAL

This section directly builds on the foregoing seven assumptions as far as the SFAP is concerned. Our final aim is to obtain a model describing the activity of all SFAPs that arise following simultaneous stimulation of a large group of fibres in a nerve causing a Compound Action Potential (CAP). In superimposing the SFAPs we encounter some new problems which give rise to three further assumptions and the use of the statistics of the distribution of arrival times.

The additional assertions are:

- 3.1 The CAP can be represented as a *linear superposition* of its elements, defined as the SFAPs volume conducted in passive surroundings.
- 3.2 All single fibres which conduct a SFAP are activated *simultaneously* at the *same point* on the nerve. This implies that the travelling distance between the site of activation and the site of observation is equal for all fibres.
- 3.3 For medullated fibres a *linear* relationship exists between fibre *radius* and *propagation* velocity.
- 3.4 The arrival times of the SFAPs form a *stochastic process* with a probability density function (PDF) that can be computed from the diameter histogram of fibres in a particular nerve.

In the following four subsections these assumptions are worked out.

2.3.1 *Linear superposition*

We may distinguish two kinds of mutual interaction between fibres which violate the linearity that is assumed in Assumption 3.1. An *active interaction* appears when the membrane activity of the fibre under consideration is significantly influenced by the activity of neighbouring fibres through their extracellular fields. Esplin (1962) could not find such influence in cat sural nerve in situ. The studies of Clark and Plonsey (1968, 1970) on nerve fibre interaction deal with unmyelinated fibres of radii 40 and 60 μm . With our geometry their results seem to confirm Assumption 3.1 because the extracellular field becomes only a very small fraction of the intracellular

field during activity. Our simulations of intrafascicular compound potentials, which resulted in potentials which never exceeded 100 μ V, also confirm that active interference can be neglected.

As the surrounding fibres are supposed to form a part of the passive environment for the fibre under consideration their activity should also not imply a *passive interaction* of the extracellular field in terms of changing conductivities in the outer region (Fig. 2.4). The membrane properties in the active state are different from those in the passive state which could change for instance the measure of anisotropy we have introduced in Sect. 2.6. The insulating sheets around fascicles and the nerve trunk form another important part of the passive environment for each fibre. Their electrical properties are not variable, which reduces the variability in the conductivities of the nerve trunk as a whole. Since quantifying data are lacking we will not go into this further.

Using the notations of the previous section we write the compound action potential as:

$$\phi_{CAP}(t) = \sum_{i=1}^N \phi_e^T(\rho_i, t-t_i, a_i) \quad (31)$$

where ϕ_{CAP} represents the compound action potential and ϕ_e^T the SFAP of an active fibre with radius a_i , arriving at time t_i and observed at a radial distance ρ_i , N fibres are supposed to be activated. It will be recalled that as a consequence of the Assumptions 2.2 and 2.6 differences in observation distances are not introduced ($\rho_i = \rho$; $i = 1, 2, \dots, N$).

2.3.2 Aspects of stimulation

At a rather high level of stimulation Buchthal and Rosenfalck (1966) found a shift in arrival time of the first positive peak in the CAP when the stimulation level was further increased. This time shift corresponded with a shift in the point of stimulation of about 5 mm for the fastest fibres. As these fastest fibres are expected to have the lowest threshold, 5 mm can be considered a 'worst case'. For a distance finger-wrist of about 15 cm this means an error in the estimation of the distance between stimulating and recording electrode of less than 3%. The duration of the stimulation pulse can be made rather short (≈ 0.1 ms), which also results in a distance error of a few percents at most.

2.3.3 Fibre radius versus propagation velocity

Assumption 3.3 can be expressed mathematically:

$$U = 2a_i C \quad (32)$$

A great deal of theoretical and experimental effort has been put into the investigation of this relationship. The determination of the fibre radius, the justification of the linear relationship and the assessment of the constant C have been topics of discussion (e.g. Gasser and Erlanger 1927, Hursh 1939, Rushton 1951, Buchthal and Rosenfalck 1966, Goldman and Albus 1968, BeMent and Olson 1977). We will return to this subject in the discussion (see also chapter 3).

Combination of (32) and (31) leads to:

$$\phi_{\text{CAP}}(t) = \sum_{i=1}^N \phi_e^T(\rho, t-t_i, a_i) \quad (33)$$

where

$$t_i = z/2a_i C \quad (34)$$

with z the distance between the point of stimulation and the point of observation. The moment of stimulation corresponds to $t = 0$ for simplicity. The term $z/2a_i C$ corresponds with the travelling time of the depolarization area.

2.3.4 Distribution of diameters and arrival times

Let us assume, by way of example, that we want to simulate the CAP of a human sural nerve on the basis of N activated single fibres. An approximation of the probability density function (PDF) of the fibre diameters in such a nerve should then be available.

In order to obtain this function we could for instance collect many sural nerves and determine an average diameter histogram with very small bin width which then would be an approximation of the wanted PDF. The actual method we used (Subsect. 2.4.2) is different as will be explained later on. To the obtained PDF of fibre diameters belongs a corresponding PDF of arrival times which can be calculated by using (34). We will call this PDF of the population of arrival times: $f_a(t)$. An example is shown in Fig. 2.6a.

As stated N fibres are supposed to be activated, each with a corresponding arrival time. A set of possible arrival times after stimulation of the nerve can be obtained by taking a random sample of size N from the PDF $f_a(t)$. The result of such a procedure is shown in Fig. 2.6b and c for $N = 500$ and 5000 respectively and using the PDF of Fig. 2.6a. It is important to note that the resolution of these presentations is not any more limited by the bin width of the original diameter histogram but only by the stepwidth which we used in the time domain (0.04 ms), i.e. arrival times in a time interval of 0.04 ms are taken together.

It can be shown (Papoulis 1965) that the occurrence of arrival times as described above forms a nonstationary Poisson point process $\underline{X}(t)$ with mean:

$$M(t) = E\{\underline{X}(t)\} = Nf_a(t) \quad (35)$$

and autocorrelation function:

$$R(t_1, t_2) = E\{\underline{X}(t_1) \cdot \underline{X}(t_2)\} = N^2 f_a(t_1) f_a(t_2) + Nf_a(t_1) \delta(t_1 - t_2) \quad (36)$$

where $\delta(t)$ is the normal Delta or impulse function. The last term of (36) represents the auto covariance expression of white noise. Equations (35) and (36) suggest that the process $\underline{X}(t)$ can also be written as a sum of two functions of time

$$\underline{X}(t) = M(t) + \underline{W}(t) \quad (37)$$

where $\underline{W}(t)$ is a non stationary white noise process with zero mean and variance:

$$\text{Var}\{\underline{W}(t)\} = Nf_a(t) \quad (38)$$

Broman and Lindström (1974) have introduced a mean and a standard deviation in calculations on compound potentials for the related problem of calculating motor unit action potentials of muscles.

The summation of (33) can be replaced by a convolution of $\underline{X}(t)$ and the SFAPs belonging to each arrival time. Or using (37) and (35):

$$\phi_{\text{CAP}}(t) = \int_0^{\infty} Nf_a(\tau) \phi_e^T(\rho, t-\tau, a_\tau) d\tau + \int_0^{\infty} \underline{W}(\tau) \phi_e^T(\rho, t-\tau, a_\tau) d\tau \quad (39)$$

where $a_\tau = d/2C\tau$.

Note that in this convolution the variable τ not only appears in the term $t - \tau$ but also in a_τ .

Note further that:

$$E\{\phi_{CAP}(t)\} = N \int_0^\infty f_a(\tau) \phi_e^T(\rho, t-\tau, a_\tau) d\tau \quad (40).$$

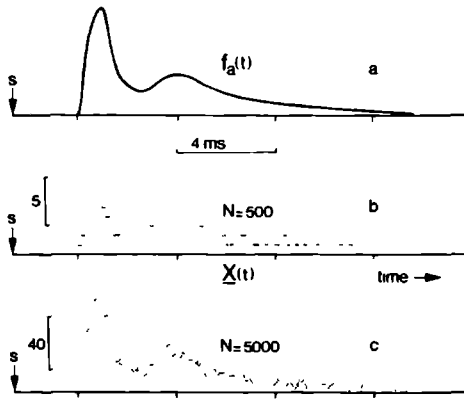


Fig. 2.6 a - c

a Probability density function (PDF) of arrival times based on the bimodal diameter histogram of Fig. 2.9. b and c

Random arrival time samples of size $N = 500$ and $N = 5000$ respectively, based on the PDF of a. S : stimulation moment.

(Travelled distance $z = 150$ mm. Conversion factor $C = 4.7 \text{ m.s}^{-1} \cdot \mu\text{m}^{-1}$)

This ends our theoretical evaluation because with (21), (29), (30) and (39) we are in the position to simulate CAPs once the physical parameters of the nerve and the SFAPs are known.

CAPs were simulated by generating $\underline{X}(t)$'s, which were based on diameter histograms found in the literature (Buchthal et al. 1975). Similar simulations of motor unit potentials of muscles have been made by Boyd et al. (1978) and Griep et al. (1978).

2.4 DISCUSSION

The theoretical framework of the foregoing sections constitutes the solution of the forward problem in CAP reconstructions. Next the appropriate choices on all the variables that arise have to be made. The sensitivity of the model in connection with the accuracy of its parameters is discussed in four subsections.

2.4.1 The intracellular fibre potential

The origin of the potential field, that we called CAP, can be found in the active processes at the nerve fibre membranes. Information about shape and amplitude of the intracellular fibre potential $\phi_1^T(t)$ forms the basis of this model. The question of how accurately $\phi_1^T(t)$ must be known has been solved mostly for the homogeneous extracellular medium (Rosenfalck 1969, Plonsey 1974, 1977). An important conclusion is that for homogeneous media the extracellular potential field can be described adequately on the basis of a triangular form of $\phi_1^T(t)$ when the observation distance is not too small. Such a triangular form corresponds with the so-called tripole concept for the transmembrane current $i_m^T(t)$. A description of $i_m^T(t)$ as a mathematical axial quadrupole on the other hand can only be used for very large values of the observation distance ρ . In terms of filter characteristics one could say that differences in the shape of $i_m^T(t) \sim d^2\phi_1^T(t)/dt^2$, that appear as high frequency components, do not give rise to differences in $\phi_e^T(\rho, t, a)$ when they are suppressed sufficiently by the filter function $H_v(\omega/U; \dots)$ as can be seen from (21).

In the *homogeneous* case the suppression of high frequency components in $i_m^T(t)$ is only influenced by the observation distance and the propagation velocity. This is illustrated in Fig. 2.7a and b where the filter function $H_1(\omega/U; \rho; a)$ is plotted in dashed lines.

In the *inhomogeneous* and eventually anisotropic cases the high frequency components are suppressed considerably as compared to the homogeneous case. In the configurations illustrated in Fig. 2.7a and b (solid lines), the lower limiting value for ρ , beyond which the tripole model (and likewise the mathematical quadrupole model) is accurate will therefore be accordingly lower. This conclusion is illustrated in Fig. 2.8. Part a of this figure shows an intracellular potential partly based on measurements reported by Paintal (1966) on mammalian nerve fibres, i.e. a monophasic shape with a duration of about 0.5 ms and an amplitude of 100 mV (solid line). The two previously mentioned approximations of this intracellular potential are also plotted. The resulting SFAPs for two observation distances (1.5 and 20 mm respectively) are shown in Fig. 2.8b and c for the homogeneous and isotropic case. Fig. 2.8d and e show SFAPs for an inhomogeneous configuration corresponding to Fig. 2.7a ④, observed at the same two distances. Note that in the case of Fig. 2.8d the tripole already yields a satisfactory approximation of the true SFAP. Volume conduction phenomena are often ex-

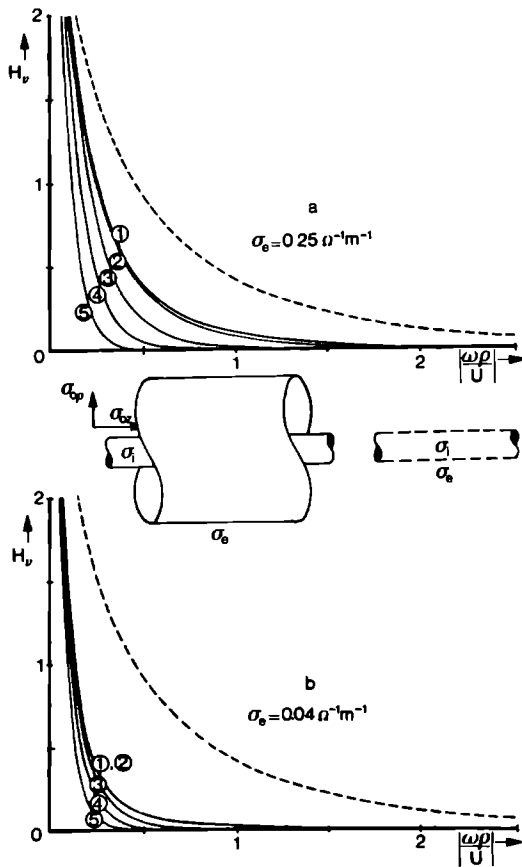


Fig. 2.7 a and b
 Various volume conduction filters H_1 (---) and H_2 (—), corresponding with Eqs. (16) and (29). Two external conductivities $\sigma_e = 0.25$ and $\sigma_e = 0.04 \Omega^{-1} \cdot m^{-1}$ are compared (a and b, solid lines). The result is different although the same configurations inside the trunk are assumed: $\sigma_{oz} = 5 \Omega^{-1} \cdot m^{-1}$; $\sigma_{op} = 5, 1, 0.1, 0.03$ and $0.01 \Omega^{-1} \cdot m^{-1}$ for the cases ①, ②, ③, ④, and ⑤ respectively. (Nerve trunk radius $b = 1$ mm. Fibre radius $a = 10 \mu m$. Observation distance $\rho = 1.5$ mm.). Both parts of the figure are compared to the homogeneous, isotropic case (dashed lines)

pressed with the help of a mathematical multipole expansion of the sources. It is well known that in homogeneous media the field at a very large distance from the sources is merely determined by the lowest order pole of the source. In our inhomogeneous configuration this will remain true as only an extra low-pass filtering is introduced. It can be further shown that the dipole moment of the source density $i_m^S(z)$ is zero as long as $\phi_i^S(z)$ returns to its resting value, which can be assumed for physiological reasons. This implies that at large distances the field is mainly determined by the quadrupole strength of the source. It can be proven easily (e.g. Burger 1968) that this strength is proportional to the length of $\phi_i^S(z)$. So it can be concluded that

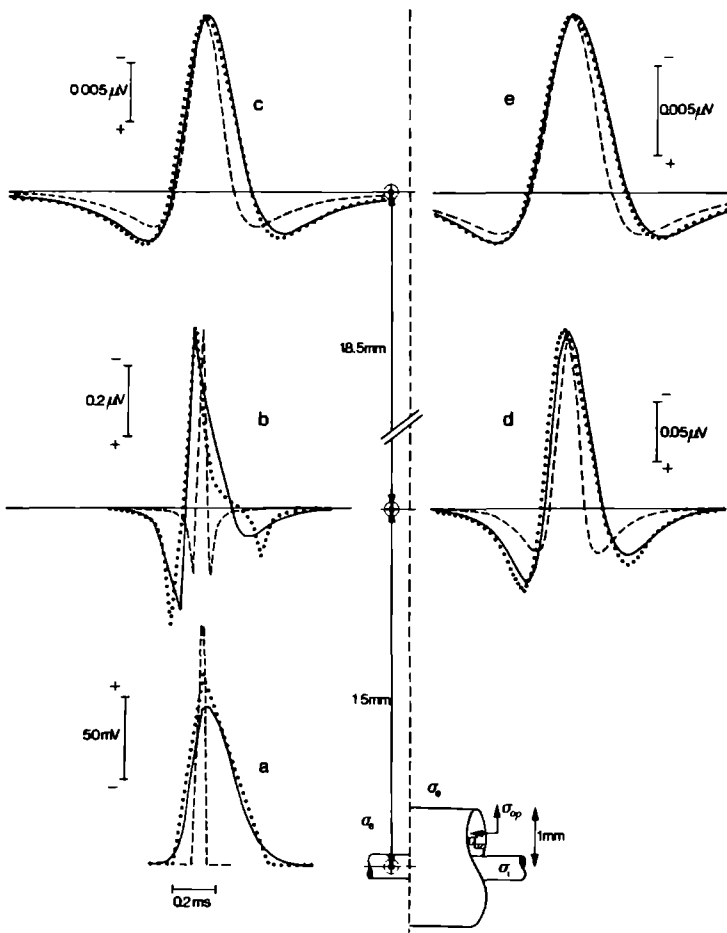


Fig. 2.8 a - e

a Intracellular single fibre action potential, based on experimental data (Paintal 1966, solid line), and two approximations which result in a tripole (dotted line) and a mathematical axial quadrupole (dashed line) when the transmembrane current function is considered. b and c These curves are calculations of extracellular single fibre potentials for a homogeneous and isotropic extracellular medium. Two observation distances are chosen: $\rho = 1.5 \text{ mm}$ for b and $\rho = 20 \text{ mm}$ for c. The solid, dotted and dashed curves are based on equally represented intracellular potentials ($\sigma_e = 0.25 \Omega^{-1} \cdot \text{m}^{-1}$). d and e The same as b and c except for the extracellular medium which is inhomogeneous and partly anisotropic ($\sigma_{o0} = 0.03 \Omega^{-1} \cdot \text{m}^{-1}$ and $\sigma_{oz} = 5 \Omega^{-1} \cdot \text{m}^{-1}$). For larger observation distances and/or increasing inhomogeneity the shapes become more similar. Note the different amplitude calibrations. ($\sigma_i = 1 \Omega^{-1} \cdot \text{m}^{-1}$; $U = 100 \text{ m} \cdot \text{s}^{-1}$; $a = 10 \text{ } \mu\text{m}$; $b = 1 \text{ mm}$)

for large observation distances an increase in duration of $\phi_1^T(t)$ essentially does affect the SFAP-*amplitude* and not its *shape*. Alternatively can be said that the SFAP in these cases is merely determined by the invariant volume conduction phenomenon and not anymore by the intracellular potential shape.

2.4.2 The diameter distribution

A smoothed version of the fibre diameter histogram, which applies to a particular nerve, can be used as an approximation of the probability density function of the fibre diameters. In view of the total number of fibres in human sensory nerve (500-15000) a binwidth corresponding to 1 μm diameter resolution seems sufficiently accurate. An extensive investigation of diameter histograms and their interpretation can be found in Olson (1973). For the smoothing procedure we used interpolation techniques via the frequency domain (Gold and Rader 1969). An example of the result of this procedure is shown in Fig. 2.9 for the diameter histogram of a human sural nerve (Buchthal et al. 1975).

2.4.3 Conductivity Parameters

Figure 2.10 shows the result of CAP simulations using experimental data from the human sural nerve (see also Fig. 2.9). The constant C (cf. (32)) was set at $4.7 \text{ m.s}^{-1} \cdot \mu\text{m}^{-1}$ as suggested by Buchthal et al. (1975). This value was based on the arrival time corresponding with the fastest fibres in the nerve (see also Subsect. 2.4.4). The distance z between the point of stimulation and the point of registration on the nerve was chosen 150 mm, a usual value in clinical investigations of the sural nerve. In the nerve under con-

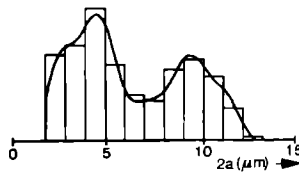


Fig. 2.9

PDF of fibre diameters in a nerve (solid line), obtained by smoothing the fibre diameter histogram. Number of fibres $N = 6600$. The histogram for a normal sural nerve was taken from Buchthal et al. (1975)

sideration 6600 fibres were counted, this being the number that we supposed to be activated ($N = 6600$). A rather small observation distance to the trunk was assumed: $\rho_1 = 1.5 \text{ mm}^1$. We took $\sigma_i = 1 \Omega^{-1} \cdot \text{m}^{-1}$, a value found in other studies on nerve fibre activity (Clark and Plonsey 1968, Moore et al. 1978). In Fig. 2.10a the result of a CAP simulation is shown for the homogeneous and isotropic conditions using filter function $H_1(\omega/U; \rho; a)$.

(We will follow physiological and clinical practice and draw negative potential values in the SFAP upwards).

The dotted line in the same figure represents the expected value of the CAP as it is defined in (40). It is clear that the stochastic character of the arrival time process introduces high frequency components in the CAP, resulting in an unexpected shape for a registration outside the trunk. Although intrafascicularly measured CAPs do show similarities with the shape in Fig. 2.10a (e.g. Burke et al. 1975), extracellularly measured CAPs normally do not show such abundant high frequency components, independent of whether they have been obtained by averaging or not. One might argue that a jitter in arrival times could be held to be responsible for a smooth waveform of averaged CAPs but the results of averaged intrafascicular CAP-registrations contradict the existence of such a time jitter. However, by virtue of Assumption 2.6 we have another physiological basis for the existence of a smoothing effect.

Generally speaking smoothing (low-pass filtering) is more pronounced because of two aspects, i.e. when current set free at a membrane surface:

- 1) flows more easily in the axial than in the radial direction (anisotropy),
- 2) encounters a less conducting medium outside the trunk.

In Fig. 2.7 two different external media were compared with conductivity $\sigma_e = 0.25$ and $0.04 \Omega^{-1} \cdot \text{m}^{-1}$ respectively. These values approximate the conductivity of muscle and fat tissue (Geddes and Baker 1967). The conductivity in the nerve trunk in the axial direction was chosen in accordance with an approximation made by Clark and Plonsey (1968) for the interstitial medium in the crayfish central nerve: $\sigma_{oz} = 5 \Omega^{-1} \cdot \text{m}^{-1}$. The other parameter values are given in the legend of Fig. 2.7. The differences between the curves ① to ⑤ in each of the Figs. 2.7a and b are explained by the first aspect mentioned. The differences between corresponding curves in Figs. 2.7a and b

¹ In order to simplify the interpretation of the results we will neglect the influence of the skin in this discussion ($\rho_2 = \infty$).

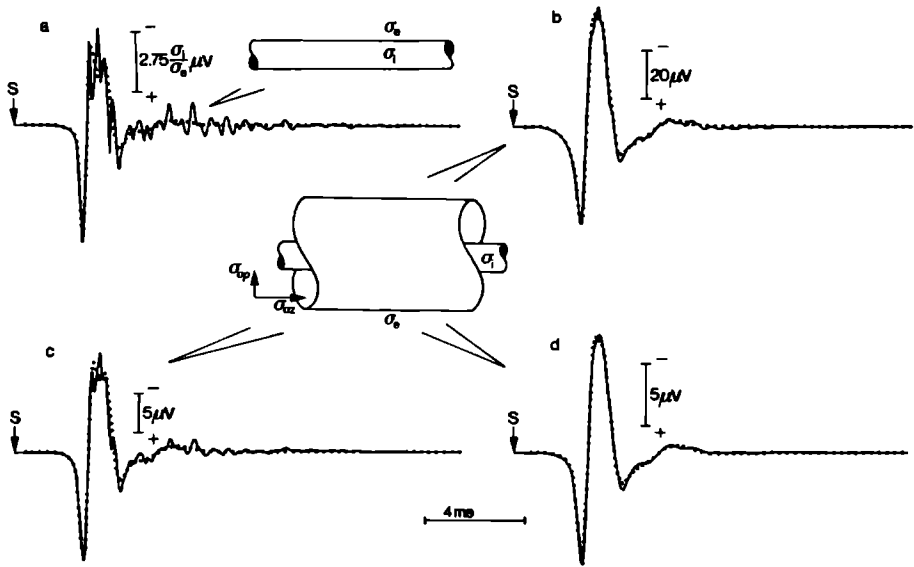


Fig. 2.10 a - d

Simulations of compound action potentials showing the influence of the three extracellular conductivities (see insets). a A homogeneous, isotropic extracellular medium (see Fig. 2.7, dashed lines). b An isotropic trunk with high conductivity $\sigma_{op} = \sigma_{oz} = 5 \Omega^{-1} \cdot m^{-1}$. The external conductivity is very low: $\sigma_e = 0.04 \Omega^{-1} \cdot m^{-1}$. c As b with a better external conductivity: $\sigma_e = 0.25 \Omega^{-1} \cdot m^{-1}$. d A highly anisotropic trunk $\sigma_{op} = 0.03$; $\sigma_{oz} = 5 \Omega^{-1} \cdot m^{-1}$. The external conductivity as in c. The dotted lines show the expected values of the CAP's based on the same PDF from which the 6600 fibres were chosen (see Fig. 2.6). S: stimulation moment. Note the different amplitude calibrations. ($\rho = 1.5 \text{ mm}$; $z = 150 \text{ mm}$; $C = 4.7 \text{ m} \cdot \text{s}^{-1} \cdot \mu\text{m}^{-1}$; $\sigma_i = 1 \Omega^{-1} \cdot m^{-1}$; $b = 1 \text{ mm}$)

can be understood with the second aspect.

Figures 2.10b and c show CAP simulations using the two inhomogeneous but isotropic cases corresponding to the curves ① of Fig. 2.7b and 2.7a respectively ($\sigma_{op} = \sigma_{oz} = 5\Omega^{-1} \cdot m^{-1}$). For anatomical reasons a conductivity in the radial direction inside the nerve trunk which is of the same order of magnitude as the conductivity of fat tissue, seems reasonable. Therefore Fig. 2.10d shows a simulation result for $\sigma_{op} = 0.03$ and $\sigma_e = 0.25\Omega^{-1} \cdot m^{-1}$ (cf. Fig. 2.7a ④).

Comparison of Fig. 2.10a, b, c and d shows:

- 1) Except for the case of Fig. 2.10d the influence of the stochastic properties of the arrival process is clearly visible. In the dotted lines this influence is excluded as already stated.
- 2) The first positive peak in the calculated CAPs is hardly affected by this statistical variation in any of the four cases.
- 3) The first positive-negative deflection is the steepest edge in a CAP. Its steepness is almost the same in all four cases and is determined by the rising phase of the arrival time - PDF (see Fig. 2.6a).
- 4) The volume conduction filters corresponding with the cases a - d do not only differ in low-pass cut-off frequency. This is for instance obvious by comparison of the Figs. 2.10c and d. While the first positive deflection of Fig. 2.10d is almost as steep as that of Fig. 2.10c, on the other hand high frequency components are much more suppressed in the former figure.

2.4.4 Propagation velocity and fibre diameter and wave shape

The propagation velocity of the SFAP is the most crucial property in the appearance of the CAP. This is most obvious in the influence of the propagation velocity on the *arrival time*. The influence of U on the *shape* of the SFAP can be observed, for instance, when only a few fibres are activated (Fig. 2.11). This figure shows that the differences in shape and amplitude of the SFAPs as a function of their arrival times can only be recognized easily when not more than ten or twenty fibres are activated. The contribution of each SFAP to a CAP consisting of several hundreds or even thousands of fibre potentials cannot be easily recognized. The dispersion in arrival times between different fibres can be conceived of as the most important indicator of the distribution of propagation velocities and therefore also of fibre diameters.

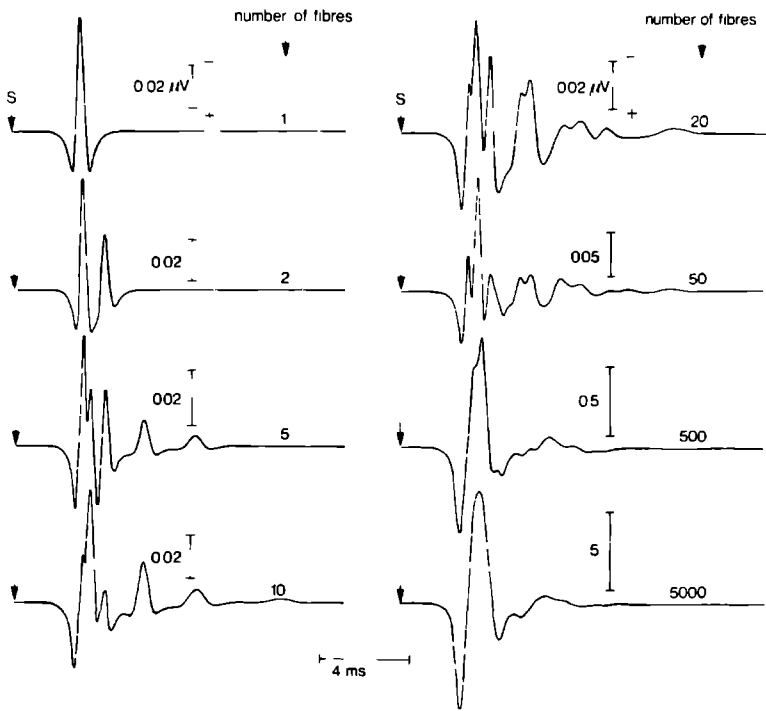


Fig. 2.11

Illustrative example to show the influence of the number of fibre action potentials on the shape and the amplitude of a compound action potential. Except for the total number of fibres, the parameters of Fig. 2.10d are used. Note the changing amplitude scale

An accurate choice of the conversion factor C is often pursued in modelling CAPs. Correlation of the maximum propagation velocity with the diameters of the largest fibres (e.g. Hursh 1939), is an obvious method. The highest value for U is in this case derived from the appearance of the first positive maximum. Our simulations confirm the reliability of this method. By comparing an arrival time distribution (Fig. 2.6) with the CAPs based on that distribution (Fig. 2.10), we see a rather good agreement between the first maximum and the arrival time of the fastest fibres.

When measured versions of both the diameter histogram and a CAP of the same nerve were available we could approximate C by simulating CAPs based on the diameter histogram for a range of C values. The calculated CAP that gives the best fit to the measured one determines an optimal value for C in which *all* the fibres are incorporated.

Equation (39) poses a problem as to what extent this equation can be replaced by a *simple* convolution integral which no longer depends on a_τ via the parameter list of ϕ_e^T . Usually a power of the diameter is introduced which only determines the amplitude of ϕ_e^T . Such an approximation can be written:

$$\hat{\phi}_{CAP}(t) = p \int_0^\infty \left(\frac{a_\tau}{a_\eta} \right)^q \underline{\chi}(\tau) \phi_e^T(\rho, t-\tau, a_\eta) d\tau \quad (41)$$

where p and q are arbitrary constants and a_η is some (intermediate) fibre diameter. The SFAP-shape belonging to that diameter is chosen as a standard wave shape. In order to investigate the difference between the two predictions of the compound action potential formulated in (39) and (41) we could first of all minimize a normalized mean square error, e.g. defined as:

$$\epsilon = \left\{ \int_0^\infty (\phi_{CAP}(t) - \hat{\phi}_{CAP}(t))^2 dt \right\} \cdot \left\{ \int_0^\infty \phi_{CAP}^2(t) dt \right\}^{-1} \quad (42)$$

by searching for an optimum set (p,q).

For the case of Fig. 2.10d with $a_\eta = 5.32 \mu\text{m}$ ($U_\eta = 50 \text{ m.s}^{-1}$) we reached very low ϵ -values within a wide range of q-values (Table 2.1). The optimum for q is found to be around 1.2. The flatness of the optimum indicates a relative insensitivity of the model to precise diameter and arrival time distributions. This should be kept in mind when discussing the possibilities of solving the "inverse problem", i.e. the construction of the fibre diameter distribution on the basis of a measured compound action potential. Such constructions could for instance be based on (41) using a deconvolution procedure.

TABLE 2.1

Conversion factor C	intermediate radius a_n (μm)	U_n (m.s^{-1})	equation (41)		equation (42)
			p	q	ϵ
3.0	5.00	30	0.65	1.3	0.010
4.7	5.32	50	0.68	0.5*	0.021
4.7	5.32	50	0.68	1.2	0.007
4.7	5.32	50	0.66	1.9*	0.020
6.0	5.00	60	0.64	1.1	0.007

* non-optimal q-values

2.5 CONCLUSIONS

This chapter primary deals with the problem of the reconstruction of compound action potentials of whole nerves in situ. This is more or less in contrast with the reversed problem in which, given the compound action potential, the range of conduction velocities of contributing fibres is estimated, ultimately resulting in a diameter histogram of active fibres. In analogy to the terminology in use for electrocardiographical studies it is proposed to adopt the term *forward* problem for reconstruction problems and *inverse* problem for the reversed situation of parameter estimation.

Our study of the forward problem is mainly based on an elaboration of volume conduction properties of the surrounding tissues and on the statistics of arrival times of different single fibre action potentials. Usually the extracellular medium has been assumed to be homogeneous and isotropic. In this chapter it is shown that this is an oversimplification leading to simulated compound action potentials much more notched than those encountered in practice. Therefore, as a first new aspect in the presented model, both an inhomogeneity and an anisotropy are introduced, in accordance with the morphological and anatomical structures of nerves *in situ*. The inhomogeneity represents the nerve trunk as a whole, a configuration with conducting properties that differ from those of the rest of the surrounding medium. Moreover the nerve trunk apparently acts as an anisotropic electrical medium where the conductivity in the axial direction is much larger than in the radial one. Although these features significantly increase the complexity of

the model one could, in order to simplify, interpret the resulting effect as a virtual enlargement of the observation distance. High frequency components of participating single fibre action potentials are now much more suppressed, which leads to simulated wave forms that closely resemble compound action potentials that can actually be measured. The second new aspect in the present model is the use of statistical concepts in the superimposition of individual nerve fibre activity. The method, essentially based on smoothing of fibre diameter histograms and the construction of a random sample of arrival times, enables the simulation of accurate compound action potential wave shapes and amplitudes even when the diameter histogram is known with a relatively poor resolution. Once the model rests on a sound theoretical basis it becomes a promising tool in the study of the influence of specific parameters on compound action potentials such as temperature (chapter 4), refractoriness (chapter 5) and block of fibres both under normal *and* pathological conditions.

In physical terms the model analyses the potential field of a single active nerve fibre in the spatial frequency domain and considers the compound potential as a linear superimposition process with Poisson-like statistical properties. Assuming cylinder symmetry, it has been shown that even for complex configurations the external field around the nerve trunk can be described in the spatial frequency domain by a low-pass filter acting upon the second derivative of the intracellular potential. By introducing an anisotropy and an inhomogeneity not only the cut-off frequency of the filter becomes lower, but also the roll-off becomes steeper. As a result, high frequency components are significantly more suppressed which also implies that approximation of the transmembrane current by a tripole model is accurate even for small observation distances.

In the second part of the model it has been demonstrated that the compound action potential can be described by a convolution of the volume conducted single fibre action potential and a nonstationary Poisson process derived from the probability density function of arrival times. The latter function in turn can be determined by using smoothed diameter histograms. The convolution is not a simple one since the single fibre potential is not uniform in shape for all fibres, but is still dependent on the fibre diameter in a rather complex way.

However, by the simplifying assumption that the volume conducted single fibre potential is uniform for all fibres with only its amplitude depending on fibre diameter, the former convolution can be reduced to a simple one with

good accuracy. This implies that theoretically the inverse problem, i.e. estimation of the range of conduction velocities from measured compound action potentials, can be solved by deconvolution.

The analysis of specific parameters that influence wave shape and amplitude of the compound action potential is the subject of the chapters 3, 4 and 5.

Acknowledgement

We wish to thank A. Heringa for many stimulating discussions on volume conduction theory.

2.6 REFERENCES

- Abramowitz, M. and Stegun, I.A. Handbook of mathematical functions. Dover, New York, 1972.
- Barker, A.T. Determination of the distribution of conduction velocities in human nerve trunks. (Ph.D. Thesis). Univ. of Sheffield 1976.
- BeMent, S.L. and Olson, W.H. Quantitative studies of sequential peripheral nerve fiber diameter histograms and biophysical implications. *Exp. Neurol.*, 1977, 57: 828-848.
- Boyd, D.C., Lawrence, P.D. and Bratty, P.J.A. On modeling the single motor unit action potential. *IEEE Trans. biomed. Eng.*, 1978, 25: 236-242.
- Broman, H. and Lindström, L. A model describing the power spectrum of myoelectric signals, Part II: Motor unit signal. Chalmers Univ. of Technology, Göteborg, 1974.
- Buchthal, F. and Rosenfalck, A. Evoked action potentials and conduction velocity in human sensory nerves. *Brain Res.*, 1966, 3: 1-122.
- Buchthal, F., Rosenfalck, A. and Behse, F. Sensory potentials of normal and diseased nerve. In: P.J. Dyck, P.K. Thomas and E.H. Lambert (Eds.), *Peripheral neuropathy*, Vol. 1. Saunders, Philadelphia, 1975: 442-464.
- Burger, H.C. Heart and vector. Philips Technical Library, Eindhoven, 1968.
- Burke, D., Mackenzie, R.A., Skuse, N.F. and Lethlean, A.K. Cutaneous afferent activity in median and radial nerve fascicles: A micro-electrode study. *J. Neurol. Neurosurg. Psychiatry*, 1975, 38: 855-864.
- Clark, J.W. and Plonsey, R. A mathematical evaluation of the core conductor model. *Biophys. J.*, 1966, 6: 95-112.

- Clark, J.W. and Plonsey, R. The extracellular potential field of the single active nerve fiber in a volume conductor. *Biophys. J.*, 1968, 8: 842-864.
- Clark, J.W. and Plonsey, R. A mathematical study of nerve fiber interaction. *Biophys. J.*, 1970, 10: 937-957.
- Dawson, G.D. The relative excitability and conduction velocity of sensory and motor nerve fibres in man. *J. Physiol.*, 1956, 131: 436-451.
- Esplin, D.W. Independence of conduction velocity among myelinated fibres in cat nerve. *J. Neurophysiol.*, 1962, 25: 805-811.
- Gasser, H.S. and Erlanger, J. The role played by the sizes of the constituent fibres of a nerve trunk in determining the shape of its action potential wave. *Am. J. Physiol.*, 1927, 80: 522-547.
- Geddes, L.A. and Baker, L.E. The specific resistance of biological material: A compendium of data for the biomedical engineer and physiologist. *Med. Biol. Engng*, 1967, 5: 271-293.
- Gold, B. and Rader, C.M. *Digital processing of signals*. McGraw-Hill, New York, 1969.
- Goldman, L. and Albus, J.S. Computation of impulse conduction in myelinated fibres; theoretical basis of the velocity-diameter relation. *Biophys. J.*, 1968, 8: 596-607.
- Griep, P.A.M., Boon, K.L. and Stegeman, D.F. A study of the motor unit action potential by means of computer simulation. *Biol. Cybernetics*, 1978, 30: 221-230.
- Hursh, J.B. Conduction velocity and diameter of nerve fibers. *Amer. J. Physiol.*, 1939, 127: 131-139.
- Jackson, J.D. *Classical electrodynamics*. Wiley & Sons, New York, London, Sydney, 1962.
- Lorente de N6, R. A study of nerve physiology. *Studies from the Rockefeller Institute for Medical Research*, 1947, 132: 384-482.
- Lowitzsch, K., Hopf, H.C. and Galland, J. Changes of sensory conduction velocity and refractory periods with decreasing tissue temperature in man. *J. Neurol.*, 1977, 216: 181-188.
- Ludin, H.P. and Beyeler, F. Temperature dependence of normal sensory nerve action potentials. *J. Neurol.*, 1977, 216: 173-180.
- Moore, J.W., Joyner, R.W., Brill, M.H., Waxman, S.G. and Najar-Ioa, M. Simulations of conduction in myelinated fibers: Relative sensitivity to changes in nodal and internodal parameters. *Biophys. J.*, 1978, 21: 147-160.

- Olson, W.H. Peripheral nerve compound action potentials and fiber diameter histograms (Ph.D. dissertation). Univ. of Michigan, Ann Arbor, Mich., 1973.
- Paintal, A.S. The influence of diameter of medullated nerve fibres of cats on the rising and falling phases of the spike and its recovery. *J. Physiol.*, 1966, 184: 791-811.
- Papoulis, A. Probability, random variables, and stochastic processes. McGraw-Hill, Tokyo, 1965.
- Patlak, C.S. Potential and current distribution in nerve: The effect of the nerve sheath, the number of fibres and the frequency of alternating current stimulation. *Bull. Math. Biophys.*, 1955, 17: 287-307.
- Plonsey, R. The biophysical basis for electrocardiography. *CRC crit. Rev. Bioeng.*, 1971, 1: 1-49.
- Plonsey, R. The active fiber in a volume conductor. *IEEE Trans. Biomed. Eng.*, 1974, 21: 371-381.
- Plonsey, R. Action potential sources and their volume conductor fields. *Proc. IEEE*, 1977, 65: 601-611.
- Rosenfalck, P. Intra- and Extracellular potential fields of active nerve and muscle fibres. *Acta Physiol. Scand.*, 1969, Suppl. 321.
- Rushton, W.A.H. A theory of the effects of fibre size in medullated nerve. *J. Physiol.*, 1951, 115: 101-122.
- Tackman, W. and Lehmann, H.J. Refractory period in human sensory nerves. *Eur. Neurol.*, 1974, 12: 277-292.
- Weerd, J.P.C. de, Notermans, S.L.H. and Vingerhoets, H.M. Measurement of the refractory period in human sensory nerve fibres (Abstract). *Electroenceph. clin. Neurophysiol.*, 1979, 47: 19p.

PART III

MODEL RECONSTRUCTIONS OF EXPERIMENTAL DATA FROM NORMAL HUMAN SURAL NERVES

Modelling compound action potentials of peripheral
nerves *in situ*.

(submitted for publication to *Electroenceph. clin. Neurophysiol.*, 1981)

- I. Model description; evidence for a nonlinear relation between fibre diameter and velocity
D.F. Stegeman and J.P.C. de Weerd (chapter 3)
- II. A study of the influence of temperature ¹
D.F. Stegeman and J.P.C. de Weerd (chapter 4)
- III. Nerve propagation in the refractory period
D.F. Stegeman, J.P.C. de Weerd and S.L.H. Notermans (chapter 5)

¹ presented in preliminary form at the 6th intern. congress of electromyography, Stockholm, 1979.

C H A P T E R 3
MODEL DESCRIPTION; THE RELATION BETWEEN
FIBRE DIAMETER AND VELOCITY

ABSTRACT

Compound sensory nerve action potentials of sural nerves of healthy volunteers have been measured at seven different distances between site of stimulation and site of recording. The results are used to adjust a model description for the generation of compound action potentials of nerves. A fairly good agreement between experiment and model is obtained when a weak nonlinear, S-shaped relation between external fibre diameter and propagation velocity of the single fibre action potentials is assumed. This result corresponds surprisingly well with findings in 'classical' reconstruction attempts reported in the literature.

3.1 GENERAL INTRODUCTION

The recording of peripheral nerve activity *in situ* is valuable as a routine investigation for diagnostic purposes. The measurement of whole nerve activity outside the nerve trunk after supramaximal electrical stimulation has become a standard tool in clinical electroneurophysiology (see Buchthal and Rosenfalck, 1966). It is not the only, nor is it the most advanced technique which has been developed. The method of microneurography can also be applied to human nerves without excision or exposure, yielding intrafascicular recordings of single nerve fibres (see Vallbo et al. 1979).

The 'whole nerve method' indeed has the disadvantage that the appearance of the fibre membrane activity is seriously hindered by the fact that extraneural recordings are made. For example, the activity of 'slower' fibres ($< 30 \text{ m.s}^{-1}$) is almost completely obscured, unless averages of several hundreds or even thousands of sweeps are made. Its advantage, however, is the relative comfort of the investigation and, what is also important, the fact that after electrical stimulation a simultaneous recording from a large group of activated nerve fibres is obtained.

The problem is to what extent do extraneurally obtained compound action potentials (CAPs) carry information about the underlying sources i.e. the activity of the fibres of various diameters that are activated by the stimulus? This chapter is a first approach to answering this question by using a model for (sensory) nerve CAP generation. The mathematical formulation was given in chapter 2. The model is, in our view, a rather precise and promising description of the actual geometry and the physiological processes that are involved. A correspondence between experimentally obtained CAPs from normal nerves and model results (for which we will use the term 'reconstructions') is not self-evident, as may be concluded for instance from the reconstructions made by Buchthal and Rosenfalck (1966, 1971). Their reconstructions are not very convincing, in particular with respect to shape correspondence. The well known reconstructions by Gasser and Grundfest (1939) of monopolar CAPs, measured on *excised* animal nerves, however, are in good agreement with experimental data. Better understanding of normal nerve CAP generation *in situ* is important for a better analysis of compound action potential wave shapes under pathological conditions (Buchthal et al. 1975, Behse and Buchthal 1978, Tackmann et al. 1976). We show that our model (Sect. 3.2 and 3.3) initially fails to predict some well defined experimental results too (Sect. 3.4 to 3.6). After thorough examination of the discrepancies (Sect. 3.7), strong evidence

is obtained that the relation between fibre diameter and propagation velocity is not strictly linear (Sect. 3.8). This and other findings are evaluated and finally the perspectives of accurate model computations in clinical electro-neurography are given (Sect. 3.9).

3.2 INTRODUCTION TO THE MODEL

The *in situ* condition has been stressed in the title of this thesis because of its importance for CAP shapes. Normally bi- or tri-phasic CAPs are observed. Intracellular potential changes (the sources of activity) on the contrary are usually monophasic with a duration of less than 1 ms and a positive amplitude of about 100 mV (Tasaki and Frank 1955)¹. The occurrence of more phases in a compound action potential indicates the outward spread of ionic currents into the extracellular surroundings of the nerve. *In situ* recordings, in contrast to measurements on excised nerves, apparently require a model description in which these *volume conductor* effects are included. Such a description is complicated by inhomogeneities and anisotropies in the extracellular medium, which cannot be neglected (as is done for simplicity by Lorente de N6 (1947) and others) if precise reconstructions are to be achieved.

A simplified presentation of the nerve trunk and its surroundings as implemented in the model is given in Fig. 3.1 (see Table 3.1(p60) for numerical values). The closest surroundings for each fibre are formed by the other fibres in the nerve and the connective tissue (Fig. 3.1 region I). The perineurium and the epineurium probably have the largest influence. These structures act as an electrical shielding around the nerve fibre and are summarized in the model as region I. One can interpret this region as the representation of the whole nerve trunk as a passive surrounding for each individual fibre. This trunk is embedded in a subcutaneous fat layer (Fig. 3.1 region II). The remainder of the limb is represented by muscle tissue (Fig. 3.1 region III). The two boundaries between regions II and III and the region II and the air (electrical insulation) are assumed to be perfectly flat².

¹ We should like to point out that the model presented here is based on findings on the single fibre level. The intracellular fibre activity is not explained in any way with this model.

² The method of images (Plonsey 1969, v. Oosterom 1978) can be applied as a repeated mirror effect caused by the boundaries air-fat and fat-muscle.

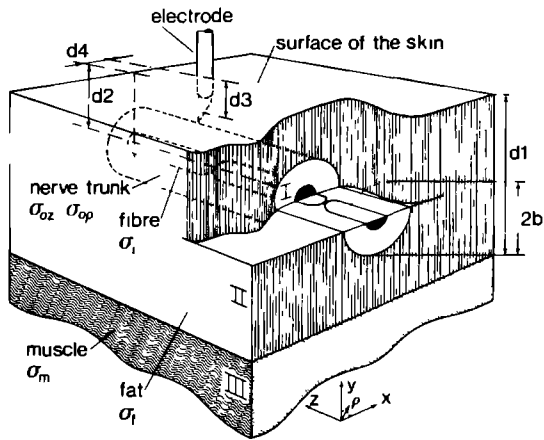


Fig. 3.1

Schematized presentation of the volume conductors around a nerve fibre as used in the model. The fibre is assumed to be localized in the centre of the nerve trunk (region I) for computational convenience. This trunk is embedded in a fat layer (region II). The layer is bounded on one side by the surface of the skin and on the other side by muscle tissue (region III). See table 3.1 for the numerical values. Note the anisotropy of the nerve trunk. In the model the leading off surface of the electrode is assumed to be infinitesimally small

This configuration and the numerical values are based on the human sural nerve, in which nerve the surrounding structures are relatively simple, compared for instance to the geometry of the structures around the arm nerves in man. It is assumed that a monopolar recording electrode with a point shaped leading-off surface is used. The effect of the simplifications concerning finite electrode dimensions (Griep et al. 1978) and curved boundaries are slight. The 'reconstructed' CAP appears as a summation of the activity of all constituent fibres (next section). Further mathematical and computational details can be found in chapter 2.

3.3 THE COMPOUND NERVE ACTION POTENTIAL

It appears that no interactions between myelinated fibres occur

(Esplin 1962). This means that the compound activity of a nerve can be conceived of as a *linear* summation of the activity of all constituent fibres. Therefore it is possible to treat each single fibre or small group of fibres separately. Each contribution can simply be added in order to obtain the final CAP.

Usually fibres of various calibres are present, as is reflected in a histogram of external fibre diameters. Such a histogram can be converted to a smooth curve that can be considered as an estimate of the distribution of fibre diameters (Fig. 3.2a). Assuming for the moment a linear relation between diameter and propagation velocity, the arrival times of the action potentials of the different fibres can easily be calculated when the propagated distance between site of stimulation and site of recording is known and a function describing the dispersion of arrival times is obtained (Fig. 3.2b). Each extracellular (extraneural) single fibre action potential is, with respect to its shape, latency and amplitude, determined by its intracellular single fibre action potential, its propagation velocity and by the configuration as sketched in Fig. 3.1.

The intracellular fibre action potential (spike) is modelled as a triangle with parameters t_{rise} , t_{fall} and A_i (see Fig. 3.2c). The same function was used for all fibres (Table 3.1), although Paintal (1966) pointed out that t_{rise} and t_{fall} increase with decreasing velocity. These modest changes appeared to be of minor importance in the model results and are therefore omitted. The three phases of an extracellular single fibre action potential are caused by two current sources and one current sink in the fibre membrane. Because of the simple triangular shape of the intracellular action potential in the model, the transmembrane current function is reduced to the so called 'tripole' (Fig. 3.2d) (Rosenfalck 1969)³. The volume conduction works on this transmembrane current tripole as a smoothing window (low pass filter) in which the propagation velocity also plays a part. That is, the lower the propagation velocity, the broader this window becomes (Fig. 3.2e). This causes a decrease in amplitude and an increase in duration of single fibre action potentials with decreasing velocity (Fig. 3.2f). In previously proposed reconstruction procedures and in solutions of the 'inverse problem' of the estimation of propagation velocity distributions (Barker et al. 1979,

³ The transmembrane current can be approximated as the second derivative of the intracellular action potential. This simplification is justified in chapter 2.

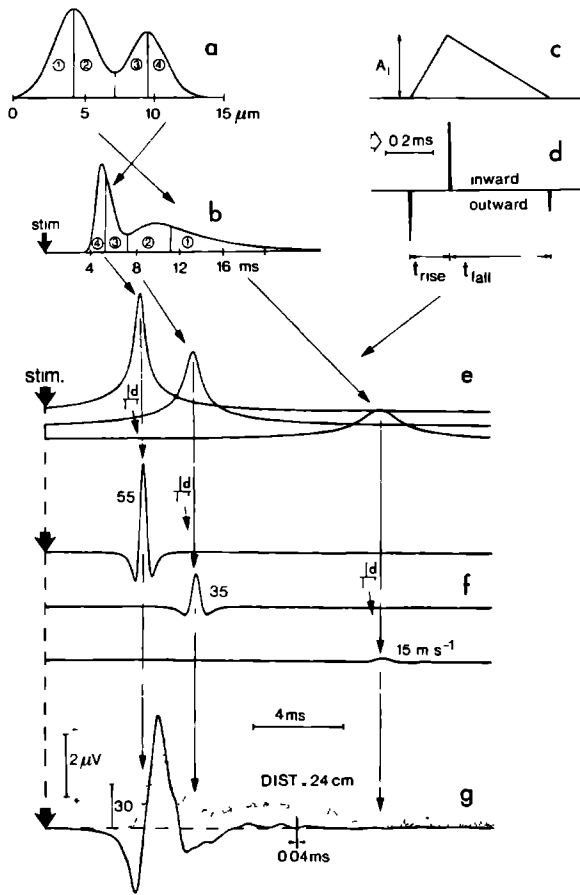


Fig. 3.2 a-g

Illustrative example to show the generation of a compound action potential by the model. A distribution of fibre diameters (a) is converted into a distribution of arrival times of the corresponding action potentials (b). For each propagation velocity a volume conduction 'window' is calculated (e). These windows are applied to the transmembrane current function (d), being the second derivative of an intracellular spike (c). The resulting extracellular single fibre action potentials are clearly diameter dependent both in shape and amplitude (f). A total number of 6600 fibres is assumed to be present. The arrival times of their action potentials, excited by the same stimulus, are indicated in g (dots). The CAP is the result of summation of all single fibre contributions (g, solid curve)

Cummins et al. 1979b) only an amplitude dependence of diameter was inserted in a rather arbitrary way, while the shapes were supposed to be equal for all fibres. For the solution of the inverse problem the aspects of duration and amplitude of the extracellular single fibre action potentials are of major interest (Cummins et al. 1979a, Kovacs et al. 1979). Therefore it is important that our model does not need any such simplifications with respect to these parameters which have not been experimentally verified so far because of the extremely low amplitude of single fibre activity (0.01 - 0.05 μ V).

An example of a simulated compound action potential (CAP) is shown in Fig. 3.2g, together with the dispersed arrival times (dots).

3.4 EXPERIMENTAL METHODS

Measurements were made on five healthy volunteers, aged 18 - 34, under carefully standardized conditions. The near-nerve electrode (teflon coated needle electrodes with a bared tip; Buchthal and Rosenfalck 1966) was placed 25 - 30 cm proximal to the heel. The indifferent electrode was placed at a transverse distance of at least 40 mm at the same level. Stimulation was done with surface electrodes at distances of 6, 9, 12, ..., 24 cm distal to the recording electrode (Fig. 3.3). It was decided to vary the position of

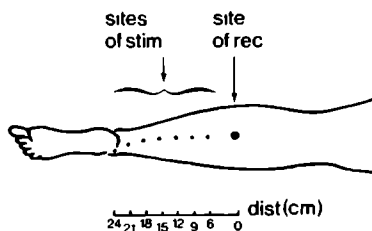


Fig. 3.3
Stimulation and recording sites
in the experimental set up
(sural nerve)

the stimulating rather than of the recording electrode in order to minimize the influences of factors other than the propagated distance alone. An electromyograph (Disa 1500 series, bandwidth 10 Hz - 10 kHz) with a digital interface to a DEC PDP 11/34 computer was used. The sample rate was 25 kHz. Each CAP was determined as an average of 64 sweeps (two per second) and stored on a magnetic disk. Additional improvement of the signal to noise ratio was obtained with a software time varying filter technique as proposed by de Weerd et al. (1981 a,b). The long tail of the stimulus artefact was removed by subtraction of a first order exponential curve from the averaged compound action potentials.

The skin temperature was kept between 34°C and 36°C with an infrared heater (Disa 31 B30/40). Stimuli of 0.1 ms in duration were applied. The current strength was increased until the stimuli were felt as sharp and pricking. This was normally at 4 - 6 times the threshold level (20 - 25 mA). At these intensities one may expect that a greater part of the group of smaller fibres (1-6 µm diameter) is stimulated as well (Vallbo et al. 1979). Further increase of the stimulus led to contraction of muscle fibres, electrically causing a time-locked artefact interfering with the last phase of the CAP. The experimental results, at the magnification used, never showed a visible contribution from the smaller fibres, a finding which has been confirmed by others. We do not expect therefore that a further increase in the stimulation level would change the CAP shapes due to further recruitment of thin fibres.

3.5 EXPERIMENTAL RESULTS

Five series, corresponding to the five subjects, of seven compound action potentials, corresponding to the seven distances (6, ..., 24 cm) were obtained. From these thirty five CAPs we calculated a propagation velocity, referring to the first positive peak, of 60.6 ± 3.3 (SD) m.s^{-1} . The inter-individual variations were small. This is shown for a distance of 12 cm in Fig. 3.4. Therefore we decided to make up the (grand) average across individuals for each distance⁴ (Fig. 3.5a). Fig. 3.5b gives the same result, but with normalized amplitudes which is advantageous when CAP shapes are inspected.

With increasing propagated distance (DIST) the most obvious changes in the compound action potentials are:

- 1) A third phase is clearly present in the CAP measured at 6 cm but hardly or not at all at larger distances. Most other CAPs are almost biphasic.
- 2) The latency to the first positive peak increases linearly with the distance as was expected.
- 3) The amplitude decreases with increasing propagated distance. In the range studied (6 - 24 cm) an almost exponential curve was found (Fig. 3.8 '▲').

⁴ This was done after correction for the latency differences by aligning the first positive peaks before averaging. For the averaged CAP the mean latency was used.

- 4) The duration from the first positive to the negative peak increases with distance.
- 5) The duration of the negative phase (for instance the width at 50% of the maximal negative amplitude) increases.
- Both aspects 4) and 5) will be referred to as 'broadness' in the subsequent sections. In general this broadness is only modestly enlarged after a four-fold increase in the propagated distance.

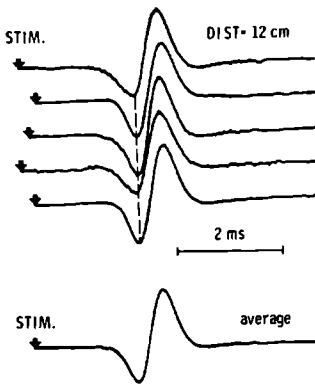


Fig. 3.4

The individual experimentally obtained CAPs for the five subjects at 12 cm propagated distance together with their average. The first positive peaks were aligned before averaging. Amplitudes are normalized in this figure

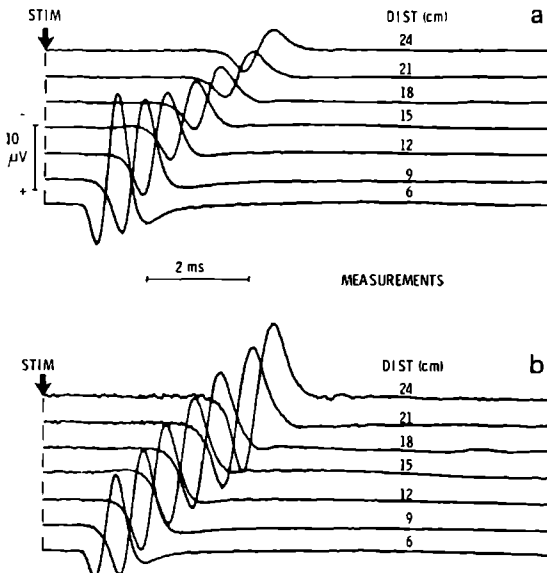


Fig. 3.5 a and b

Compound action potentials obtained for different propagated distances. Each trace represents the average of five CAPs, measured on different subjects. In part a absolute amplitudes are plotted, in part b the CAP amplitudes are normalized

3.6 A FIRST MODEL APPROACH

A large number of model parameter values has to be assumed. For most of them there are values available from the literature, but their reliability is not always known. Fortunately not all values are critical to the final result. In Table 3.1 the model parameters along with the assigned values are summarized. When no reference is given (C , σ_{oz}), the model outcomes are used to derive an appropriate value. The following comments are relevant:

The distribution of external fibre diameters is described by six parameters, defining two summated Gaussian curves (Fig. 3.6b). The values have been extracted from a histogram of fibre diameters (Fig. 3.6a, Buchthal et al. 1975). The gaussian curves are fitted to the histogram by means of a least mean square error algorithm (Bevington 1969). Histograms from other authors

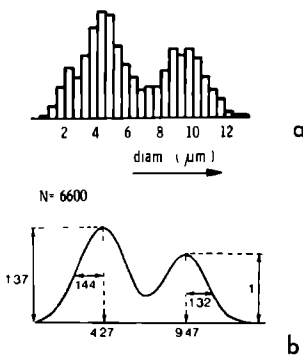


Fig. 3.6 a and b

a Diameter histogram of a normal sural nerve, as measured by Buchthal et al. (1975). The number of fibres was 6600

b An optimal fit to histogram a, assuming the existence of two Gaussian distributed groups of fibres. The heights are given in arbitrary units

show bimodal distributions as well, but the positions and widths of the two peaks sometimes exhibit systematically different values (e.g. Dyck et al. 1971, O'Sullivan and Swallow 1968, Tackmann et al. 1976). Differing methods of preparation and counting are probably in part responsible for these discrepancies. The histogram used here had the narrowest peaks and was chosen for that reason (see next section).

External fibre diameter and propagation velocity are proportionally related according to theoretical descriptions (Rushton 1951, Goldman and Albus 1968, Moore et al. 1978). Numerous experimental data seem to confirm this relation (for references see Sect. 3.8), which is usually expressed by means of the so called 'conversion factor' (C). A value of $4.74 \text{ m.s}^{-1} \cdot \mu\text{m}^{-1}$ gives a close latency fit for most of the seven CAPs. This value is in good

agreement with the value proposed by Buchthal et al. (1975) for the nerve under consideration at body temperature ($C = 4.7$). The total number of fibres present in that nerve (6600) was assumed to be activated.

The value for the axoplasm conductivity (σ_1) is calculated from the data of Tasaki and Frank (1955). They measured a resistance of $15 \text{ M}\Omega$ per mm fibre length. The fibre had an outside diameter of $13 \mu\text{m}$. When a fibre contains only axoplasm, as is assumed in the model, this axoplasm then must have a conductivity of $0.5 \Omega^{-1} \cdot \text{m}^{-1}$ ($= (\pi \cdot (6.5)^2 \cdot 15 \cdot 10^{-3})^{-1}$). The conductivity of the 'real' axoplasm (half the cross section actually contains myelin) must be estimated at about $1 \Omega^{-1} \cdot \text{m}^{-1}$ to give the same resistance.

For computational convenience no anisotropy in the muscle tissue was assumed. The value used ($\sigma_m = 0.25$) lies in between the longitudinal and transverse conductivity for such tissue.

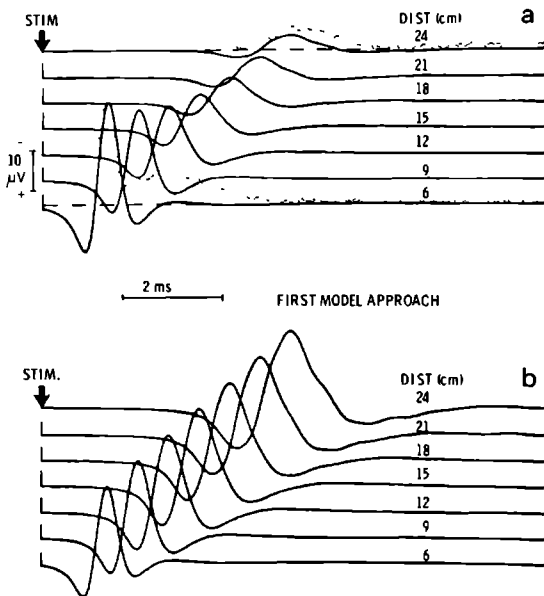


Fig. 3.7 a and b

A first attempt at CAP reconstructions with the proposed model (presentation as in Fig. 3.5). The dots in the first and the last trace of part a indicate the arrival times of the constituent single fibre action potentials for propagated distances of 24 and 6 cm respectively. The relation between single fibre diameter and velocity is assumed to be linear ($C = 4.74 \text{ m} \cdot \text{s}^{-1} \cdot \mu\text{m}^{-1}$)

The model reconstructions are shown in Fig. 3.7 with both real and normalized amplitudes. The correspondence in shape and amplitude (Fig. 3.8) is not very convincing. The typical changes in the measured CAPs with increasing propagated distance as summarized at the end of the previous section are not reproduced, especially not with respect to the broadness and the vanishing third phase.

TABLE 3.1 Summary of model parameters and their assigned values.

parameter	meaning	value	reference	see Fig.
C	conversion factor	$4.74 \text{ m.s}^{-1} \cdot \mu\text{m}^{-1}$	-----	3.10
d1	thickness of the subcutaneous layer.	10 mm	Boileau Grant 1962	
d2	depth of the nerve below the skin.	9 mm	Boileau Grant 1962	
d3	insertion depth of the electrode.	9 mm	estimated	
d4	transverse distance of the electrode.	5 mm	estimated	
b	radius of the nerve trunk.	1 mm	Boileau Grant 1962	
σ_i	axoplasm conductivity.	$0.5 \Omega^{-1} \cdot \text{m}^{-1}$	Tasaki and Frank 1955	3.1
σ_{op}	radial nerve trunk conductivity (I).	$0.01 \Omega^{-1} \cdot \text{m}^{-1}$	Tasaki 1964	
σ_{oz}	axial nerve trunk conductivity (I).	$1.0 \Omega^{-1} \cdot \text{m}^{-1}$	-----	
σ_f	conductivity of fat layer (II).	$0.04 \Omega^{-1} \cdot \text{m}^{-1}$	Geddes and Baker 1967	
σ_m	conductivity of muscle tissue (III).	$0.25 \Omega^{-1} \cdot \text{m}^{-1}$	Geddes and Baker 1967	
t_{rise}	rising phase duration of single fibre spike.	0.12 ms	Paintal 1966 T = 34°C	3.2c
t_{fall}	falling phase of spike.	0.40 ms	Paintal 1966	
A_i	amplitude of a spike	100 mV	Tasaki and Frank 1955	
m_α	mean A α fibre diameter	9.47 μm	} Buchthal et al. 1975	3.6
m_δ	mean A δ fibre diameter	4.27 μm		
s_α	standard deviation A α	1.32 μm		
s_δ	standard deviation A δ	1.44 μm		
A_α	amplitude (relat.) A α	1		
A_δ	amplitude (relat.) A δ	1.37		
N	number of fibres	6600		

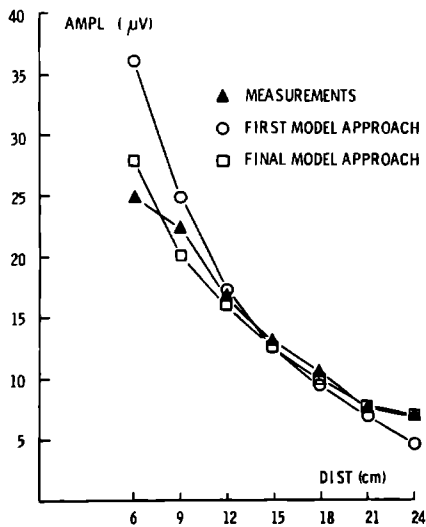


Fig. 3.8

The amplitude behaviour of the measured CAPs (\blacktriangle) as a function of the propagated distance together with the model predictions in the first model approach (\circ) and in the final one (\square)

3.7 PARAMETER INSPECTION

A re-examination of the model and its parameters is necessary. The peak to peak duration of the calculated CAPs increases more with increasing propagated distance than that of the measured CAPs (see also Fig. 3.9a and 3.9b). The only plausible reason for this is an over-estimation of the increase in the *dispersion of arrival times*. As already mentioned we intentionally took a narrow histogram of fibre diameters from the literature. The use of another histogram is demonstrated in Fig. 3.9c (Tackmann et al. 1976). It makes the discrepancy even larger.

In the choice of parameters we disregarded an important point which needs further consideration. A fibre diameter histogram, based on one single cross section of a nerve or nerve fascicle, only represents a 'sample' of the diameters of the fibres present. Local variations in fibre diameter in the course of one and the same fibre cannot be detected in this way (BeMent and Olson 1977). These local variations have been investigated in cat nerves (Hursh 1939, Matsumoto and Mori, 1975, BeMent and Olson 1977) and in the human median nerve (Sunderland and Roche 1958). Values between 0.4 and 0.7 μm for the standard deviation were found. Data regarding the sural nerve are, as far as we know, not available. When the standard deviations are known the

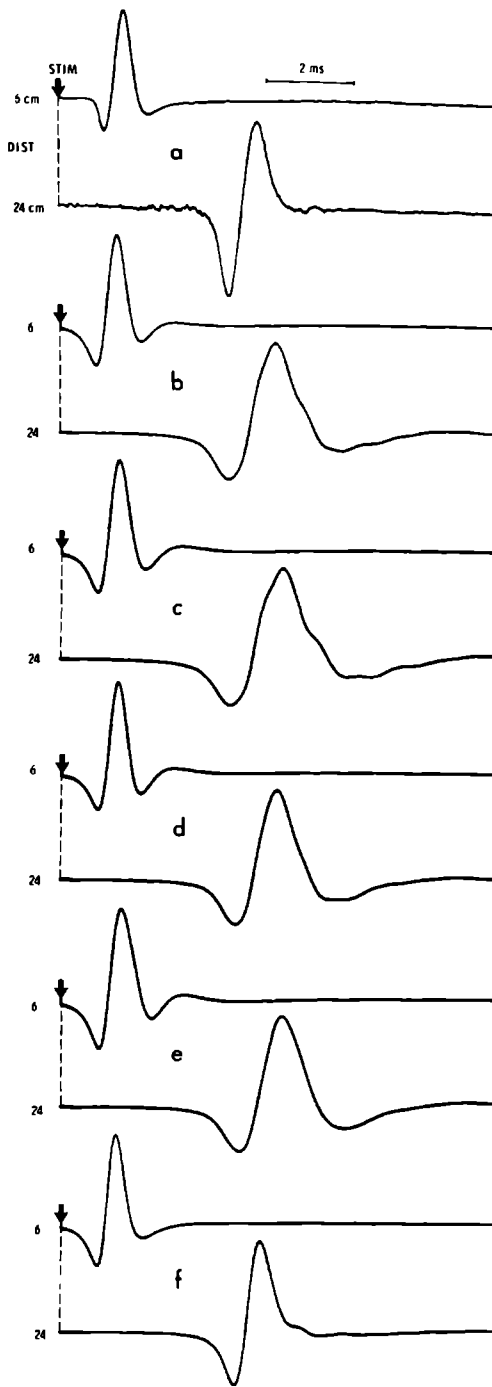


Fig. 3.9 a-f

a: The measured CAPs for propagated distances 6 and 24 cm. The amplitudes are normalized

b: Replot of the first model approach for these distances ($s_{\alpha} = 1.32 \mu\text{m}$, $m_{\alpha} = 9.47 \mu\text{m}$, $t_{\text{fall}} = 0.4 \text{ ms}$)

c: Same as b with a different diameter distribution taken from the literature (Tackmann et al. 1976) ($s_{\alpha} = 1.67 \mu\text{m}$, $m_{\alpha} = 10.73 \mu\text{m}$)

d: Same as b after a correction of the diameter distribution in order to obtain the distribution of mean fibre diameters ($s_{\alpha} = 1.12 \mu\text{m}$, $m_{\alpha} = 9.47 \mu\text{m}$, $t_{\text{fall}} = 0.4 \text{ ms}$)

e: Same as d with a prolonged falling phase of the intracellular single fibre action potentials ($t_{\text{fall}} = 0.8 \text{ ms}$)

f: Replot of the final model approach for the two propagated distances. A non-linear relation between fibre diameter and propagation velocity was assumed

cross section histogram can be corrected and an estimate of the histogram of *mean* fibre diameters, which is the important factor in propagation velocity, is thereby obtained. The correction makes the distribution of diameters narrower, which could be helpful in improving the calculated results. In Fig. 3.9d the CAPs are shown using a standard deviation of $0.7 \mu\text{m}$ to correct the original distribution of diameters shown in Fig. 3.6b. A gaussian distribution was also assumed for the variation in diameter. The broadness of the second CAP (24 cm) actually decreases (although not by enough) but the CAP is still triphasic.

In the context of the model one may expect a decrease in the third phase of a CAP when the *repolarization* is slowed, i.e. an increase in t_{fall} is introduced. Therefore we recalculated the CAPs of Fig. 3.9d with an increased value for t_{fall} ($\times 2$). The result is shown in Fig. 3.9e. It is clear that this modification does not improve the results. A decrease in the third phase is present in the first CAP (6 cm) but not at all in the second one (24 cm). This observation is confirmed when t_{fall} is further increased. The first CAP becomes almost biphasic, the second one, on the contrary, maintains its three phases and becomes much broader. These results, along with strong doubt about the physiological validity of the modification, made us discard this approach.

The *volume conductor* parameters (dimensions and conductivities) will not be discussed here (see chapter 2.). Suffice it to say that a large number of simulations showed that a simultaneous improvement in the broadness, the amplitude and the suppression of a third phase cannot be obtained. The results of this section justify the conclusion that with the actual model a rough correspondence between the experimental and reconstructed CAPs can be obtained at best, as long as a linear relation between the fibre diameter and the propagation velocity is assumed.

3.8 FIBRE DIAMETER AND PROPAGATION VELOCITY

The linear (proportional) relation between external fibre diameter and the propagation velocity has been accepted as an established fact (e.g. Hursh 1939, Cragg and Thomas 1957, Boyd and Kalu 1979, McLeod and Wray 1967, Hutchinson et al. 1970, Schnepf et al. 1971). Little attention has been paid to the finding of Gasser and Grundfest (1939) that a good fit in their CAP reconstructions could only be obtained if slight, but systematic deviations from a strictly proportional relation were introduced. An S-shaped curve was

more appropriate in almost all of the cases that they studied. The same tendency is found in the study by Olson (1973). Without introducing different (linear) relations for the thinner and the thicker fibres no close fitting reconstructions of monophasic CAPs were obtained (cat saphenus nerve). The distinction between a straight line and the sigmoid curves found by Gasser and Grundfest is not observed with direct electrophysiological experiments, perhaps because these data always show a considerable scatter⁵.

The mismatch of our first model approach, together with the above observations, caused us to reject the assumption of a linear relation between the two quantities. Instead, we searched for an 'optimal' distribution of propagation velocities, such that the seven reconstructed CAPs fitted as closely as possible to the measured ones. A strict definition of optimal was not given but attention was paid to (i) a correct description of the peak to peak durations, (ii) the relative amplitudes to third phases (if present) and (iii) the absence of any elevation caused by the group of small fibres. The conversion from the resulting velocity distribution into the original diameter distribution would lead to an empirical relation between diameter and velocity. This method is essentially the same as the one used by Gasser and Grundfest (1939). The result of the above procedure is shown in Fig. 3.10. The diameter distribution (Fig. 3.6b) and the final velocity distribution are drawn along the abscissa and the ordinate respectively. The dotted diameter distribution and the dotted curve in the figure refer to the estimated distribution of *mean* fibre diameters (see Sect. 3.7, Fig. 3.9d). Note the small difference between the two curves. The S-shaped character is preserved in both curves and seems to be essential. The final CAP reconstructions and the amplitude behaviour are shown in Fig. 3.11 and Fig. 3.8 (squares). The CAPs for the extreme distances (6 and 24 cm) are redrawn in Fig. 3.9f.

The improvements are substantial and concern all three above mentioned aspects. Also the amplitude and the broadness of the negative phase are better reproduced in these reconstructions. The empirical diameter-velocity relation has much in common with the curves found by Gasser and Grundfest (1939). The change to smaller conversion factors for the small fibres was also found by Olson (1973). These similarities are striking and give evidence that a sigmoid diameter-velocity relation is more appropriate for mammalian

⁵ One of the reasons could be the defective determination of the desired *mean* fibre diameter as described in the previous section.

medullated fibres. Both monophasic CAPs, measured *in vitro*, as well as bi- or tri-phasic CAPs *in situ* as we measured, appear to depend strongly on this relation.

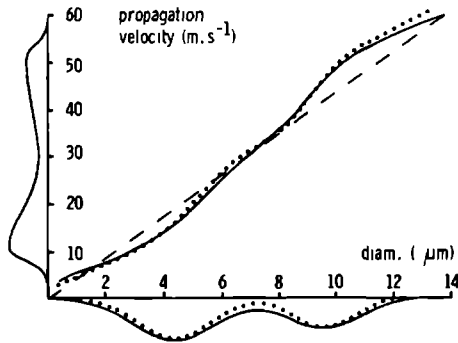


Fig. 3.10

The nonlinear relation between fibre diameter and propagation velocity. The distributions of diameters and velocities are plotted along the abscissa and the ordinate respectively. The dotted functions refer to the diameter distribution of mean fibre diameters as estimated from the original distribution (see Fig. 3.6)

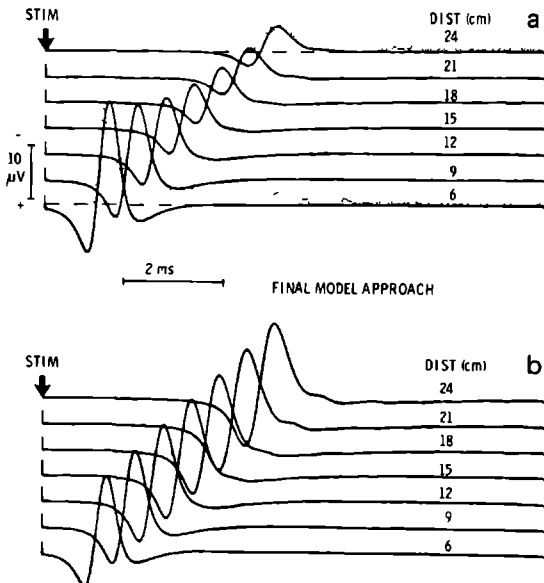


Fig. 3.11 a and b

The final CAP reconstructions, obtained after an optimization of the velocity distribution (see the ordinate of Fig. 3.10). The presentation is as in Fig. 3.7

3.9 DISCUSSION AND CONCLUSIONS

Based on the assumption that compound action potentials are a linear summation of the activity of all constituent fibres, CAP reconstructions can be performed. The dispersive character of single fibre activity, caused by differences in propagation velocity, is the most prominent characteristic. The model presented is based on the description of volume conduction of currents leaving (and entering) the fibre membrane in the anisotropic and inhomogeneous medium around this fibre. The model predictions were verified with experimental outcomes on human sural nerves. We chose this nerve on the one hand because of its surveyable surroundings and on the other hand because of the availability of many biopsy studies in the literature. We assume that the sural nerve is a 'normal' sensory nerve. It is not likely that our results apply solely to this particular nerve. A more complex structure (bone, blood vessels, tapering etc.) may, however, disturb the validity of the described model.

The distributions of external fibre diameters, when inserted into the model, must be combined with an S-shaped relation between fibre diameter and propagation velocity in order to give a satisfactory fit between model and experiment. The deviation from a straight (linear) relation is consistent but weak, considering the substantial differences in CAP shapes (compare e.g. Fig. 3.9b and 3.9f). No adjustment of any of the other parameters in the model (their effects were extensively studied) led to comparable improvements. The evidence for a deviation from linearity (Fig. 3.10) for the thicker fibres in this curve is fairly strong and the results are quantitatively reliable. The deviation of the thin fibres is dictated by the absence of elevations caused by this group and can only be justified qualitatively. Some support is present in the study of Olson (1973) and in some measurements on human biopsy material (Dyck et al. 1971). In some cases the last authors measured monopolar CAPs in which the peak from the small fibres seemed to be more delayed than a linear relation with a conversion factor of about $5.0 \text{ m.s}^{-1} \cdot \mu\text{m}^{-1}$ would bring about.

A physiological explanation for this systematic deviation is not easy to give. Synchronization of the largest fibres would only partly explain the results. Moreover there is evidence against such a supposition (Esplin 1962, Freeman 1972). Direct measurements of the diameter-velocity relation are not suited to a demonstration of minor deviations from linearity. Even when the *mean* fibre diameter is known exactly, it cannot be ruled out that the

propagation velocity shows scatter within one subject when more fibres of the same diameter are studied. Nerve models, describing propagation according to the concept of Hodgkin and Huxley for medullated fibres, also yield a linear relation (see Moore et al. 1978, Waxman 1980). Such models deviate from this behaviour when diameter dependent values for the node and internode parameters are inserted; there is no strict objection to the presence of such a dependence. The lack of experimental data makes further discussion on this point too speculative to be useful.

The volume conduction phenomenon has been expressed in terms of a smoothing window (Fig. 3.2e). It is not easy to test the correctness of this description. Some remaining differences between predicted and measured CAPs indicate some slight model imperfections. The first positive peak for instance is larger in the measurements than in the reconstructions and the rising phase of these peaks is less steep in the reconstructions. Although the axial conductivity σ_{oz} exceeds the value suggested by Tasaki (1964) of $\sigma_{oz} = 0.5 \Omega^{-1} \cdot m^{-1}$, which leads to more suppression of the high frequency components in the CAPs (see chapter 2), there are still some separate late phases present in the calculated CAPs, especially at the largest propagated distances (Fig. 3.11). These observations may indicate that the tails of the volume conduction windows (Fig. 3.2e) are less extensive than the theory predicts.

In most volume conduction studies amplitudes are given in arbitrary units, not in μV . We obtained a surprisingly good correspondence with respect to the absolute CAP amplitudes (Fig. 3.8). The surprise lies in the fact that almost all parameters (conductivities, number of fibres, the intracellular spike characteristics and the distribution of velocities) play a part in the generation of this parameter.

A rather subtle aspect of the results obtained is the appearance of almost biphasic CAPs, while all extracellular single fibre potentials are triphasic and almost symmetrical. A transition from tri- to bi-phasic CAPs with increasing propagated distance can also be observed in most of the examples given in the systematic study reported by Buchthal and Rosenfalck (1966). This result has some consequences for solutions of the 'inverse problem' of the estimation of the propagation velocity distribution. When a procedure is based on two CAPs at different propagated distances (Barker et al. 1979, Cummins et al. 1979b), one of these CAPs should be measured at a short (< 9 cm) distance. Otherwise an estimation procedure will probably not 'recognize' the triphasic nature of the single fibre action potentials and

an incorrect velocity distribution will then be obtained as the final solution.

Peripheral sensory nerve activity is measured more and more in routine clinical practice. Shape inspection of a CAP is not usual however. A decreased propagation velocity and a severely diminished amplitude are the most frequently used indications of nerve dysfunction. With the model proposed here it may be possible to be more specific about the influence of underlying processes on the CAP shape. In the model the outcomes of physiological experiments on single fibre level can be evaluated or used to predict measurements on compound activity level.

The chapters 4 and 5 deal with the influence of temperature and the refractory state respectively. Both aspects emerge in discussions about nerve function from time to time. The final aim is to gain more insight into the type of malfunction of peripheral nerves which can be detected from their CAPs and which can only be determined using alternative methods of investigation.

3.10 REFERENCES

- Barker, A.T., Brown, B.H. and Freeston, I.L. Determination of the distribution of conduction velocities in human nerve trunks. *IEEE Trans. biomed. Engng*, 1979, BME-26: 76-81.
- Behse, F. and Buchthal, F. Sensory action potentials and biopsy of the sural nerve in neuropathy. *Brain*, 1978, 101: 473-493.
- BeMent, S.L. and Olson, W.H. Quantitative studies of sequential peripheral nerve fiber diameter histograms and biophysical implications. *Exp. Neurol.*, 1977, 57: 828-848.
- Bevington, P.R. Data reduction and error analysis for the physical sciences. McGraw-Hill, New York, 1969.
- Boileau Grant, J.C. An atlas of anatomy. Williams and Willins, Baltimore, 1962.
- Boyd, I.A. and Kalu, K.U. Scaling factor relating conduction velocity and diameter for myelinated afferent nerve fibres in the cat hind limb. *J. Physiol.*, 1979, 289: 277-297.
- Buchthal, F. and Rosenfalck, A. Evoked action potentials and conduction velocity in human sensory nerves. *Brain Res.*, 1966, 3: 1-122.
- Buchthal, F. and Rosenfalck, A. Sensory potentials in polyneuropathy. *Brain*, 1971, 94: 241-262.

- Buchthal, F., Rosenfalck, A. and Behse, F. Sensory potentials of normal and diseased nerve. In: P.J. Dyck, P.K. Thomas and E.H. Lambert (Eds.), *Peripheral neuropathy*, Vol. 1. Saunders, Philadelphia, 1975: 442-464.
- Cragg, B.G. and Thomas, P.K. The relationships between conduction velocity and the diameter and internodal length of peripheral nerve fibres. *J. Physiol.*, 1957, 136: 606-614.
- Cummins, K.L., Perkel, D.H. and Dorfman, L.J. Nerve fiber conduction-velocity distributions. I. Estimation based on the single-fiber and compound action potentials. *Electroenceph. clin. Neurophysiol.*, 1979a, 46: 634-646.
- Cummins, K.L., Dorfman, L.J. and Perkel, D.H. Nerve fiber conduction-velocity distributions. II. Estimation based on two compound action potentials. *Electroenceph. clin. Neurophysiol.*, 1979b, 46: 647-658.
- Dyck, P.J., Lambert, E.H. and Nichols, P.C. Quantitative measurements of sensation related to compound action potential and number and sizes of myelinated and unmyelinated fibres of sural nerve in health, Friedreich's ataxia, hereditary sensory neuropathy and tabes dorsalis. In: A. Rémond (Ed.), *Handbook of Electroencephalography and Clinical Neurophysiology*, Vol. 9. Elsevier, Amsterdam, 1971: 83-118.
- Esplin, D.W. Independence of conduction velocity among myelinated fibres in cat nerve. *J. Neurophysiol.*, 1962, 25: 805-811.
- Freeman, W.J. Spatial divergence and temporal dispersion in primary olfactory nerve of cat. *J. Neurophysiol.*, 1972, 35: 733-744.
- Gasser, H.S. and Grundfest, H. Axon diameters in relation to the spike dimensions and the conduction velocity in mammalian A fibers. *Amer. J. Physiol.*, 1939, 127: 393-414.
- Geddes, L.A. and Baker, L.E. The specific resistance of biological material: A compendium of data for the biomedical engineer and physiologist. *Med. Biol. Engng*, 1967, 5: 271-293.
- Goldman, L. and Albus, J.S. Computation of impulse conduction in myelinated fibres; theoretical basis of the velocity-diameter relation. *Biophys. J.*, 1968, 8: 596-607.
- Griep, P.A.M., Boon, K.L. and Stegeman, D.F. A study of the motor unit action potential by means of computer simulation. *Biol. Cybernetics*, 1978, 30: 221-230.
- Hursh, J.B. Conduction velocity and diameter of nerve fibers. *Amer. J. Physiol.*, 1939, 127: 131-139.

- Hutchinson, N.A., Koles, Z.J. and Smith, R.S. Conduction velocity in myelinated nerve fibres of *Xenopus laevis*. *J. Physiol.*, 1970, 208: 279-289.
- Kovacs, Z.L., Johnson, T.L. and Sax, D.S. Estimation of the distribution of conduction velocities in peripheral nerves. *Comp. Biol. Med.*, 1979, 9: 281-293.
- Lorente de N6, R. A study of nerve physiology. Studies from the Rockefeller Institute for Medical Research, 1947, 132: 384-482.
- Matsumoto, A. and Mori, S. Number and diameter distribution of myelinated afferent fibers innervating the paws of cat and monkey. *Exp. Neurol.*, 1975, 48: 261-274.
- McLeod, J.G. and Wray, S.H. Conduction velocity and fibre diameter of the median and ulnar nerves of the baboon. *J. Neurol. Neurosurg. Psychiat.*, 1967, 30: 240-247.
- Moore, J.W., Joyner, R.W., Brill, M.H., Waxman, S.G. and Najar-Ioa, M. Simulations of conduction in myelinated fibers: Relative sensitivity to changes in nodal and internodal parameters. *Biophys. J.*, 1978, 21: 147-160.
- Olson, W.H. Peripheral nerve compound action potentials and fiber diameter histograms (Ph.D. dissertation). Univ. of Michigan, Ann Arbor, Mich., 1973.
- Oosterom, A. van. Cardiac potential distributions (Ph.D. dissertation). Univ. of Amsterdam, Amsterdam, 1978.
- O'Sullivan, D.J. and Swallow, M. The fibre size and content of the radial and sural nerves. *J. Neurol. Neurosurg. Psychiat.*, 1968, 31: 464-470.
- Paintal, A.S. The influence of diameter of medullated nerve fibres of cats on the rising and falling phases of the spike and its recovery. *J. Physiol.*, 1966, 184: 791-811.
- Plonsey, R. Bioelectric phenomena. McGraw-Hill, New York, 1969.
- Rosenfalck, P. Intra- and extracellular potential fields of active nerve and muscle fibres. *Acta Physiol. Scand.*, 1969, Suppl. 321.
- Rushton, W.A.H. A theory of the effects of fibre size in medullated nerve. *J. Physiol.*, 1951, 115: 101-122.
- Schnepf, G., Schnepf, P. and Spaan, G. Faseranalytische Untersuchungen an peripheren Nerven bei Tieren verschiedener Grösse. *Z. Zellforschung*, 1971, 119: 77-98.

- Sunderland, S. and Roche, A. Axon myelin relationships in peripheral nerve fibers. *Acta Anat.*, 1958, 33: 1-37.
- Tackmann, W., Spalke, H.J. and Oginszus, H.J. Quantitative histometric studies and relation of number and diameter of myelinated fibres to electrophysiological parameters in normal sensory nerves in man. *J. Neurol.*, 1976, 212: 71-84.
- Tasaki, I. and Frank, K. Measurement of the action potential of myelinated nerve fiber. *Amer. J. Physiol.*, 1955, 182: 572-578.
- Tasaki, I. A new measurement of action currents developed by single nodes of Ranvier. *J. Neurophysiol.*, 1964, 27: 1199-1205.
- Vallbo, Å.B., Hagbarth, K.-E., Torebjörk, H.E. and Wallin, B.G. Somatosensory, proprioceptive and sympathetic activity in human peripheral nerves. *Physiol. Rev.*, 1979, 59: 919-957.
- Waxman, S.G. Determinants of conduction velocity in myelinated nerve fibers. *Muscle Nerve*, 1980, 3: 141-150.
- Weerd, J.P.C.de A posteriori time-varying filtering of averaged evoked potentials. I. Introduction and conceptual basis. *Biol. Cybernetics*, 1981a(in press).
- Weerd, J.P.C.de and Kap, J.I. A posteriori time-varying filtering of averaged evoked potentials. II. Mathematical and computational aspects. *Biol. Cybernetics*, 1981b(in press).

C H A P T E R 4
A STUDY OF THE INFLUENCE OF TEMPERATURE

ABSTRACT

Compound nerve action potentials of sural nerves of healthy volunteers have been measured at different temperatures. In the range from 21 to 39°C a linear temperature dependence of the propagation velocity was found (slope $1.9 \text{ m.s}^{-1}.\text{°C}^{-1}$). The causes of amplitude and shape alterations in the compound action potentials (CAPs) with changing temperature are analysed with the help of a model. It appears that the changes in the measured CAPs are well explained by known temperature effects at the single fibre level. Both the considerable increase in CAP duration after cooling and the relative constancy of the CAP amplitude were reproduced by the model. Close fits to the actually measured CAPs can be obtained when some crucial parameter values are optimized. The results of this procedure are presented.

4.1 INTRODUCTION

The influence of the temperature on nerve propagation appears predominantly in the propagation velocity, for which a linear dependence on temperature has been well established (e.g. Paintal 1965). The impacts of temperature on other features of nerve activity are revealed by visual inspection of the wave shapes of evoked compound action potentials (CAPs). In particular, a substantial increase in the total CAP duration (broadness) is seen with decreasing temperature (Buchthal and Rosenfalck 1966).

A number of authors (McLeod 1966, Ludin and Beyeler 1977, Hulley et al. 1979, Gutjahr 1979) further observed the intuitively somewhat dissatisfying effect of decreasing *amplitudes* with temperature increase, particularly in the range beyond 30°C. Since the average decrease is modest, it is perhaps more appropriate to emphasize the remarkable lack of consistency in the amplitude dependence on temperature, as was done by Buchthal and Rosenfalck (1966). They apparently observed both slightly increasing and slightly decreasing amplitudes. Their explanation which suggests that the influence of auxiliary factors (shift of the electrode during the experiment) rather than the temperature itself is predominant, indicates that this amplitude behaviour was rather unexpected.

In this study we compare experimental results, obtained from normal human sural nerves *in situ* at different temperatures, to the results of model predictions. The model used has been described in the chapters 2 and 3. Basically, the model assumes the CAP to be a summation of single fibre action potentials. Thus we can refer to results from electrophysiological investigations obtained from excised single nerve fibres. It will be shown that the typical changes in CAP parameters (including its amplitude) caused by the temperature changes, can be fully explained by physiological changes which are known to occur at the single fibre level.

Ludin and Beyeler (1977) were aware of the possibility of such an explanation when they pointed to the complex interaction of different single nerve fibre characteristics which change with temperature. However, they were unable to explain these interactions in a satisfactory way, due to the lack of a proper model description. In this respect, the present study illustrates the usefulness of such a description for the clarification of phenomena that cannot easily be understood intuitively.

A precise understanding of the factors which influence the CAP, such as the effect of temperature, is also indispensable when CAPs are used to

extract more detailed information from the nerve, for instance the velocity distribution of the various constituent fibres (e.g. Cummins et al. 1979). A further motivation for studying the influence of the temperature quantitatively is the observation that the pathophysiology of nerve conduction in demyelinating diseases can be recognized in the electrophysiological effects of slight temperature changes (Rasminsky 1973, Davis et al. 1975, Low and McLeod 1977).

Sect. 4.2 concerns the experimental methods and Sect. 4.3 a description, in general terms, of our experimental results. A short survey over the literature with respect to the influence of temperature on nerve fibre propagation is presented in Sect. 4.4. In Sect. 4.5 model-'reconstructions' are given. The calculated results appear to fit closely to the experimental results so that estimations concerning underlying processes in single nerve fibres can be given. A dissection of the model results is given in the discussion (Sect. 4.6) to illustrate some important aspects. For details concerning the model and its various parameters chapter 3 should be consulted. Details of the modelling procedure have been combined in an appendix (Sect. 4.7) in order to avoid a disturbance of the reasoning of this chapter.

4.2 EXPERIMENTAL METHODS

Monopolar recordings of compound action potentials from sural nerves were obtained using six healthy volunteers (3 male, 3 female, 20-30 years of age). Teflon-coated needle electrodes with a bared tip (Buchthal and Rosenfalck 1966) were used. Stimulation was carried out with surface electrodes at a supramaximal level (4-6 times threshold, duration 0.1 ms) at the lateral malleolus. The stimulus strength was adjusted at each temperature because of a possible change in threshold with temperature (Schoepfle and Erlanger 1941). The position of the different recording electrode was adjusted until a maximal CAP amplitude was registered.

Prior to insertion of the electrodes the leg was cooled in water to 18°C. During the experiment it was warmed up stepwise with an infrared heater (Disa 31B30/40). Recordings were not made until the temperature of the leg had stabilized after a warming up period. Recordings were made at intervals of 10-15 minutes. The temperature was measured at the stimulus site (surface of the skin) and at the recording site (subcutaneous). The mean value was taken (difference always less than 2°C). Recordings were obtained in the temperature range from 21 to 39°C for each subject. An electromyograph

(Disa 1500 series) with a digital interface to a DEC PDP 11/34 computer was used. Each CAP was determined from 64 sweeps (chapter 3), and stored on a magnetic disk.

4.3 EXPERIMENTAL RESULTS

The *propagation velocity* changed drastically with the temperature. In agreement with other authors we found that a linear relation fits the data very well (Fig. 4.1). The linear regression line through all the data had a slope of $1.9 \text{ m.s}^{-1} \cdot \text{°C}^{-1}$, which is in good agreement with the measurements of Buchthal and Rosenfalck (1966) and de Jesus et al. (1973) on human nerves. After extrapolation, the regression line crosses the abscissa (zero velocity) at a temperature of 7°C , which is in good agreement with the measurements of Paintal (1965) on single fibres. Ludin and Beyeler (1977) and Lowitzsch et al. (1977) obtained a significantly slower propagation for all temperatures

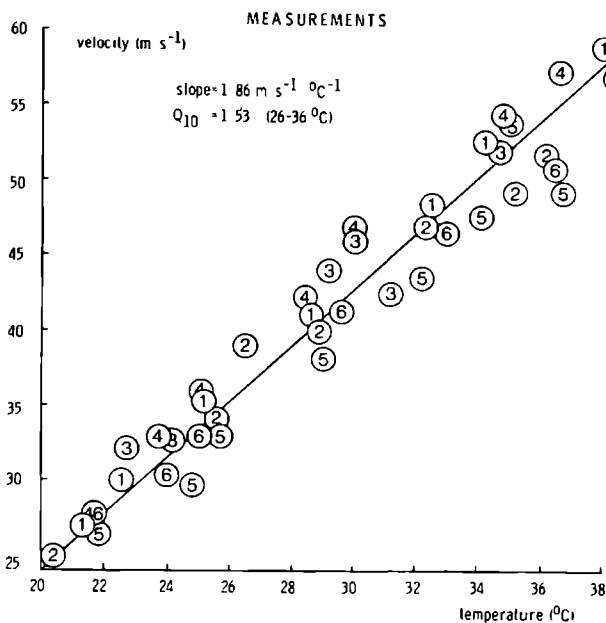


Fig. 4.1

The experimental propagation velocities, calculated from the latencies to the first positive peak, as a function of the temperature. The subjects are indicated by numbers

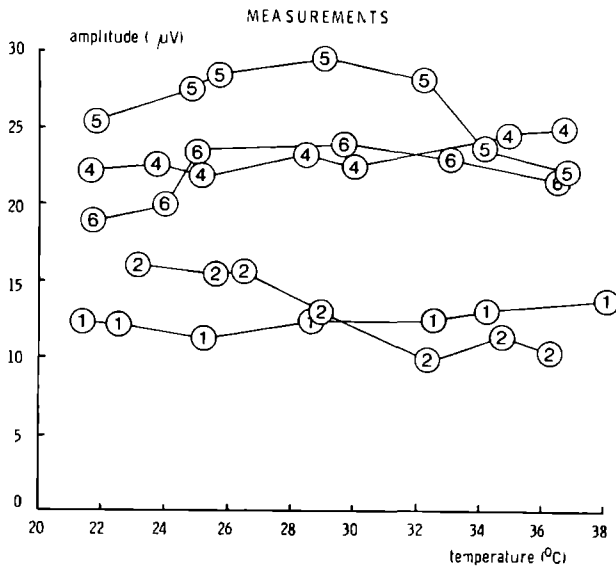


Fig. 4.2

The experimental CAP amplitudes of five of the six subjects as a function of the temperature

and an accordingly lower slope in their regression lines. Table 4.1 summarizes the results from various authors, including data on single nerve fibres and data from model studies. Temperature coefficients (Q_{10}) are given for the restricted temperature range 26 to 36°C¹, since the Q_{10} itself is temperature dependent as soon as no exponential dependence is present. There appears to be more agreement in the literature about the Q_{10} values than about the slopes. This supports the observation of Paintal (1965) that the relative temperature dependence is equal for fast and slow fibres.

The CAP amplitudes (peak-to-peak) at different temperatures in five of the six subjects are presented in Fig. 4.2. One case is omitted (③) because the stimulus strength was not supramaximal. Like Ludin and Beyeler (1977) we did not find a consistent trend in the relationship of amplitude and temperature. In subjects ⑤ and ⑥ the maximum amplitude appeared at about 30°C, in subjects ① and ④ this occurred at the highest and in subject ②

¹ The Q_{10} is defined as the ratio of the velocities at 36°C and 26°C.

at the lowest temperature. In two subjects (② and ⑤) a clear diminution in the amplitude with temperature increase beyond 30°C was present.

The measured CAPs of all subjects, again with the exception of subject ③ are shown in Fig. 4.3. These five cases will be treated separately throughout the paper. Because of large inter-individual differences, a compression of results by averaging over all subjects, as was practiced in chapter 3, seemed inappropriate in this case. All amplitudes shown in Fig. 4.3 have been normalized for sake of shape inspection. The mean temperature (TEMP) is given at the right hand side in each trace. The distance between site of stimulation and site of recording (DIST) is also shown. The most frequently used distance was 12 cm. The most dominant aspect in the shape change is undoubtedly the increase in the CAP duration with decreasing temperature. In two subjects (④ and ⑥) the CAPs are rather irregularly shaped. Such irregularities are also produced by the model. We will come back to this point in the appendix. In accordance with the results presented in chapter 3 the CAPs are almost biphasic, with the exception of case ②. We will argue that a narrow distribution of propagation velocities must be responsible for the appearance of triphasic CAPs in the latter case.

TABLE 4.1 The influence of temperature on nerve propagation velocity.

reference	Q_{10} (26-36°C)	slope m/s/°C	nerve *
Buchthal and Rosenfalck (1966)	1.5	2.0	human median
de Jesus et al. (1973)	1.5	2.0	human median
Ludin and Beyeler (1977)	1.4	1.7	human median
Lowitzsch et al. (1977)	1.5	1.3	human ulnar
this chapter	1.5	1.9	human sural
Paintal (1965)	1.6	2.0	cat single fibre (60)
Hutchinson et al. (1970) (30-36°C after extrapolation)	1.3	1.5	xenopus laevis single fibre (70)
Lee and Bowen (1975)	1.5	1.7	dog ulnar
Roberts and Trollope (1979)	1.7	2.1	rat saphenous
Hutchinson et al. (1970) (30-36°C after extrapolation)	1.6	1.8	membrane model Hodgkin-Huxley (50)
Moore et al. (1978)	1.7	2.0	idem (60)

* for single fibres the velocity (at 36°C) is given in brackets (m.s⁻¹).

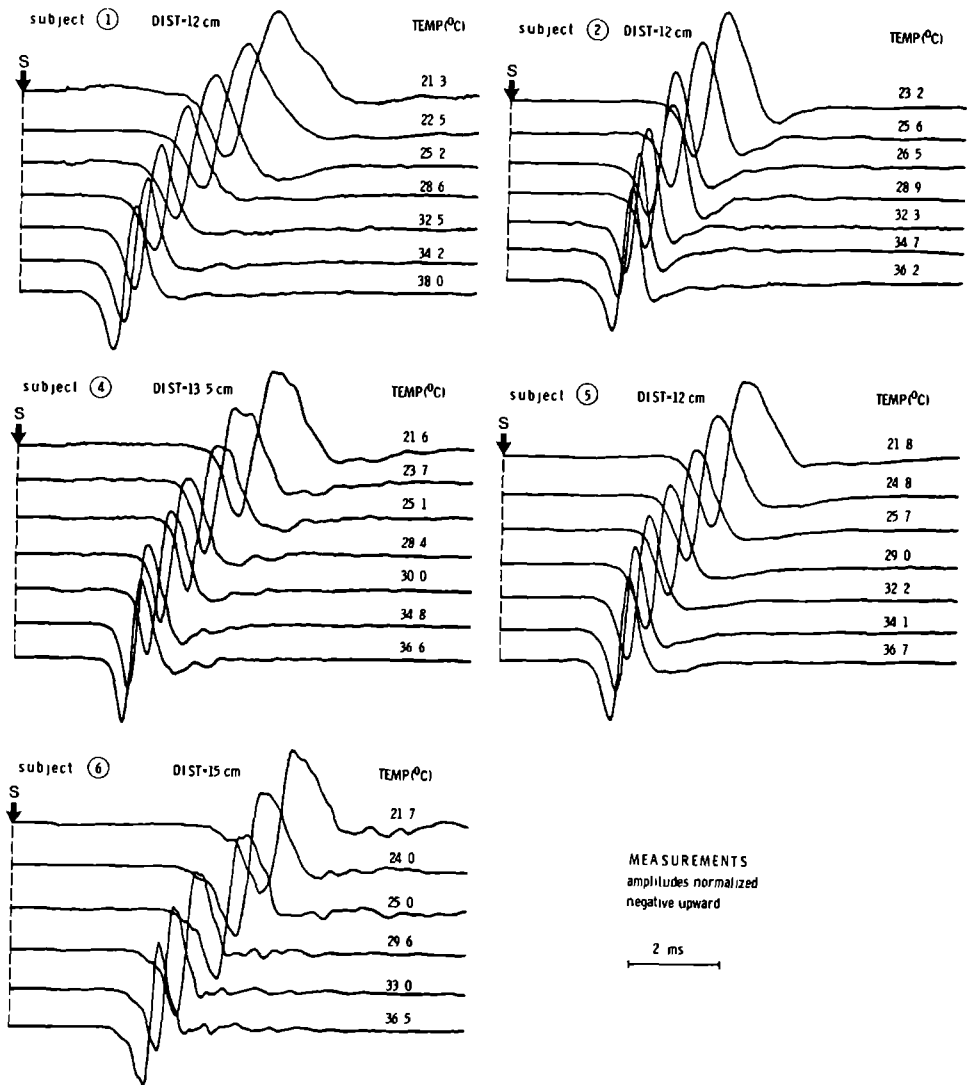


Fig. 4.3

The experimental CAP shapes from five subjects at different temperatures (indicated by 'TEMP').

The amplitudes (peak-to-peak) are normalized. The moment of stimulation is indicated by an arrow. 'DIST' is the distance between the site of stimulation and the site of recording

4.4 TEMPERATURE AND SINGLE FIBRE CHARACTERISTICS

It is well known that the process of depolarization and repolarization along the axon membrane is retarded after cooling (e.g. Gasser 1931). This can be observed as an increase in the rise-time and the fall-time of the monophasic intracellular action potential. This monophasic potential change will be denoted by the term *spike* from now on. An increase of the total spike duration with temperature decrease was clearly demonstrated by Tasaki and Fujita (1948) for motor nerve fibres of the spring toad, by Hodgkin and Katz (1949) for the giant axon of the squid and by Schoepfle and Erlanger (1941) for medullated nerve fibres of the frog. In the latter two papers it is shown that the decline of the spike (t_{fall} , Fig. 4.4a) has a higher Q_{10} than the rising phase (t_{rise} , Fig. 4.4a). For the increase of the total spike duration Q_{10} values between 2.5 and 3.5 were found. Gasser (1931) did not observe different Q_{10} 's for the rise- and fall-time. Paintal (1966) extensively studied the dependence of t_{rise} and t_{fall} on temperature in mammalian nerve fibres (cat). For fast fibres (say $> 30 \text{ m.s}^{-1}$), which mainly determine the CAP shapes *in situ*, Paintal found a logarithmic dependence for t_{rise} ($Q_{10} \approx 2.5$), whereas t_{fall} varied linearly with temperature ($Q_{10} \approx 3.3$)

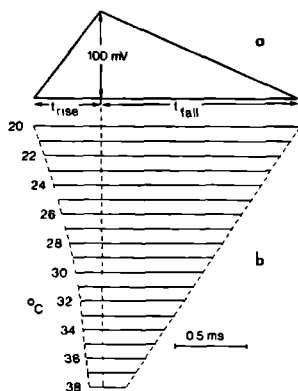


Fig. 4.4 a and b

a: A schematic presentation of the intracellular action potentials of an active nerve fibre as a function of time. This triangular shape is used in the model calculations. It is characterized by the rise-time: t_{rise} , the fall-time: t_{fall} and the amplitude: 100 mV

b: A presentation of t_{rise} and t_{fall} as a function of the temperature as measured by Paintal (1966) for a fast fibre

between 26 and 36°C). In Fig. 4.4b his data for a fast fibre (64 m.s^{-1} at body temperature) are given. In what follows we shall often refer to these data. Although most authors found it difficult to define the spike duration the results taken altogether, do give a rather coherent impression.

This is in notable contrast to the results concerning the spike *amplitude*. It is not entirely clear in how far amplitudes, either measured extracellularly at the cut end of a nerve fibre, or with the fibre membrane penetrated, are interpretable in terms of the intracellular spike amplitude. Most studies indicate that the spike amplitude is almost constant beyond 25°C until a heat block occurs (Gasser 1931, Trautwein et al. 1953, Tasaki and Frank 1955, Hutchinson et al. 1970², Frankenhaeuser 1973²). The amplitude slightly decreases with decreasing temperature below 25°C according to the first two papers. The same was found by Tasaki and Fujita (1948). Schoepfle and Erlanger (1941) found the opposite behaviour in a temperature range below 25°C³. Since the temperature influence on the amplitude always appeared to be slight in the range actually studied (21 - 39°C) a constant amplitude (100 mV) was assumed. In our model the spike amplitude determines the CAP amplitude proportionally, whereas the CAP shape remains unaltered, so that an a posteriori evaluation can easily be made (see Sect. 4.5).

Some authors have stressed the influence of the temperature on *electrical conductivities* in the extracellular medium, which is important in the volume conduction of ionic currents (Tasaki 1949, Zipp 1977, Ludin and Beyeler 1977). Although such an influence is undoubtedly present, there is no reason to assume that the conductivities of the intra- and the extracellular tissues have a different temperature dependence. Since theoretically equal Q_{10} values for all tissue conductivities do not alter the extracellular potential field (chapter 2), this influence can be ignored in the calculations.

² From mathematical studies, based on the 'Hodgkin-Huxley equations' for the active excitable membrane.

³ In the unmyelinated giant axon of the squid the amplitude also increases with decreasing temperature.

Since a CAP can be considered as a summation of single fibre contributions, all temperature influences on its appearance must be related to the underlying single fibre characteristics. Three parameters were taken into consideration in order to 'simulate' the influence of the temperature, namely the spike propagation velocity, its rise-time (t_{rise}) and its fall-time (t_{fall}). Supported by the observations of Paintal (1965, 1966) and given the fact that slow fibres provide hardly any contribution to a CAP *in situ*, we assumed that all fibres have the same intracellular spike and further that their propagation velocity is influenced by the same proportional factor. For the five cases that were presented in Fig. 4.3 we first tried a 'forward' method for reconstructing the CAPs with the model. To this end parameter values established in chapter 3 were used. For the *rise-time* and the *fall-time* the values presented in Fig. 4.4b were used (Paintal 1966). The *velocities* were adjusted until the first positive peaks of model CAPs and experimental CAPs coincided. These primary results showed that only global properties of the measured CAPs could be reproduced by the model, both with respect to shape and amplitude. As in chapter 3 we next applied the model 'inversely'. A number of model parameters (see the appendix, Table 4.2) were adjusted simultaneously until the calculated results fitted as close as possible to the experimental data. Such an optimization procedure is not without pitfalls. The number of parameters varied must be restricted in order to avoid interdependencies which can undermine the uniqueness of the results and thus their validity. Details concerning these problems can be found in the appendix.

A strict criterion for optimality, for instance the mean square error, was not evaluated. Within the restrictions of the model, however, further improvements beyond the results to be presented can only be marginal. The results for CAP shapes and CAP amplitudes, obtained after optimization, are presented in Fig. 4.5 and 4.6 respectively. We concentrated on good shape correspondences. The dotted traces in Fig. 4.5 represent the measured data of Fig. 4.3. The open circles in Fig. 4.6 are replots of the measured peak-to-peak amplitudes (Fig. 4.2) scaled to the maximum value. The lack of a consistent trend in the amplitude is also obvious from the calculated data. The causes of this variability will be discussed later. The remaining discrepancy in amplitude between model results and measurements suggests that the single fibre spike amplitude is also influenced by the temperature. This

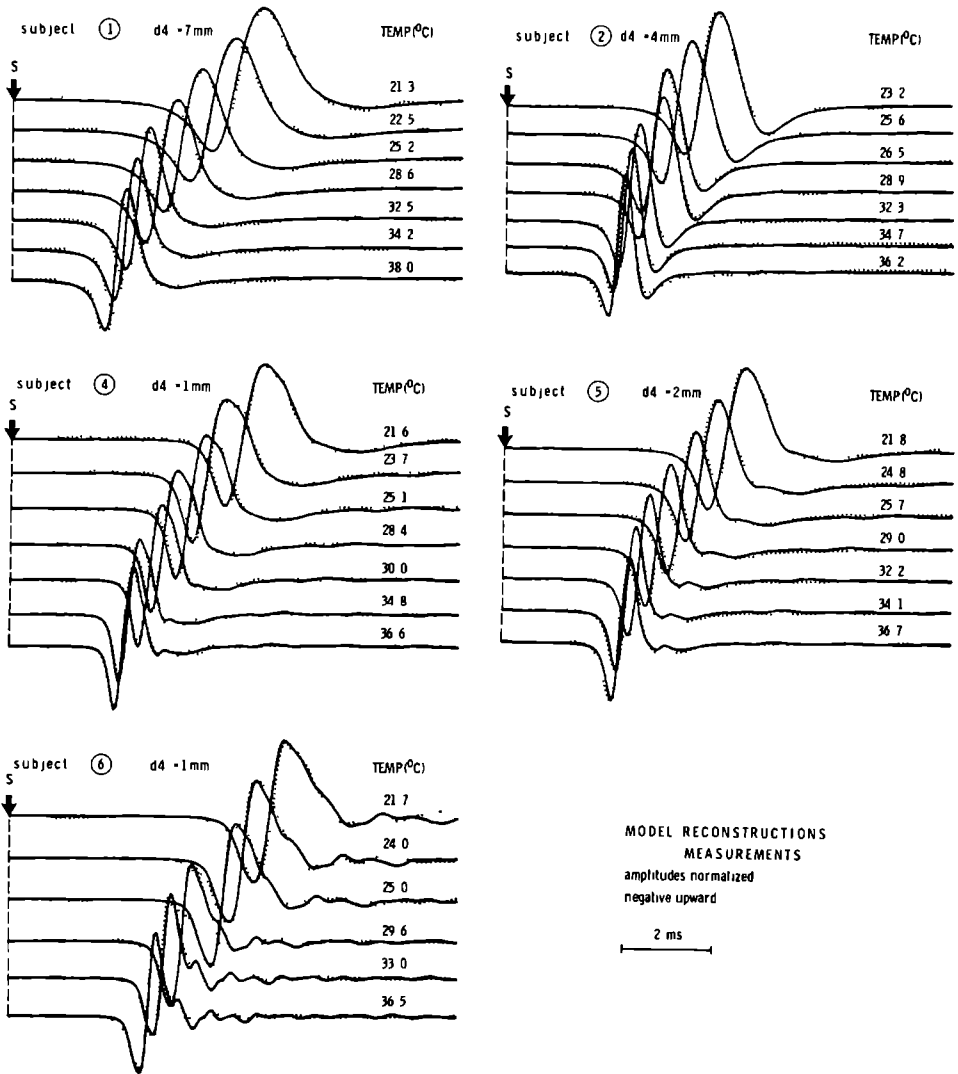


Fig. 4.5

The calculated CAP shapes after parameter optimization. The experimental data (Fig. 4.3) are represented by dots. The amplitudes are normalized. The moment of stimulation is indicated by an arrow. 'd4' is the estimated transverse observation distance nerve(-centre) to electrode

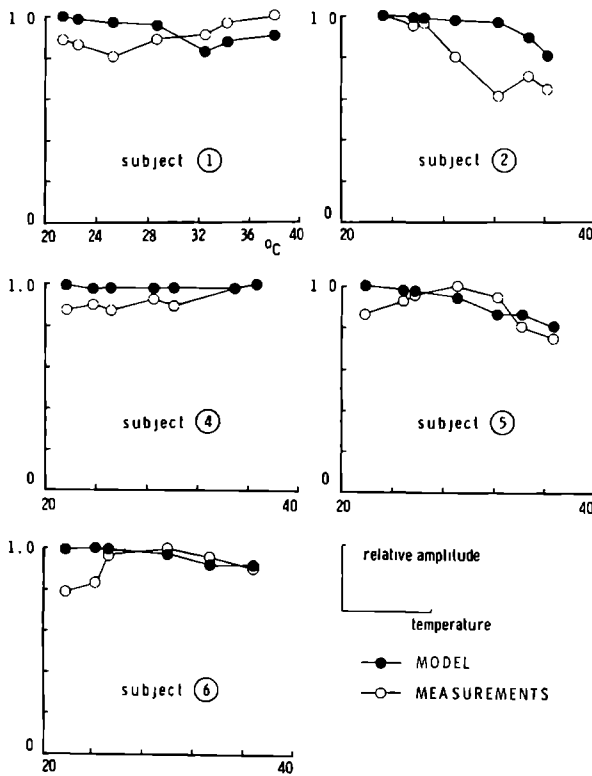


Fig. 4.6

The amplitudes, relative to the maximum value, of measured CAPs a function of the temperature (open circles) and the amplitudes of the calculated CAPs after parameter optimization (filled circles)

influence shows, with the exception of subject ②, the same tendency as found in most single fibre measurements (see previous section). Fig. 4.7 shows estimates of the total spike duration ($t_{\text{rise}} + t_{\text{fall}}$) as a function of the temperature. The estimated durations approximate the experimental data of Paintal (1966) (Fig. 4.7 broken lines). In most cases the duration at the highest temperature exceeds Paintal's values. This deviation might be caused by a hysteresis type of behaviour, as already described by Paintal (1965) and Franz and Iggo (1968). We will come back to this point in the next section.

Fig. 4.8 shows estimates (after parameter optimization) of the distribution of propagation velocities between 20 and 60 m.s⁻¹ at the highest

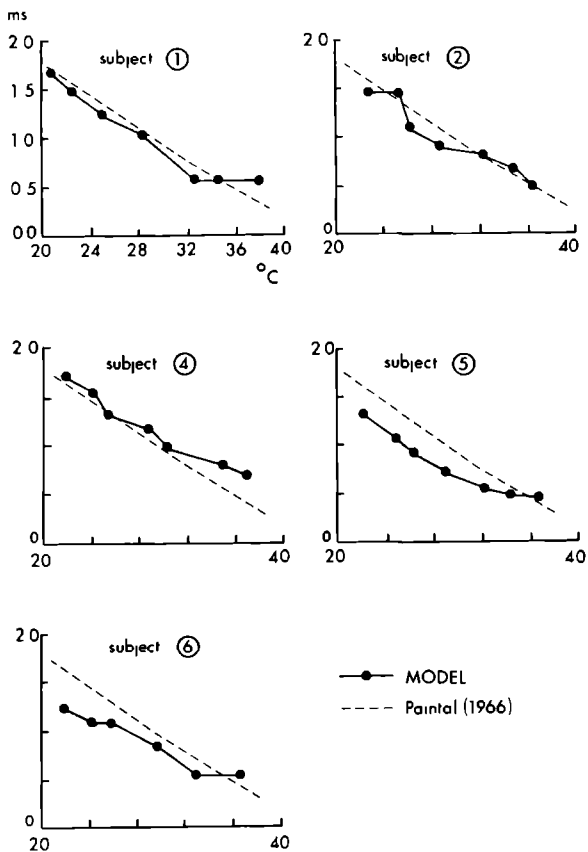


Fig. 4.7

The estimated total duration of the intracellular action potential of a single fibre (Fig. 4.4a) as a function of the temperature, obtained after parameter optimization. The broken line represents the measurements of Paintal (1966) (c.f. Fig. 4.4b)

temperature. The velocity distributions at lower temperatures were obtained by adjusting all single fibre propagation velocities by the same factor until the positive peak of the model generated CAP coincided with that of the measured CAP. All velocity distributions are skew. The measure of skewness varies between individuals. The elevations in the distributions below 30 m.s^{-1} (A δ fibres) stems from the previous chapter and has not been estimated from the actual data. Their influence on the CAP shapes is, however,

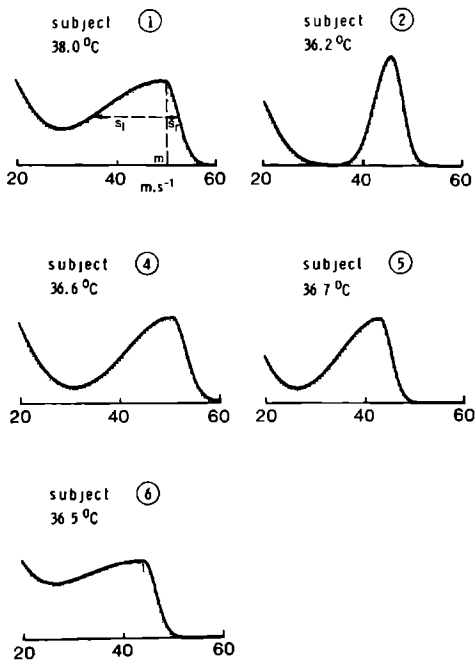


Fig. 4.8

Distributions of propagation velocities of the constituent fibres at the highest temperature, estimated from the measurements. (In the model all velocities are assumed to decrease by the same proportional factor when the temperature decreases.)

marginal.

The transverse observation distance from nerve to electrode (d_4) was the last parameter to be extracted from the measurements (see the appendix). The values are inserted in Fig. 4.5 for each subject. They strongly influence the steepness and the amplitude of the first positive elevation in a CAP.

4.6 DISCUSSION AND CONCLUSIONS

The use of available temperature data for single nerve fibre characteristics led to model results which did not optimally fit the measured data. We therefore applied an 'inverse' procedure and estimated some important parameters from the measurements themselves. The precision by which the measured CAPs could be fitted was unexpected and is promising for future work. The resulting estimates of the influence of the temperature on single fibre characteristics (velocity, spike duration) appear to be acceptable from a physiological point of view. Although it is not easy to prove that a unique set of optimal parameters exists, other sets will readily lead to unphysiological values. It can be concluded that both with respect to shapes

(Fig. 4.5) and amplitudes (Fig. 4.6) the appearance of nerve propagation on a 'macro'-level (CAPs) can be deduced from the 'micro'-level of single fibre activity to a good degree of accuracy. This is not intuitively evident, especially with respect to the CAP amplitudes.

Some basic aspects of the model results will be further analyzed. We noticed, while optimizing the results, that at higher temperatures the CAP amplitude is strongly related to the spike duration. This can be illustrated by comparison of figures 4.6 and 4.7 (filled circles). A decreasing CAP amplitude with rising temperature beyond 34°C (subjects ② and ⑤) is coupled with a relatively short spike duration (comparable to Paintal's data) in that temperature region. At lower temperatures the spike duration mainly influences the CAP shape and not its amplitude.

We have already mentioned the observations of Paintal (1965) and Franz and Iggo (1968) that warming up and cooling a nerve fibre might lead to different temperature dependencies. In our results the nerve propagation velocity (calculated from the latency to the first positive peak) at 'normal' temperatures (35°C), after the nerve was warmed up, was indeed significantly lower than expected on the basis of other experiments (see for instance chapter 3). Long spike durations at higher temperatures (cf. Fig. 4.7) provide another indication that some 'virtual' temperature apparently lags behind the measured temperature when a fibre is warmed up. This implies that the calculated slope of the relation between temperature and nerve propagation velocity should be interpreted with care. Departure from a warm nerve and measuring during a gradual cooling of the nerve, might lead to a higher slope (about 2.2 instead of 1.9 m.s⁻¹.°C⁻¹). This higher value may be more suitable as the correction factor in routine clinical work. In the clinical literature this hysteresis has also been discussed by Low and McLeod (1977).

In the model the temperature dependence of two parameters, namely the propagation velocities of the fibres and their spike duration, is essential for a satisfactory explanation of the temperature influence on CAP changes. An interesting property of the model is the possibility of studying each of these parameter dependencies separately in order to gain insight into the extent and the character of the changes caused by a particular factor. This is illustrated in Fig. 4.9 for the series of experiments belonging to subject ⑤. Firstly the influence of the temperature on the spike duration is neglected: the duration belonging to the highest temperature (36.7°C) is maintained (Fig. 4.9a). Fig. 4.9b shows what happens if the propagation velocity of all fibres is kept constant at a value corresponding with the

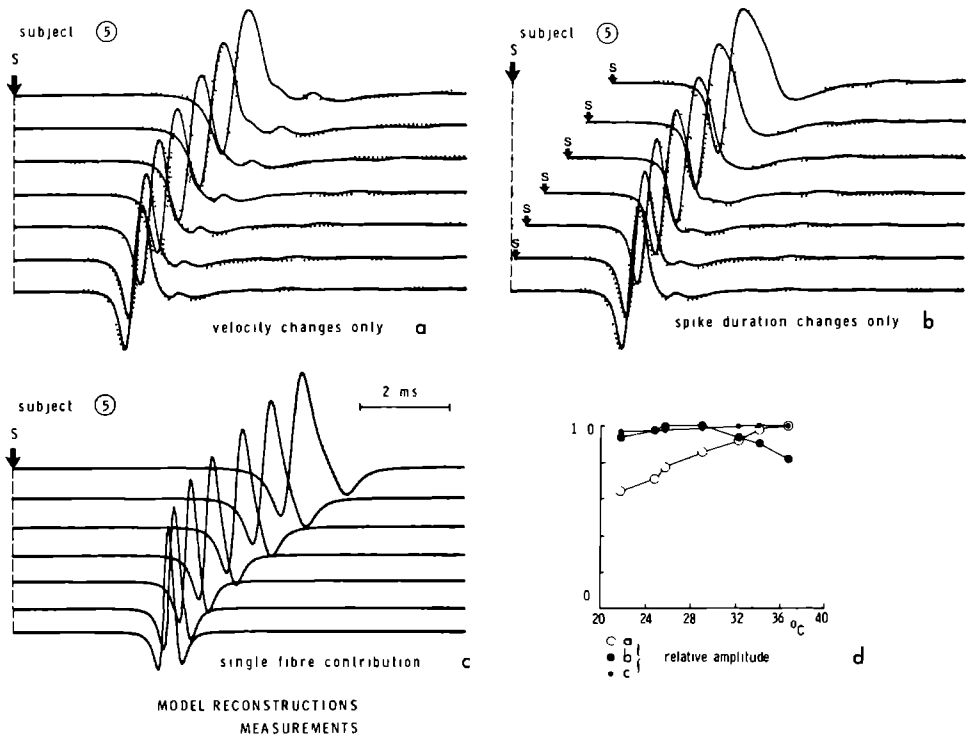


Fig. 4.9 a-d

a: Model results of CAP shapes, belonging to subject ⑤, after omission of the increased duration of the intracellular spike duration with decreasing temperature. The measured CAPs are represented by dots

b: As a, but now with omission of the decreased propagation velocity after cooling. Note the shifting moment of stimulation (arrows) after aligning the first positive peaks to those of the measured CAPs

c: Single fibre action potentials of one fibre, taken from the model calculations of subject ⑤, at different temperatures

d: The amplitudes, relative to their maximum, of the calculated action potentials, presented in this figure

highest temperature. From Fig. 4.9a and b it is obvious that neither the increased spike duration, nor the decreased velocity can be neglected in explaining the CAP shapes at low temperature (compare the dotted curves). An illustration of the influence of spike duration on the calculated shapes of an extracellular single fibre action potential at different temperatures is shown in Fig. 4.9c. In Fig. 4.9d the peak-to-peak amplitudes of the traces presented in Fig. 4.9a-c are shown. This figure again illustrates that a CAP's amplitude, as a function of the temperature, cannot be understood intuitively. Comparison of the amplitudes in Fig. 4.9d with those in Fig. 4.6 (for subject ⑤) reveals that the latter can in no way be predicted by a straightforward combination of the former.

In chapter 3 we paid attention to the relation between fibre diameters and propagation velocities; evidence was given for a nonlinear dependence. In the present chapter we have demonstrated that the velocity distribution shows a certain interindividual variation (Fig. 4.8). The question can be raised whether this variation should be ascribed to the existence of significantly different diameter distributions among healthy subjects, or to a variability in the diameter-velocity relation, or, what is most likely, to both. This question can only be answered when biopsy data from electrophysiologically studied nerves become available. As far as an estimation of the velocity distribution is desirable, eventually together with other parameters (e.g. spike duration), we are optimistic about the possibilities of a simultaneous optimization procedure.

We fitted the measured CAP data by a 'trial and error' procedure, which was very time consuming. A computer aided formalization of this 'fit by reconstruction' of the measured CAPs will be developed. It is likely that such a procedure will become a powerful tool in the acquisition of interpretable parameters from normal and diseased nerves.

Acknowledgement

The authors wish to express their appreciation for the support of H.M. Vingerhoets with respect to the acquisition of the experimental data.

TABLE 4.2 Model parameters and the assigned values
(for details see chapter 3)

description	value
thickness of the subcutaneous layer (d1)	10 mm
depth of the nerve below the skin (d2)	9 mm
insertion depth of the electrode (d3)	9 mm
transverse distance nerve to electrode (d4)	1 - 7 mm *
radius of the nerve trunk (b)	1 mm
axoplasm conductivity (σ_i)	$0.5 \Omega^{-1} \cdot m^{-1}$
axial nerve trunk conductivity (σ_{oz})	$0.3 \Omega^{-1} \cdot m^{-1}$
radial nerve trunk conductivity (σ_{op})	$0.01 \Omega^{-1} \cdot m^{-1}$
conductivity of the subcutaneous fat layer (σ_f)	$0.04 \Omega^{-1} \cdot m^{-1}$
conductivity of the muscle tissue (σ_m)	$0.25 \Omega^{-1} \cdot m^{-1}$
spike duration ($t_{rise} + t_{fall}$)	0.4 - 1.7 ms *
number of myelinated fibres (incl. A δ)	8000
ratio s_r/m in the velocity distribution (Fig. 4.8)	0.05
ratio s_1/m in the velocity distribution (Fig. 4.8)	0.07 - 0.42 *

* estimated from the inverse procedure (Figs. 4.5, 4.7 and 4.8).

Some 'technical' comments:

The distribution of velocities for the fast fibres ($> 30 \text{ m} \cdot \text{s}^{-1}$) is expressed in three parameters: its modus (m), and two 'standard deviations' (s_1 and s_r) (see Fig. 4.8 subject ①). This distribution is generated by a combination of two one side Gaussian distributions with different standard deviations and the same mean. For each subject the ratios s_1/m and s_r/m were taken to be constant over the whole temperature range, which is equivalent to proportionally changing the velocities of all fibres with temperature. The ratio s_r/m mainly determines the widening of the CAPs with increasing distance between site of stimulation and site of recording. Such data are not available for the present cases. We took the value that was determined in chapter 3. The ratio s_1/m is used in the parameter optimization procedure. The values for t_{rise} and t_{fall} were coupled according to the data from Paintal (1966) (Fig. 4.4b) and simultaneously estimated. In the

assessment of the observation distance from nerve to electrode (d_4) we used the measurements from subject ⑥ as a standard. During the insertion of the electrode this subject felt the electrode touch the nerve, so that the distance from the electrode to the nerve trunk could be considered to be negligible. The trunk radius (b) was set to 1 mm and in case ⑥ $d_4 = b = 1$ mm. Calculations with the values for σ_{op} and σ_{oz} as presented in Table 4.2 led to a good fit in this case. These values for b , σ_{op} and σ_{oz} were maintained for all subjects. With these assumptions the observation distance d_4 (≥ 1 mm) can be estimated for the other subjects as well.

Some remarks with respect to the sensitivity of individual parameters:

At high temperatures the CAP *shapes* are mainly determined by the distribution of propagation velocities, combined with the smoothing effect of the volume conductor around the nerve fibres. The precise spike configuration (t_{rise} , t_{fall}) does not have significant influence in this case. At lower temperatures the spike duration increases rapidly and its form becomes more and more important with respect to the CAP shapes. Concerning the CAP *amplitudes* the situation is more or less the reverse. For a very short spike duration it is easy to prove that the CAP amplitude is proportionally related to this duration (see chapter 2). This holds true to a good approximation for the high temperature region (35-40°C). For lower temperatures (in the range 20-35°C) the calculations reveal that the spike duration has hardly any influence on the CAP amplitude. For still lower temperatures (< 20°C) the amplitude starts to go down. Dimitrova (1973) has previously demonstrated, on the basis of model calculations, that the amplitude of an individual fibre action potential is maximal at an intermediate spike duration.

The estimation of the observation distance d_4 has been justified before. Some consideration of the sensitivity of this parameter still seems necessary. It was estimated so that the first positive peaks in the calculated series belonging to the same subject never exceeded the measured ones in size.

Another aspect which is strongly related to this observation distance is the measure of 'irregularity' of the CAPs. It is best observed in subject ⑥ (Fig. 4.5). Calculations reveal, in general, that this effect can be explained by the essentially finite number of fibres in a nerve. The irregularity becomes more and more suppressed with increasing observation distance. The statistical nature of this variability implies that only the magnitude of the irregularities, rather than their precise waveshapes, are predictable. In this respect the measured data are not always well reproduced by the model.

For subject ⑤ the model generates an 'afterpotential', which is not present in the experimental data. For subject ④, on the other hand the magnitude of the irregularity is underestimated by the model. These discrepancies indicate that still more detailed information from each individual set of CAPs can be extracted. An underestimation of the degree of irregularity by the model may indicate, for instance, that the number of fibres has been estimated too high and vice versa. When a large fraction of the fibres is blocked, as may happen under pathological conditions, the 'irregular' part of the CAP comes to dominate in the CAP appearance (e.g. Buchthal et al. 1975). A more extensive discussion on the finiteness of the number of fibres can be found in chapter 2. 2.

4.8 REFERENCES

- Buchthal, F. and Rosenfalck, A. Evoked action potentials and conduction velocity in human sensory nerves. *Brain Res.*, 1966, 3: 1-122.
- Buchthal, F., Rosenfalck, A. and Behse, F. Sensory potentials of normal and diseased nerve. In: P.J. Dyck, P.K. Thomas and E.H. Lambert (Eds.), *Peripheral neuropathy*, Vol. 1. Saunders, Philadelphia, 1975: 442-464.
- Cummins, K.L., Perkel, D.H., Dorfman, L.J. Nerve conduction velocity-distributions. I. Estimation based on the single-fiber and compound action potentials. *Electroenceph. clin. Neurophysiol.*, 1979, 46: 634-646.
- Davis, F.A., Schauf, C.L., Reed, B.J. and Kesler, R.L. Experimental studies of the effects of extrinsic factors on conduction in normal and demyelinated nerve. I. Temperature. *J. Neurol. Neurosurg. Psychiat.*, 1975, 39: 442-448.
- Dimitrova, N. Extracellular potential field of a single unmyelinated nerve fibre. *Electromyogr. clin. Neurophysiol.*, 1973, 13: 547-558.
- Frankenhaeuser, B. The nerve impulse. In: J.E. Desmedt (Ed.), *New developments in electromyography and clinical neurophysiology*, Vol. 2. Karger, Basel, 1973: 42-44.
- Franz, D.N. and Iggo, A. Conduction failure in myelinated and non-myelinated axons at low temperatures. *J. Physiol.*, 1968, 199: 319-345.
- Gasser, H.S. Nerve activity as modified by temperature changes. *Amer. J. Physiol.*, 1931, 97: 254-269.

- Gutjahr, L. The partial regression coefficients of predictor variables on nerve conduction velocity and other neurographic parameters. In: A. Persson (Ed.), Abstracts 6th international congress of electromyography in Stockholm. Munksgaard, Copenhagen, 1979: 275.
- Hodgkin, A.L. and Katz, B. The effect of temperature on the electrical activity of the giant axon of the squid. *J. Physiol.*, 1949, 109: 240-249.
- Hulley, W.C., Wilbourne, A.J. and McIntyre, K. Sensory nerve action potential amplitudes; alterations with temperature. *Electroenceph. clin. Neurophysiol.*, 1978, 45: 24P.
- Hutchinson, N.A., Koles, Z.J. and Smith, R.S. Conduction velocity in myelinated nerve fibres of *Xenopus Laevis*. *J. Physiol.*, 1970, 208: 279-289.
- Jesus, P.V. de, Hausmanowa-Petrusewicz, I. and Barchi, R.L. The effects of cold on nerve conduction of human slow and fast nerve fibres. *Neurology*, 1973, 23: 1182-1189.
- Lee, A.F. and Bowen, J.M. Effects of tissue temperature on ulnar nerve conduction velocity in the dog. *Am.J.Vet.Res.*, 1975, 36: 1305-1307.
- Low, P.A. and McLeod, J.G. Refractory period, conduction of trains of impulses, and the effect of temperature on conduction in chronic hypertrophic neuropathy. *J. Neurol. Neurosurg. Psychiat.*, 1977, 40: 434-447.
- Lowitzsch, K., Hopf, H.C. and Galland, J. Changes of sensory conduction velocity and refractory periods with decreasing tissue temperature in man. *J. Neurol.*, 1977, 216: 181-188.
- Ludin, H.P. and Beyeler, F. Temperature dependence of normal sensory nerve action potentials. *J. Neurol.*, 1977, 216: 173-180.
- McLeod, J.G. Digital nerve conduction in the carpal tunnel syndrome after mechanical stimulation of the finger. *J. Neurol. Neurosurg. Psychiat.*, 1966, 29: 12-22.
- Moore, J.W., Joyner, R.W., Brill, M.H., Waxmann, S.G. and Najjar-Ioa, M. Simulations of conduction in myelinated fibres: Relative sensitivity to changes in nodal and internodal parameters. *Biophys. J.*, 1978, 21: 147-160.
- Paintal, A.S. Effects of temperature on conduction in single vagal and saphenous myelinated nerve fibres of the cat. *J. Physiol.*, 1965, 180: 20-49.
- Paintal, A.S. The influence of diameter of medullated nerve fibres of cats on the rising and falling phases of the spike and its recovery. *J. Physiol.*, 1966, 184: 791-811.

- Rasminsky, M. The effects of temperature on conduction in demyelinated single nerve fibers. *Arch. Neurol.*, 1973, 28: 287-292.
- Roberts, D.V. and Trollope, I.E. Nerve conduction velocity and refractory period as parameters of neurotoxicity. *Electroenceph. clin. Neurophysiol.*, 1979, 46: 351-354.
- Schoepfle, G.M. and Erlanger, J. The action of temperature on the excitability, spike height and configuration, and the refractory period observed in the responses of single medullated nerve fibers. *Amer. J. Physiol.*, 1941, 134: 694-704.
- Tasaki, I. The excitatory and recovery processes in the nerve fibre as modified by temperature changes. *Biochim. biophys. acta*, 1949, 3: 498-509.
- Tasaki, I. and Frank, K. Measurement of the action potential of myelinated nerve fiber. *Amer. J. Physiol.*, 1955, 182: 572-578.
- Tasaki, I. and Fujita, M. Action currents of single nerve fibers as modified by temperature changes. *J. Neurophysiol.*, 1948, 11: 311-315.
- Trautwein, W., Gottstein, U. and Federschmidt, K. Der Einfluss der Temperatur auf den Aktionsstrom des excidierten Purkinje-Fadens, gemessen mit einer intracellulären Elektrode. *Pflügers Archiv ges. Physiol.*, 1953, 258: 243-260.
- Zipp, P. Temperature dependent alterations of the surface-emg and ecg: An investigation of the electrical transfer characteristics of the human skin. *Europ. J. appl. Physiol.* 1977, 37: 275-288.

C H A P T E R 5
NERVE PROPAGATION IN THE REFRACTORY PERIOD

ABSTRACT

Compound nerve action potentials (CAPs) of sural nerves of healthy persons have been measured in the relative refractory period of the fibres. Double stimuli were used with interstimulus intervals ranging from 0.7 to 4.0 ms. The CAP latency increase, its amplitude decrease and its wave shape alterations with decreasing interstimulus interval are discussed using a model description. Recovery functions for the single fibre action potential in the relative refractory period are defined. These recovery functions, however, cannot sufficiently explain the CAP amplitude diminutions, actually measured. Apparently in the relative refractory period an increasing number of fibres ceases to propagate an action potential when the stimulus interval is shortened. This effect, which is caused by subthreshold stimulation, predominantly involves the slower fibres. The usual derivation of refractory period parameters in clinical practice is discussed.

5.1 INTRODUCTION

The states of inexcitability and reduced excitability of nerve fibres after the passage of an action potential are known as the absolute and the relative refractory period. Their durations are well-defined when the response of a single nerve fibre to closely spaced stimuli is considered. The absolute refractory period (ARP) ends with the interstimulus interval, which is just short enough to prohibit the generation of a *propagated* action potential as a response to the second stimulus even if its strength is unlimited. The relative refractory period (RRP) is, according to the original definition, the period during which the nerve has an increased threshold to stimulation, due to the passage of a previous action potential.

In a *compound* action potential of a nerve (CAP) signs of refractoriness can also be observed. It is not possible, however, simply to maintain the above definitions, since a whole population of fibres, with a certain *range* of refractory periods, is involved. Clearly, an operational definition must be found. The ARP could obviously be defined as the interval where it has just become impossible to evoke a second CAP response. A practical problem, however, is the stimulus amplitude. Usually it is expressed on the basis of the strength to evoke a just maximal amplitude (supramaximal) (e.g. Tackmann and Lehmann 1974) or on the sensory threshold for stimulation (Buchthal and Rosenfalck 1966). In a conscious subject the stimulus strength cannot be made arbitrarily large, so that, even for the most excitable fibres, propagation failure can take place before the ARP is reached.

With respect to the relative refractory period of a whole nerve an 'increased threshold' to stimulation of the most excitable fibres can be used as a criterion. This was actually done by Gilliatt and Willison (1963) in a systematic study of human (median) nerve in the RRP. The limited signal-to-noise ratio makes such a definition unattractive for practical use. A current principle is the detection of the first signs of an increased latency and of the first notable decrease of the CAP amplitude with decreasing interstimulus interval (Buchthal and Rosenfalck 1966, Lowitzsch et al. 1973, Tackmann and Lehmann 1974). The relation between such operational definitions and more fundamental properties at the single fibre level will be the central theme in this chapter. A sound quantitative basis for what happens to a CAP when the constituent fibres are in the RRP may yield us new perspectives for the use of this phenomenon. Its diagnostic value was discussed in a relatively large number of papers describing the effects of experimentally induced

neuropathies on the refractory period in mammals (e.g. Cragg and Thomas 1964, Lehmann 1967, McDonald and Sears 1970, Tackmann and Lehmann 1971, Lehmann et al. 1971a,b, Low and McLeod 1977, Smith and Hall 1980). A prolongation of the refractory state appeared to be particularly caused by demyelination. Initially, it was thus concluded that perhaps a specific test could be established for this type of disorder. However, it was shown that in patients with neuropathies, causing a primary axonal degeneration, the refractory periods can also be significantly prolonged (Tackmann et al. 1974a, b). Later on the interest in the refractory period in clinical practice declined.

In this chapter we use the model description for the generation of CAPs which has been described in the chapters 2 and 3. It will be shown with the help of model calculations that the procedures involved in the determination of the RRP have some shortcomings, which may degrade the diagnostic value of this parameter.

Sect. 5.2 deals with the experimental methods and the acquisition of the data. In Sect. 5.3 the important aspects of CAP appearance in the refractory state are introduced. The effect that a single nerve fibre action potential *recovers* from refractoriness 'on its way' to the recording electrode is clarified in Sect. 5.4. This recovery is related to the measured data using model reconstructions.

It appears that propagation failure, caused by subthreshold stimulation in the RRP of the fibres, is likely to occur even at relatively large inter-stimulus intervals (Sect. 5.5). Evidence will be given that such 'relative block' occurs predominantly in the slower fibres (Sect. 5.6). A general discussion on the results and the conclusions can be found in Sect. 5.7. Some mathematical aspects concerning nerve fibre propagation in the RRP are given in the appendix (Sect. 5.8).

5.2 METHODS

Monopolar recordings from sural nerves of volunteers (18-40 years of age) were obtained. All subjects were healthy and showed no signs of a neurological disorder. Stimulation and recording was done with subcutaneous, teflon-coated, needle electrodes. The nerve was stimulated at the lateral malleolus and the recording electrode was placed 12 cm proximal. Its position was adjusted until a maximal CAP amplitude was obtained. Double and single stimuli were given alternately (64 of each). The rate of stimulation was two per second and the stimulus duration 0.1 ms.

In the nerve's response to a double stimulus the first (conditioning) stimulus evokes a 'normal' CAP (R2 in Fig. 5.1). Since this CAP may interfere with the response to the second (test) stimulus (R3 in Fig. 5.1), R2 was removed by subtracting the subsequent single stimulus response (R1 in Fig. 5.1). In this way 64 R3 responses were obtained. These CAPs were averaged and stored on a magnetic disk (see chapter 3).¹

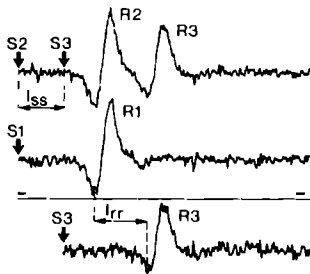


Fig. 5.1
Principles of data acquisition with the nomenclature used (partly after Kopec et al. 1978)

The stimulus strengths (S1, S2, S3 in Fig. 5.1) were equal. From each nerve two series of seven CAPs were obtained at a stimulus intensity of 1.0 and 1.5 times the level that was necessary to evoke a maximal CAP amplitude.

The skin temperature was controlled by an infrared heater (Disa 31B 30/40) and kept between 35°C and 37°C.

5.3 EXPERIMENTAL RESULTS

Four representative series of measured CAPs are shown in Fig. 5.2. The upper trace in each is the 'normal' CAP response (=R1). The subsequent traces are R3 responses (CAPs evoked by the second stimulus). The interstimulus intervals (I_{ss} , see Fig. 5.1) were chosen approximately equidistantly on a logarithmic scale. Note that all signs of the preceding R2 responses are suppressed after subtraction of the R1 responses.

At the left hand side two examples (subjects ①, ③) of a high stimulus level (1.5 times supramaximal) and at the right hand side two of a lower level (just supramaximal, subjects ②, ④) are given. It is clear at first sight that the amplitudes in the latter series decline earlier and more strongly with decreasing I_{ss} . The broken lines through the first positive

¹ An electromyograph with a digital interface to a DEC PDP 11/34 computer was used (Disa 1500 series). Similar procedures were described by Betts et al. (1976), Kopec et al. (1978) and Smith (1980).

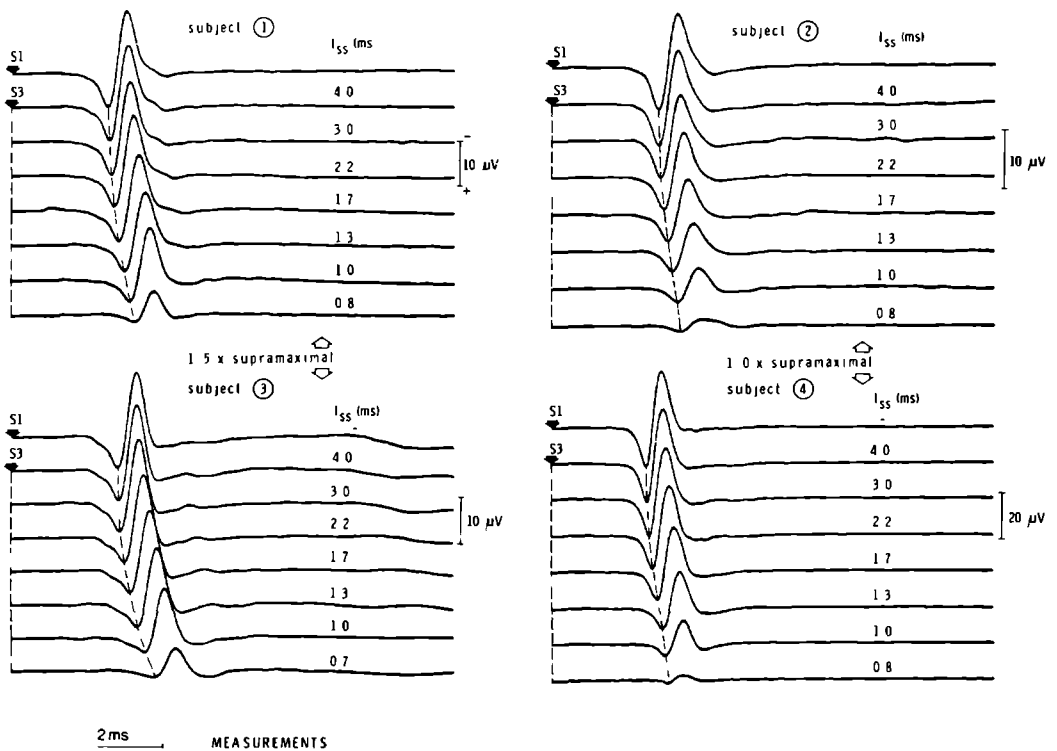


Fig. 5.2

Experimentally obtained compound action potentials (R3) from four subjects at different interstimulus intervals (I_{ss}). The moment of stimulation is indicated by an arrow. The upper traces represent the normal CAP (R1). Note the different amplitude calibrations. The temperature was about 36°C

peaks of the CAPs indicate the increasing CAP latencies with decreasing interval. Another phenomenon that will have our attention is the tendency of the CAP to exhibit a more pronounced third phase for the shortest intervals. For the rest a remarkable constancy of the CAP shapes can be observed.

5.4 SINGLE FIBRE PROPAGATION IN THE RELATIVE REFRACTORY PERIOD

The reduced excitability of the fibre membrane in the RRP is coupled with signs of retardation in the single fibre action potential. The duration of the intracellular fibre action potential (spike) can be prolonged, its

amplitude diminished and, most importantly, the *velocity* of propagation reduced. Because of this reduced velocity, the second spike lags more and more behind the first one, so that the velocity gradually approaches the normal value (Tasaki 1953). Consequently the spike amplitude and duration will also regain their normal values when the action potential recovers 'on its way' from refractoriness. A description of these dynamic aspects in nerve fibre propagation asks for a relatively complicated interference in the existing model description. The principles of calculation are outlined in the appendix (Sect. 5.8).

For muscle fibres an increased spike duration in the RRP was described by Buchthal and Engbaek (1963). A mathematical study concerning a nerve fibre in the refractory state demonstrates that the spike duration recovers very fast (within a few nodes of Ranvier), even when an action potential starts just beyond the ARP (Waxman et al. 1979). Moreover, advanced experimental studies on myelinated nerve fibres (Tasaki 1953, Paintal 1965, 1966) never reported an increased duration during the RRP. Therefore we assumed, in the model calculations a normal spike duration at the site of recording.

When the amplitude of a single fibre action potential at the site of stimulation is less than 40% of the normal amplitude the response will only be a local one. Beyond this value an action potential starts propagating along the fibre (Tasaki 1953, Paintal 1966). According to Waxman et al. (1979) the restoration of the amplitude then goes relatively fast (to 96% after 12 cm). Yet we did not assume *a priori*, as was suggested by Buchthal and Rosenfalck (1966) and Tackmann and Lehmann (1974), that the amplitude has recovered completely at the site of recording.

Irrespective of the travelled distance or the interstimulus interval, it is only the time elapsed since the passage of a previous action potential that determines the state of the membrane. Therefore, a basic description of the spike velocity and amplitude in the RRP can be given when these quantities are expressed as a function of the actual interval between two succeeding single fibre action potentials. In the model the *velocity* recovery has been estimated with the exponential recovery function:

$$U = U_n \left[1 - \beta e^{-\alpha I_{rr}^{(sf)}} \right] \quad I_{rr}^{(sf)} > \text{ARP} \quad (1)$$

where: U_n is the normal velocity of the fibre,
 U the actual velocity, and

$I_{rr}^{(sf)}$ the actual time interval between the first and the second single fibre action potential.

A similar expression is used for the *amplitude*:

$$A = A_n \left[1 - \delta e^{-\gamma I_{rr}^{(sf)}} \right] \quad I_{rr}^{(sf)} > ARP \quad (2)$$

where the amplitudes A and A_n are defined like U and U_n ². The values for α and γ are by their nature 'rates of recovery'. We assumed that α , β , γ and δ are constant within the group of fibres with velocities above 30 m.s⁻¹, which dominates a CAP of a nerve *in situ*. With respect to the parameters α and β this is to some extent supported by the observations of Paintal (1965). It is shown in the appendix that, if α and β are known, the effect of the refractory period on the arrival time of a particular fibre at the site of recording only depends on the normal arrival time of that fibre. From the appendix it also follows that slow fibres are more (extra) retarded than fast fibres.

5.5 ESTIMATION OF SINGLE FIBRE RECOVERY FUNCTIONS

In clinical neurophysiology the start of a CAP latency increase and the first diminution of the CAP amplitude are used to determine the RRP of a nerve. The latency increase is usually preferred because its determination is easier and more accurate (Lowitzsch et al. 1973, de Weerd et al. 1979). There can hardly be any doubt about the origin of this increase. The most plausible cause is a velocity decrease of the single fibre action potentials. An alternative explanation, namely propagation failure in the fastest fibres is very unlikely in view of the observations that fast fibres have the lowest threshold for stimulation (e.g. Vallbo et al. 1979). With respect to the amplitude decrease the explanation is less obvious. An incomplete recovery of the intracellular action potential amplitude at the site of recording certainly is not the only factor. The velocity decrease will be of importance too. Usually a decreased fibre velocity is coupled with an increase of the dispersion of the arrival times, which also causes a decrease of the amplitude.

We started the model calculations with initial estimates of α and β (equation (1)), after which these parameters were simultaneously adjusted until the latencies of measured and calculated CAPs coincided for all seven interstimulus intervals (4.0 - 0.7 ms). Most of the parameter values in the

² The constants γ and δ are related so that: $A = 0.4 A_n$ if $I_{rr}^{(sf)} = ARP$.

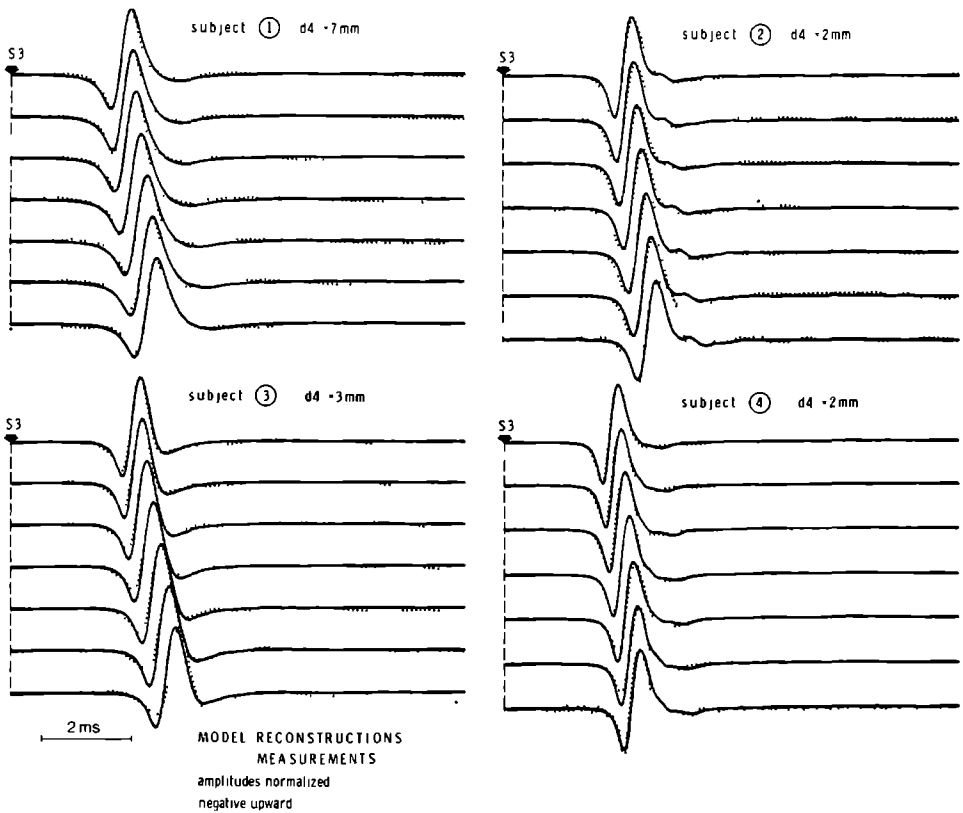


Fig. 5.3

Calculated compound action potentials (solid lines) after optimization of the velocity recovery parameters α and β (see equation (1)). The experimental data (Fig. 5.2) are reproduced by dots. The moment of stimulation (S3) is indicated by an arrow. The large negative phases are amplitude-normalized. 'd4' is the estimated transverse observation distance nerve (-centre) to electrode

model can be found in chapter 4 (Table 4.2). The distribution of 'normal' velocities (U_n in equation (1)) and the transverse observation distance nerve (-centre) to electrode were estimated from the RI responses (see Fig. 5.2, upper traces). At first an instantaneous recovery of the spike amplitude was inserted. Model calculations for the four subjects are shown in Fig. 5.3. The measured data are reproduced in dots. The amplitudes are, for sake of shape inspection, normalized ³. It appears that an exponential velocity recovery, as expressed in equation (1), is flexible enough to allow for a satisfactory CAP latency correspondence between calculated and experimental results. The estimated recovery functions for the velocity are given in Fig. 5.4. The functions are drawn between 0.7 and 4.0 ms, which is the range of interstimulus intervals used. The squares in this figure indicate an experimental result of Paintal (1965) for a short section of a fast fibre at 36°C (cat vagal nerve). We cannot offer an explanation for the difference between the estimated functions and the squares, which may, of course, be accidental. Unfortunately, more systematic quantitative data on single nerve fibres at body temperature are lacking in the literature.

Fig. 5.5 shows the amplitudes of the calculated CAPs, (closed circles), together with the measured amplitudes (open circles) for the cases where high stimulus intensities were used (① and ③). The amplitudes are plotted relative to the maximum which occurs at $I_{ss} = 4.0$ ms. The effect of a dispersion of arrival times on the amplitude is not nearly enough, however, to explain the amplitude diminutions actually measured. It will be clear that this is even the more true for the cases ② and ④ (cf. Fig. 5.2). The next logical step would thus be to estimate that value for the amplitude recovery rate γ (equation (2)), that provides us with an amplitude correspondence between calculated and measured data. Smith (1980) did not find absolute refractory periods in single nerve fibres at body temperature in excess of 1.0 ms. Therefore, above 1.0 ms we have tried to explain the CAP amplitude diminution completely by the spike amplitude recovery function. We found γ values being an order of magnitude smaller than seems reasonable in view of the results of membrane model simulations of Waxman et al. (1979). From this study it can be concluded that the amplitude recovery rate γ must be about two times the velocity recovery rate α . Although Paintal's (1965, 1966) data cannot easily be consulted on this point, they are roughly in accordance

³ The normalization is applied with respect to the main negative phases of the CAPs.

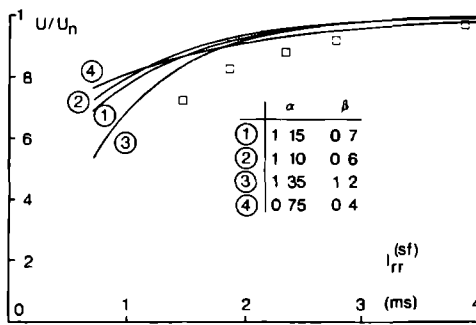


Fig. 5.4

Estimated velocity recovery functions (equation (1)) for the four subjects. The values for α and β are listed. The curves have been calculated for the range 0.7 to 4.0 ms, which is the range of interstimulus intervals used. The squares indicate the result of a velocity determination over a short fibre section, measured by Paintal (1965) at body temperature (36°C)

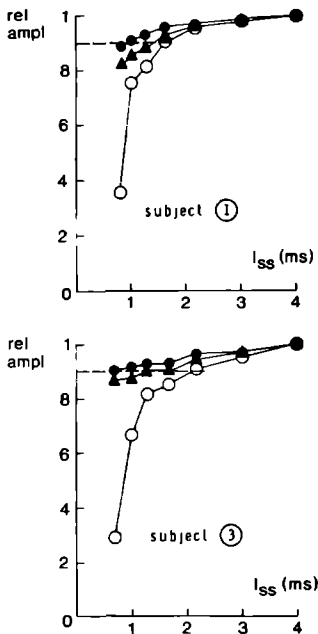


Fig. 5.5

Peak-to-peak amplitudes of measured (open circles) and calculated (closed symbols) CAPs for two subjects. The closed circles are based on calculations assuming a complete recovery of the amplitude of the intracellular fibre action potential at the site of recording. The triangles are based on a rate of recovery of this amplitude (equation (2)) which is about two times the velocity recovery rate ($\gamma = 2.5 \text{ (ms)}^{-1}$). No propagation failure in the relative refractory period was assumed in the calculations. The broken lines indicate the 90% amplitude level, a usual indicator for the RRP in clinical practice

with the above. The calculations for the subjects ① and ③ were repeated, now with $\gamma = 2.5 \text{ (ms)}^{-1}$. The results for the CAP amplitudes are presented in Fig. 5.5 in closed triangles. The present result forces us to conclude that no satisfactory explanation for amplitude diminutions in the RRP is possible without the additional supposition of propagation failure.

5.6 RELATIVE BLOCK OF FIBRES

After the foregoing estimations we know more or less quantitatively which part of the amplitude diminution must be explained by propagation failure in the RRP. As already stated, alterations in the CAP wave shape can be observed beside the amplitude diminutions. Especially the third phase is larger for the shorter interstimulus intervals. That both changes strongly depend on the stimulus intensity is illustrated in Fig. 5.6. Both CAPs are recorded from the same nerve under identical conditions, except for the stimulus strength. A value higher than 1.5 times supramaximal was not applied since this causes pain when using double stimuli. The differences with respect to amplitude and wave shape are evident.

We again applied the model in an inverse way and estimated the distribution of velocities (and the percentage of active fibres) for each interstimulus interval separately. For the subjects ① and ④ the results are shown in Fig. 5.7. The amplitude recovery was described once more with $\gamma = 2.5 \text{ (ms)}^{-1}$. The 'normal' velocities of the fibres (U_n in equation (1)) are presented. The areas under the curves are proportional to the total number of fibres. The estimates of the distributions of arrival times for subject ④ are shown in Fig. 5.8, now including the slowing of the action potentials in the RRP. The simulated CAPs on which the previous estimates for the distributions have been based are shown in Fig. 5.9. The amplitudes are again normalized for sake of shape inspection of the diminished CAPs at

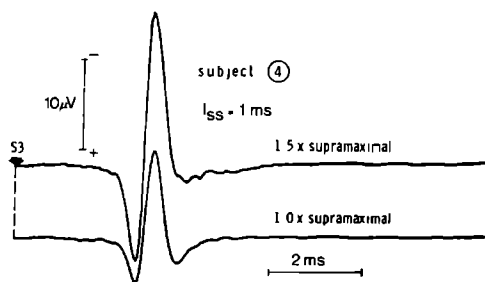


Fig. 5.6
Two measured CAPs from the same subject under identical conditions, except for the stimulus intensity. A range of 10 ms after the stimulus is shown. Note the differences in amplitude and wave shape

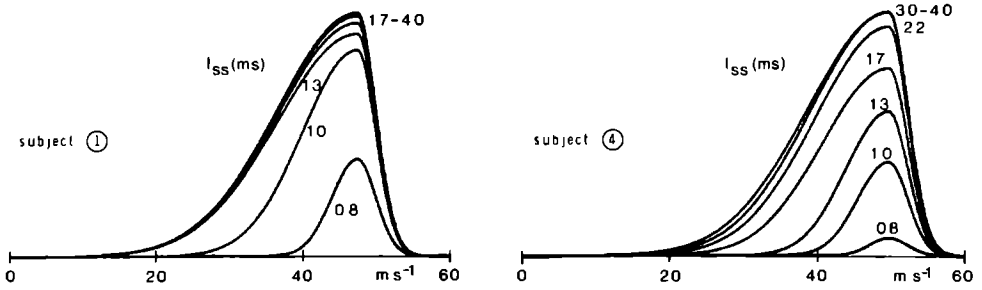


Fig. 5.7

Estimation of the velocity distributions for the subjects ① and ④ with decreasing interstimulus interval. The velocity decrease in the RRP is not implemented in this figure, i.e. the same fibre keeps the same place on the velocity scale. The areas under the curves indicate the number of fibres activated

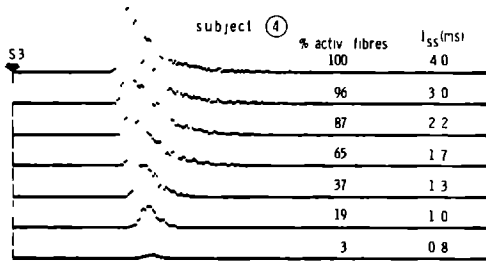


Fig. 5.8

The arrival times, which are the basis of the calculated CAPs in Fig. 5.9 for subject ④ (compare also Fig. 5.2). The estimated percentage of activated fibres is indicated. The irregularities follow from the finiteness of the number of activated fibres

short intervals.

Both examples lead to the conclusion that an increasing number of fibres ceases to propagate an action potential with decreasing interval. This, what could be called, 'relative block of fibres' starts earlier (at higher intervals) in subject ④, apparently because of the lower stimulus strength (see Fig. 5.6). It can also be concluded that the slower fibres ($< 45 \text{ m.s}^{-1}$) are predominantly involved. The general rule that it is easier to activate

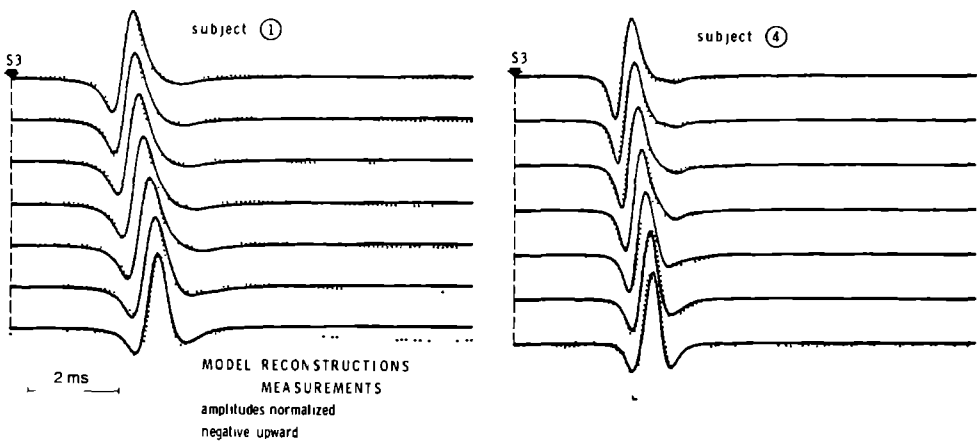


Fig. 5.9

Calculated compound action potentials (solid lines) after estimation of the velocity recovery parameters α and β (see Fig. 5.4) and the distributions of activated fibres (see Fig. 5.7) for the subjects ① and ④. The measured data are reproduced with dots

fast fibres is confirmed. The most obvious indication of 'loss' of slower fibres is the relative increase of the third phase in the CAPs. To the lowest trace of subject ④ no satisfactory model CAP could be generated with the present parameter set.

5.7 DISCUSSION AND CONCLUSIONS

In the previous sections CAPs, measured in the relative refractory period, using electrical double stimuli, were evaluated. Latency, amplitude and wave shape were analysed by means of a model description. By using the model in an inverse way, estimates of the properties of the single fibres in the RRP were obtained. This could be accomplished by defining *recovery functions* for the velocity and the amplitude of intracellular single fibre action potentials, describing the fibre behaviour in the RRP.

The velocity recovery functions (Fig. 5.4) suggest that the propagation velocity of single fibres does not reach values much lower than 50% of the normal velocity before the fibres become absolute refractory. This is a high value, if compared to the velocities that can be found at low temperatures. Values as low as 10% of the normal velocity are observed before a cold block

occurs (e.g. Paintal 1965).

Although we assumed that the recovery functions are equal for all fibres, it was shown that with decreasing interstimulus interval an increased dispersion of the arrival times of the fibres follows from the calculations. This effect can be explained using Fig. 5.10 (appendix). The lower the normal propagation velocity (U_n), the longer the normal fibre action potential latency (z/U_n) and the stronger the effect of slowing of propagation in the RRP is (see shaded areas in Fig. 5.10a and b). This means that determination of the RRP on the basis of a fixed *latency increase* (e.g. 0.1 ms) depends on the normal propagation velocity of the nerve under consideration, caused by the fact that slow fibres tend to show more latency increase than fast fibres, even when the velocity recovery properties are the same. In determining the relation between the propagation velocity and the RRP of a nerve Lowitzsch and Hopf (1973) ignored this aspect. The relation which they actually found is fully explained by the effect mentioned above. From the foregoing we can draw the conclusion that the determination of the RRP should be based on a relative rather than on a fixed latency increase.

The results presented also show the difficulties in the interpretation of CAP *amplitude* diminutions in the RRP. Lowitzsch and Hopf (1973) used a 10% diminution as indicative for the RRP. Other authors did not explicitly mention this value, but probably used a comparable percentage. This 10% value is indicated by broken lines in both parts of Fig. 5.5. It will be clear that the I_{ss} value corresponding to the 10% diminution is, to a large extent, determined by the strength of the stimulus. Since, for single fibres, no absolute refractory periods beyond 1 ms have to be expected an increasing stimulus strength will cause more and more fibres to be activated above their increased, but still finite, thresholds. In principle, all fibres can be activated beyond their ARP, but apparently a 1.5 times supramaximal stimulus is not strong enough to reach the latter situation. To avoid the effect of propagation failure in the RRP, stimuli must be applied that are not tolerated by most subjects. This problem can probably be solved by controlling the strengths of the first (S2) and the second stimulus (S3) independently. The first one can be kept at a normal (supramaximal) level, whereas the second one should be increased when I_{ss} is shortened. The total sensation will remain about the same since the second stimulus can be made about equally effective for all intervals.

With respect to the decrease in the *number* of active fibres we gave evidence for the assertion that the thinner fibres within the group of A α

fibres are predominantly involved. The A δ fibres have not been taken into account at all, since we expect them to be blocked at all interstimulus intervals which have actually been used.

The possibility of evaluating the behaviour of a range of velocities in the nerve is an important acquisition to the usual CAP interpretations, which is nicely illustrated in Fig. 5.7. This type of estimations must be refined in future. In principle accurate determinations concerning the group of fibres with velocities between 30 and 60 m.s⁻¹ appear to be possible.

5.8 APPENDIX: VELOCITY CALCULATIONS IN THE RELATIVE REFRACTORY PERIOD

The propagation velocity of a fibre depends on the interval between the second (test) stimulus and the preceding (conditioning) stimulus. This is expressed in equation (1) (see Sect. 5.4):

$$U = U_n \cdot \left[1 - \beta e^{-\alpha I_{rr}^{(sf)}} \right] \quad (1).$$

The interval $I_{rr}^{(sf)}$ is equal to or larger than the interval between the two stimuli (the index 'sf' for single fibre will be omitted in the following):

$$I_{rr} \geq I_{ss} > \text{ARP} \quad (A1).$$

When calculating the contribution of a single fibre action potential at the site of recording the arrival time of the action potential is a main characteristic. This moment is determined by the *mean velocity* between the site of stimulation and the site of recording. It can be calculated on the basis of equation (1).

To travel over an infinitesimally small distance dz , a normally propagating action potential with velocity U_n needs:

$$dT = \frac{dz}{U_n} \quad \text{seconds} \quad (A2).$$

For an action potential in the RRP it takes

$$dT' = \frac{dz}{U} = \frac{dz}{U_n (1 - \beta e^{-\alpha I_{rr}^{(sf)}})} \quad \text{seconds} \quad (A3).$$

Over this distance dz the interval between the two impulses has increased by:

$$dI_{rr} = dT' - dT \quad (A4).$$

Thus the differential equation:

$$\frac{dz}{U_n} \cdot \left[\frac{1}{1 - \beta e^{-\alpha I_{rr}}} - 1 \right] = dI_{rr} \quad (A5)$$

is obtained. After separation of variables and integration it follows that:

$$\frac{z}{U_n} = (\alpha\beta)^{-1} \cdot e^{\alpha I_{rr}} - I_{rr} - T_1 \quad (A6).$$

The constant T_1 must be chosen in such a way that at the site of stimulation ($z=0$): $I_{rr} = I_{ss}$.

So:

$$T_1 = (\alpha\beta)^{-1} \cdot e^{\alpha I_{ss}} - I_{ss} \quad (A7).$$

The arrival time of the conditioning action potential following S2 (see Fig. 5.1) is:

$$T = \frac{z}{U_n} \quad (A8).$$

The arrival time of the test action potential following S3, with S3 as the reference time, equals:

$$T' = \frac{z}{U_n} + I_{rr} - I_{ss} \quad (A9).$$

When the normal arrival time $T = z/U_n$ of an action potential is known, T' can be calculated for each I_{ss} by application of (A6), (A7) and (A9).

An example is visualized in Fig. 5.10 ($\alpha = 1(\text{ms})^{-1}$, $\beta = 1$, $I_{ss} = 2 \text{ ms}$). Fig. 5.10a shows the relation (A6). The intersection of this curve with the line $I_{rr} = I_{ss}$ (= 2 ms in this example) determines $z=0$. The vertical difference (shaded) gives $I_{rr} - I_{ss}$ as a function of z/U_n . In Fig. 5.10b the arrival times of the conditioning and the test action potentials are constructed. The interval I_{rr} at the site of recording finally determines the velocity of the action potential under the electrode via equation (1). This velocity is

needed in the calculation of the wave shape and amplitude of the single fibre action potential (see chapter 2).

The prerequisites for using the above principle in the simulation of a whole CAP in the RRP are the distribution of normal velocities U_n and the distance between site of stimulation and site of recording. Calculation then proceeds as follows. For each fibre the normal arrival time is calculated. Based on an initial choice of α and β the actual arrival time in the RRP is then calculated using (A6)-(A9). From this procedure the velocity under the electrode can be computed by using equation (1). The single fibre contribution now can be calculated and the CAP is obtained by adding all individual contributions. If the resulting CAP does not fit the measured one optimally, the distribution of velocities U_n , α and β must be re-estimated.

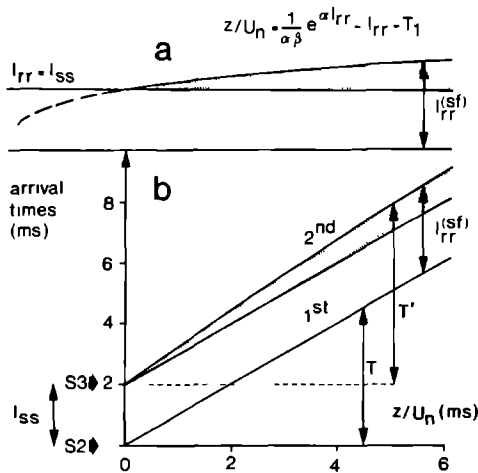


Fig. 5.10 a and b

Principles of calculating the response interval $I_{rr}^{(sf)}$ (a) and the arrival times (b) of a nerve fibre action potential in the relative refractory period. Both the arrival times of the first (conditioning) and the second (test) response are presented. The interstimulus interval (I_{ss}) is chosen 2 ms by way of example

5.9 REFERENCES

- Betts, R.P., Johnston, D.M. and Brown, B.H. Nerve fibre velocity and refractory distributions in nerve trunks. *J. Neurol. Neurosurg. Psychiat.*, 1976, 39: 694-700.
- Buchthal, F. and Engbaek, L. Refractory period and conduction velocity of the striated muscle fibre. *Acta Physiol. Scand.*, 1963, 59: 199-220.
- Buchthal, F. and Rosenfalck, A. Evoked action potentials and conduction velocity in human sensory nerves. *Brain Res.*, 1966, 3: 1-122.
- Cragg, B.G. and Thomas, P.K. Changes in nerve conduction in experimental allergic neuritis. *J. Neurol. Neurosurg. Psychiat.*, 1964, 27: 106-115.
- Gilliatt, R.W. and Willison, R.G. The refractory and supernormal periods of the human median nerve. *J. Neurol. Neurosurg. Psychiat.*, 1963, 26: 136-147.
- Kopec, J., Delbeke, J. and McComas, A.J. Refractory period studies in a human neuromuscular preparation. *J. Neurol. Neurosurg. Psychiat.*, 1978, 41: 54-64.
- Lehmann, H.J. Zur Pathophysiologie der Refraktärperiode peripherer Nerven. *Dtsch. Z. Nervenheilk.*, 1967, 192: 185-192.
- Lehmann, H.J., Lehmann, G. and Tackmann, W. Refraktärperiode und Uebermittlung von Serienimpulsen im N. tibialis des Meerschweinchens bei experimenteller allergischer Neuritis. *Z. Neurol.*, 1971a, 199: 67-85.
- Lehmann, H.J., Tackmann, W. and Lehmann, G. Funktionsänderung markhaltiger Nervenfasern im N. tibialis des Meerschweinchens bei postdiphtherischer Polyneuritis. *Z. Neurol.*, 1971b, 199: 86-104.
- Low, P.A. and McLeod, J.G. Refractory period, conduction of trains of impulses, and effect of temperature on conduction in chronic hypertrophic neuropathy. *Electrophysiological studies on the trembler mouse. J. Neurol. Neurosurg. Psychiat.*, 1977, 40: 434-447.
- Lowitzsch, K. and Hopf, H.C. Refraktärperioden und frequente Impulsfortleitung im gemischten N. ulnaris des Menschen bei Polyneuropathien. *Z. Neurol. Neurosurg.*, 1973, 205: 123-144.
- Lowitzsch, K., Hopf, H.C. and Schlegel, H.J. Conduction of two or more impulses in relation to the fibre spectrum in the mixed human peripheral nerve. In: J.E. Desmedt (Ed.), *New developments in electromyography and clinical neurophysiology*, Vol. 2 Karger, Basel, 1973: 272-278.
- McDonald, W.I. and Sears, T.A. The effects of experimental demyelination on conduction in the central nervous system. *Brain*, 1970, 93: 583-598.

- Paintal, A.S. Effects of temperature on conduction in single vagal and saphenous myelinated nerve fibres of the cat. *J. Physiol.*, 1965, 180: 20-49.
- Paintal, A.S. The influence of diameter of medullated nerve fibres of cats on the rising and falling phases of the spike and its recovery. *J. Physiol.*, 1966, 184: 791-811.
- Smith, K.J. A sensitive method for the detection and quantification of conduction deficits in nerve. *J. Neurol. Sci.*, 1980, 48: 191-199.
- Smith, K.J. and Hall, S.M. Nerve conduction during peripheral demyelination and remyelination. *J. Neurol. Sci.*, 1980, 48: 201-219.
- Tackmann, W. and Lehmann, H.J. Refraktärperiode and Serienimpulse im N. tibialis des Meerschweinchens bei akuter Thalliumpolyneuropathie. *Z. Neurol.*, 1971, 199: 105-155.
- Tackmann, W. and Lehmann, H.J. Refractory period in human sensory nerve fibres. *Europ. Neurol.*, 1974, 12: 277-292.
- Tackmann, W., Ullerich, D. and Lehmann, H.J. Transmission of frequent impulse series in sensory nerves of patients with alcoholic polyneuropathy. *Europ. Neurol.*, 1974a, 12: 317-330.
- Tackmann, W., Ullerich, D., Cremer, W. and Lehmann, H.J. Nerve conduction studies during the relative refractory period in sural nerves of patients with uremia. *Europ. Neurol.*, 1974b, 12: 331-339.
- Tasaki, I. *Nervous Transmission*. Thomas, Springfield, 1953.
- Vallbo, Å.B., Hagbarth, K.-E., Torebjörk, H.E. and Wallin, B.G. Somatosensory, proprioceptive, and sympathetic activity in human peripheral nerves. *Physiol. Rev.*, 1979, 59: 919-957.
- Waxman, S.G., Kocsis, J.D., Brill, M.H. and Swadlow, H.A. Dependence of refractory period measurements on conduction distance: a computer simulation analysis. *Electroenceph. clin. Neurophysiol.*, 1979, 47: 717-724.
- Weerd, J.P.C. de, Notermans, S.L.H. and Vingerhoets, H.M. Measurement of the refractory period in human sensory nerve fibres. *Electroenceph. clin. Neurophysiol.*, 1979, 47: 19P.

PART IV

SURVEY AND SUMMARY

C H A P T E R 6
A SURVEY OF SOME ESSENTIAL ASPECTS IN MODELLING
COMPOUND NERVE ACTIVITY

6.1 INTRODUCTION

The analysis of compound nerve action potentials (CAPs) in clinical neurophysiology is commonly restricted to the determination of the propagation velocity of the nerve and a rough estimation of the action potential amplitude. Attempts to understand the CAPs obtained from nerves *in situ* as a summation of the activity of individual fibres are rare in the literature (e.g. Buchthal and Rosenfalck 1966). This is in notable contrast to the effort which has been put into such 'reconstruction' attempts in the 'classical' neurophysiological literature (e.g. Gasser and Grundfest 1939). The latter studies are based on *monophasic* action potentials of excised animal nerves. A number of fundamental insights into nerve propagation stem from these studies.

With modern emg-equipment rather precise registrations of CAPs of nerves *in situ* can be made, which brings shape analysis of such potentials within reach. Their relatively low amplitude is largely due to the presence of an extensive medium outside the nerve trunk conducting electrical current. For a single nerve fibre the ratio between the intracellular and the extracellular resistance is so large that the considerable transmembrane potential changes (100 mV) are almost short-circuited in the extracellular medium. Another effect of the large dimensions of the extracellular tissues around a nerve fibre *in situ* is the transition from the (almost) monophasic intracellular potential change to a triphasic extracellular action potential. Since a CAP can be considered as a summation of many of such triphasic single fibre action potentials, it also shows more phases.

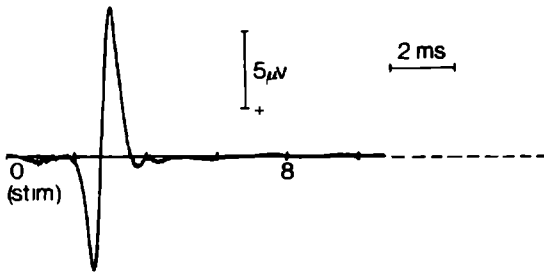


Fig. 6.1

Experimentally obtained compound nerve action potential recorded with subcutaneous needle electrodes (sural nerve of a 25 year old female subject)

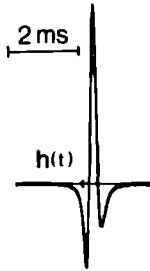


Fig. 6.2

A calculated single fibre action potential

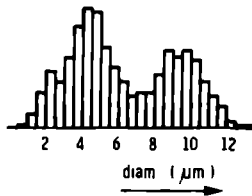


Fig. 6.3

A histogram of external fibre diameters of a sural nerve (Buchthal et al. 1975)

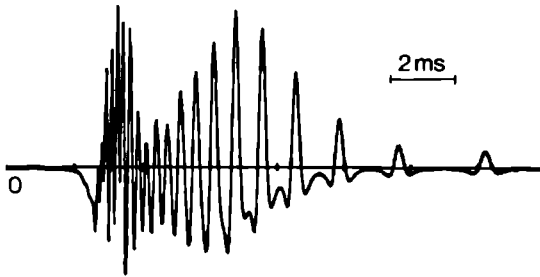


Fig. 6.4

A compound nerve action potential, based on straight-forward calculations, departing from the histogram of fibre diameters (Fig. 6.3)

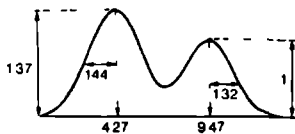


Fig. 6.5

Probability density function of fibre diameters, fitted to the histogram of Fig. 6.3

The development of a model for computer simulations of CAPs appeared to be no triviality. Essential aspects of the resulting model description are recapitulated in this chapter.

6.2 DISPERSION OF ARRIVAL TIMES

In Fig. 6.1 a measured compound action potential of a human sural nerve is presented. The temperature was about 34°C . The distance between the site of stimulation and the site of recording was 15 cm. Fig. 6.2 shows a calculated single fibre action potential. It was obtained using data from Paintal (1966) on the duration and the shape of the intracellular potential changes under the assumption that the extracellular medium is infinitely extended and has the same electrical conductivity all over (homogeneity, isotropy). The transverse distance taken between the tip of the recording electrode and the centre of the nerve fibre was 2 mm. The propagation velocity in the example of Fig. 6.2 was 50 m.s^{-1} . The difference in the wave shape of the calculated single fibre action potential and the measured CAP is evident. It can partly be explained by the differences in the propagation velocities and consequently in the 'arrival times' of the various single fibre action potentials at the site of recording. A so-called dispersion in the arrival times arises. The velocities are strongly related to the different diameters of the individual myelinated fibres (unmyelinated fibres do not noticeably contribute to CAPs *in situ*). The relation between the external diameter and the propagation velocity of such fibres is about proportional. Fibre diameters are usually expressed in a histogram (Fig. 6.3). An obvious procedure for reconstructing a compound action potential as shown in Fig. 6.1 would be to take a histogram of fibre diameters of the particular nerve, convert it to velocities and to summate the calculated single fibre action potentials as they appear after being propagated over a distance of 15 cm. The result of this procedure on the basis of the histogram of Fig. 6.3 can be found in Fig. 6.4. The relation between diameter and velocity (conversion factor) was set to $4.7 \text{ m.s}^{-1} \cdot \mu\text{m}^{-1}$ (Buchthal et al. 1975). Each bin of the histogram gives its own contribution to the calculated result. Apparently the used bin width ($0.5 \mu\text{m}$) determines the main characteristics of this CAP which strongly deviates from the measured result. The notion 'dispersion of arrival times' may become clear by inspection of Fig. 6.4.



Fig. 6.6
Calculated probability density function of arrival times



Fig. 6.7
A sample $a(t)$ of size 6000 from $f_a(t)$ (Fig. 6.6)

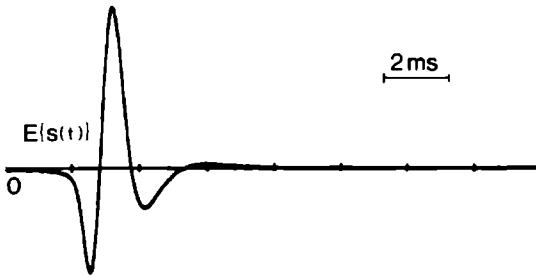


Fig. 6.8
The expected value of the compound action potential on the basis of $f_a(t)$ (Fig. 6.6) and $h(t)$ (Fig. 6.2)

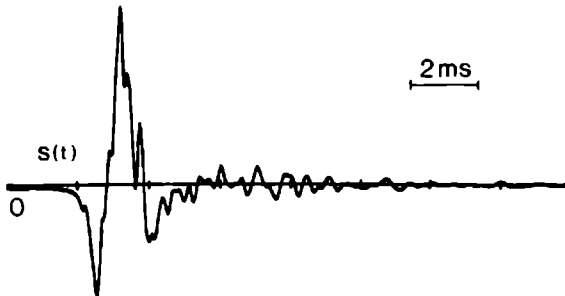


Fig. 6.9
The compound action potential based on $a(t)$ (Fig. 6.7) and $h(t)$ (Fig. 6.2)

6.3 THE STOCHASTIC PROCESS OF ARRIVAL TIMES

In order to get rid of the discrete character of the histogram it is possible, of course, to fit it with a smooth curve. An arbitrary precision along the abscissa can be obtained in that way. We can further assume that the population of the thicker fibres as well as that of the thinner fibres in the histogram did arise as a realization of a normally distributed variable. The optimally fitted distribution of diameters is given in Fig. 6.5. It should be interpreted as the probability density function of diameters in the particular nerve. Since the relation between diameter and velocity, and thus between diameter and arrival time is supposed to be known, it is possible to convert the diameter density function to the probability density function of arrival times. The latter function is given in Fig. 6.6 for the same conversion factor as was used in Fig. 6.4. The arrival time of the action potential of each of the stimulated fibres in the nerve is an independent event on a time scale. The arrival times together can be described as a (Poisson) point process with a non-uniform density (e.g. Papoulis 1965). The human sural nerve contains about 6000 fibres. To 'simulate' their arrival times we took a *random sample* of size 6000 from the function $f_a(t)$. The result is presented in Fig. 6.7. All arrival times within 40 μ s are taken together. Note how this function, so presented, consists of a superposition of the shape $f_a(t)$ (Fig. 6.6) and 'white' noise with zero mean. The noise amplitude is proportional to the square root of $f_a(t)$ for any t .

6.4 THE 'FROZEN NOISE' IN COMPOUND ACTION POTENTIALS

How is it possible that the compound action potential apparently does not show random characteristics when the arrival times of the individual fibres can be described as a stochastic process? Using the distribution function of Fig. 6.6 the expected value of the compound action potential can be determined at any moment of time. The result is given in Fig. 6.8. It is the convolution of $h(t)$ (Fig. 6.2) and $f_a(t)$ (Fig. 6.6), taking into account that the shape of the single fibre action potentials gradually changes with propagation velocity¹. When the stochastic properties of the arrival times are ignored a reasonable shape correspondence between measured and calculated CAPs can be obtained, in contrast to the result which appears

¹ This can also be observed in Fig. 6.4. It is of minor importance, however, in this context.

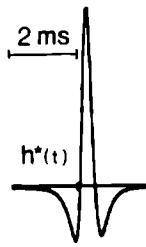


Fig. 6.10

A calculated single fibre action potential in an inhomogeneous, anisotropic volume conductor

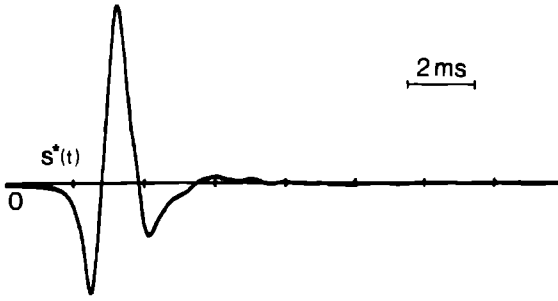


Fig. 6.11

The compound action potential based on $a(t)$ (Fig. 6.7) and $h^*(t)$ (Fig. 6.10)

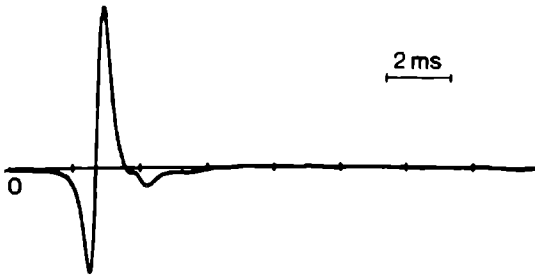


Fig. 6.12

As Fig. 6.11 with the non-linear diameter-velocity relation as presented in Fig. 6.13

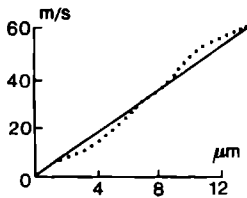


Fig. 6.13

Estimated relation between external fibre diameter and propagation velocity (dots)

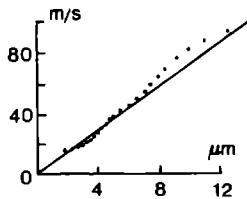


Fig. 6.14

A 'classical' estimation of the diameter-velocity relation obtained from a monophasic compound action potential of a nerve in vitro. (Gasser and Grundfest 1939)

after a calculation on the basis of a finite number of fibres. This is illustrated by taking the random sample $a(t)$ as presented in Fig. 6.7, instead of the probability density function $f_a(t)$ in the convolution with the single fibre action potential. The resulting CAP (Fig. 6.9) now shows noise components which cannot be neglected. The result of this excursion in stochastic signal theory was rather surprising at first sight. It will be further discussed in the next section.

6.5 THE PASSIVE ELECTRICAL PROPERTIES OF THE NERVE TRUNK

Fig. 6.7 can be conceived of as a superposition of the probability density function $f_a(t)$ (multiplied with the number of fibres) and white, non-stationary, noise. In this interpretation $s(t)$ (Fig. 6.9) can be regarded as a superposition of $E\{s(t)\}$ (Fig. 6.8) and filtered white noise. The single fibre action potential $h(t)$ (Fig. 6.2) is the impulse response of the filter. The noise component of $s(t)$ is more or less suppressed, depending on the characteristics of $h(t)$. We will return to the subject of the calculation of $h(t)$. In contrast to the assumption underlying the previous calculation, the structure of the nerve trunk as a passive conductor is rather *anisotropic*: the nerve fibres, lying side by side, are electrically isolated by connective tissue, which has a low electrical conductivity. Measurements of Tasaki (1964) indicate the existence of a conductivity ratio of about 50 between the fibre direction and perpendicular to it. The nerve acts as an electrical shield for its fibres. We are thus forced to implement an *inhomogeneous*, partly *anisotropic*, volume conductor around every fibre when its extraneural potential field must be reliably 'simulated'. An 'anisotropic counterpart' of $h(t)$ is presented in Fig. 6.10. Convolution of this wave shape with $a(t)$ (Fig. 6.7) clearly leads to a suppressed 'arrival time noise' (Fig. 6.11). The shape correspondence with measured CAPs improves substantially.

Similar studies in literature do not take the statistics of the essentially finite number of fibres into account. On the contrary, we have demonstrated how crucial the waveshape of the single fibre action potential is in the appearance of 'noisy' components in the CAP.

6.6 DIAMETER AND PROPAGATION VELOCITY

Not more than a global correspondence between experiment and model has been obtained so far. The main deviation lies in the overestimated amplitude of the third phase in the calculated CAPs. After an extensive study of all model parameters we were left with the possibility that the distribution of fibre diameters cannot be translated to a distribution of velocities by means of a single conversion factor. The discrepancy is indicative of a more complex relation between both quantities. A calculated CAP which fits the measured one (Fig. 6.1) better is shown in Fig. 6.12. It is obtained with an 'inverse' procedure in which the optimal velocity distribution was estimated. The resulting relation between fibre diameter and velocity is presented in Fig. 6.13. With this curve the diameter distribution (Fig. 6.5) is translated to the desired velocity distribution (see also Fig. 3.10). This result gets all the more significance when compared to the figures, presented by Gasser and Grundfest (1939). They also found a non-linear S-shaped curve for the relation between external fibre diameter and propagation velocity in most of the nerves that they studied. One of their examples (cat saphenous nerve) is given in Fig. 6.14.

6.7 PARAMETER VARIATION

Beside the morphology of the nerve there are several other factors which influence the appearance of a compound nerve action potential. It will be clear that the distance chosen between the site of stimulation and the site of recording is of crucial importance since the travelling time strongly influences the CAP characteristics. But also the physiological condition of the fibre membrane can be modified by changing the temperature or by stimulating the nerve in the refractory state.

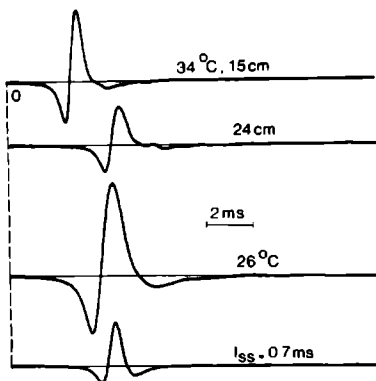
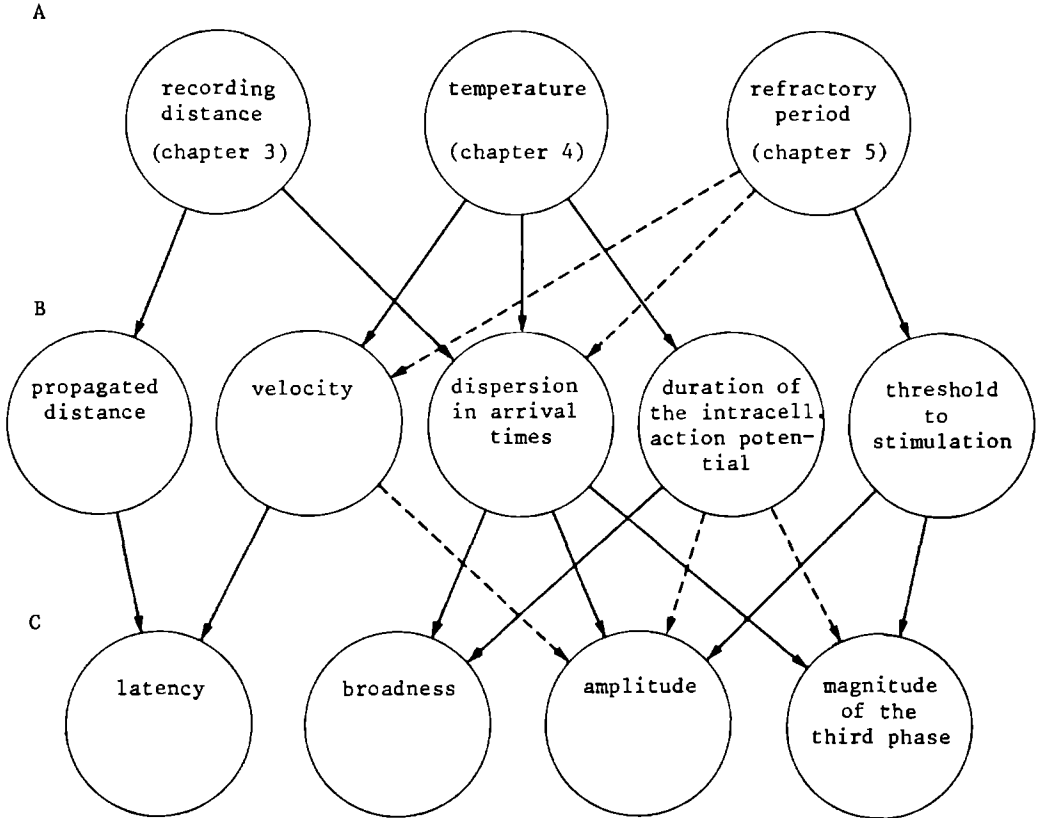


Fig. 6.15
Compound action potentials (calculated) from the same nerve under different 'experimental' conditions (see Table 6.1)

In Fig. 6.15 four CAPs are shown, originating from the same nerve. The first trace is calculated similarly to Fig. 6.12. The other ones show the result after introducing a longer propagated distance, a lower temperature and a relative refractory state of the fibres. From this figure the influence of these factors on the CAP appearance is obvious. The basic causes for the change in wave shape and amplitude are summarized in Table 6.1.

TABLE 6.1



———— strong influence

- - - - - slight influence

A: experimental variation

B: effect at the single fibre level

C: effect on the compound action potential

6.8 IN CONCLUSION

Modelling the compound electrical activity of a peripheral nerve has not been as simple as could be expected from the underlying structure. A number of complicating factors plays a part. This chapter has summarized the most important aspects from a more 'technical' point of view. The description of the model in chapter 2 has been purely in terms of the 'forward' problem, i.e. the calculation of the extraneural potential field when the sources of activity are known. In the subsequent chapters preliminary attempts for an 'inverse' estimation procedure were made. Parameters at a single fibre level such as the duration of the intracellular single fibre action potential, the distribution of velocities and fibre thresholds for stimulation were estimated quantitatively. This way of using the model has led to accurate predictions of these parameters which cannot be gathered directly from the CAP registrations.

The close agreement between experimental and calculated results under various experimental conditions gives strong evidence that a valid description of compound nervous activity has been obtained. It has given us considerable insight in the determinants of CAP generation.

Subsequent studies will be directed to the application of the model in peripheral nerve diseases, whereby its use in connection with nerve biopsy data will form a central theme.

6.9 REFERENCES

- Buchthal, F. and Rosenfalck, A. Evoked action potentials and conduction velocity in human sensory nerves. *Brain Res.*, 1966, 3: 1-122.
- Buchthal, F., Rosenfalck, A. and Behse, F. Sensory potentials of normal and diseased nerve. In: P.J. Dyck, P.K. Thomas and E.H. Lambert (Eds.), *Peripheral neuropathy*, Vol. 1. Saunders, Philadelphia, 1975: 442-464.
- Gasser, H.S. and Grundfest, H. Axon diameters in relation to the spike dimensions and the conduction velocity in mammalian A fibers. *Amer. J. Physiol.*, 1939, 127: 393-414.
- Paintal, A.S. The influence of diameter of medullated nerve fibres of cats on the rising and falling phases of the spike and its recovery. *J. Physiol.*, 1966, 184: 791-811.
- Papoulis, A. *Probability, random variables, and stochastic processes*. McGraw-Hill, Tokyo, 1965.

Tasaki, I. A new measurement of action currents developed by single nodes of Ranvier. *J. Neurophysiol.*, 1964, 27: 1199-1205.

CHAPTER 7
SUMMARY OF RESULTS

- 7.1 The wave shape of a compound action potential (CAP) is determined by (i) the *duration* of the intracellular fibre action potentials, (ii) the *dispersion* of the arrival times of these action potentials and (iii) the effects of *volume conduction*. None of these three factors can be ignored.
- 7.2 In describing *extracellular* single fibre action potentials by volume conduction theory, the anisotropy of the nerve trunk as a passive conductor must be taken into account.
- 7.3 The anisotropy *ratio* between the conductivity in the axial and that in the radial direction in the nerve trunk has been chosen between 30 and 100 in the presented model calculations.
- 7.4 A compound action potential can, fairly accurately, be described as the *convolution* of the distribution of arrival times and a single fibre action potential with fixed wave shape and variable amplitude.
- 7.5 This variation in amplitude (7.4) is often described in the literature by a *power* function of the fibre diameter. Following this approach a relatively low value in the range 0.5 - 1.5 must be introduced. Simulated CAPs appear to be rather insensitive to the actual choice (B.M. Kloppenburg; unpublished data).
- 7.6 Because of the triphasic, transient nature of extracellular single fibre action potentials, contributions from *slower fibres* (< 35 m/s) are strongly suppressed. Extinction between phases of opposite polarity occurs almost directly beyond the first onset of the compound action potential.

- 7.7 The latency of the *first positive peak* of a CAP coincides, according to model calculations, with the arrival time of the fastest action potentials under the electrode.
- 7.8 The *initial deflection* preceding this peak (7.7) must be conceived of as the forerunner of activity to come. It is caused by volume conducted, but not yet arrived, membrane activity and should therefore *not* be interpreted in terms of arrival time of the fastest fibres.
- 7.9 The latency of the main negative peak of a CAP coincides with the arrival time of the *largest number* of fibres.
- 7.10 There is strong evidence for the existence of a nonlinear, weakly *S-shaped* relation between the fibre diameter and propagation velocity. Especially the increase in velocity of the largest fibres gradually levels off with increasing diameter.
- 7.11 The CAP *amplitude* varies approximately inversely proportional with the distance between the stimulation and the recording site. This behaviour is, fairly accurately, explained by the dispersion of arrival times.
- 7.12 Usually a *third phase* can hardly be observed in CAPs. When the distance between the stimulation and the recording site is short however (< 12 cm), the magnitude of the third phase increases. This supports the model prediction of clearly triphasic single fibre action potentials.
- 7.13 The increased *broadness* of a compound action potential after cooling is about half explained by the increased dispersion of arrival times and half by the increased duration of the intracellular fibre action potentials.
- 7.14 For the CAP *amplitude* the increased dispersion of arrival times and the increased duration of the intracellular fibre action potential are opposite effects. As a result the amplitude as a function of the temperature remains approximately constant in the range between 20 and 35°C.
- 7.15 Signs of a *hysteresis* type of behaviour in the influence of the temperature are found.

- 7.16 The amplitude of a CAP in the *relative refractory period* is diminished. Three factors can be held responsible. The model reconstructions reveal that conduction failure in individual fibres, caused by increased thresholds to stimulation, predominates.
- 7.17 In the relative refractory period slow fibres have higher *thresholds* for stimulation than fast fibres. This can be concluded from the change in wave shape of a CAP with decreasing interstimulus interval.
- 7.18 A number of parameters of fundamental interest, such as the distribution of velocities, the duration of the intracellular action potentials and the thresholds of the fibres can be estimated. This can be done by using the model, presented in this thesis, in an *inverse* way.
- 7.19 The *irregular shapes* of compound action potentials that can sometimes be observed indicate that in reconstructions the essentially finite number of activated fibres must always be taken into account.
- 7.20 The model calculates '*real*' CAP amplitudes (in μV). Except for the reconstructions, presented in chapter 3, the model overestimates the measured amplitudes (not shown). The origin must, most probably, be sought in an overestimation of the number of activated fibres or in an overestimation of the intracellular tissue conductivity.
- 7.21 The presupposition that a compound action potential can be interpreted as a *linear summation* of the contributions of the activated single fibres is not contradicted in the presented results.

SAMENVATTING

Overdracht van informatie via zenuwvezels is gebaseerd op elektrochemische processen. Door in de buurt van een vezel een voldoende sterk stroomveld aan te leggen gaat deze vanaf die plaats een zogenaamde *aktiepotentiaal* voortgeleiden. De snelheid waarmee de voortplanting van een actiepotentiaal gebeurt hangt onder meer af van de dikte van de vezel en ligt voor het type vezels met een myelineschede, waar het in dit proefschrift over gaat, ongeveer tussen 10 en 100 meter per seconde.

De vezels liggen niet los verspreid, maar zijn gegroepeerd in zenuwbundels. Een actiepotentiaal van een enkele zenuwvezel manifesteert zich intracellulair als een potentiaalverandering van zo'n 100 mV. Daarvan kan in het extracellulaire medium en met name buiten de zenuwbundel (*extraneuraal*) niet veel meer worden waargenomen (minder dan 0.1 μ V). De gesommeerde (*samengestelde*, 'compound') activiteit van een (grote) groep vezels in een zenuw die simultaan op dezelfde plaats zijn gestimuleerd kan echter wel goed worden gemeten. Omdat de vezels verschillende geleidingssnelheden hebben en omdat de stimulatie- en de meetplaats meestal tien tot twintig centimeter uit elkaar liggen zal het resultaat van deze meting een uitgesmeerd karakter hebben.

De hierboven geschetste procedure van stimuleren en meten heeft een belangrijke plaats verworven in het klinisch neurofysiologisch onderzoek aan perifere zenuwen. Doorgaans besteedt men niet veel aandacht aan het samengestelde karakter van het gemeten signaal en wordt slechts de latentie (vanaf het moment van stimuleren) van de vroegste komponent bepaald. Hoewel deze bepaling een belangrijk diagnostisch hulpmiddel blijkt te zijn, levert ze zeker niet alle informatie die in het signaal opgesloten ligt.

Om de samengestelde actiepotentiaal van een perifere zenuw in zijn geheel te begrijpen is een model ontwikkeld dat, uitgaande van de over het vezelmembran optredende spanningsvariaties, beschrijft hoe de extraneurale potentiaalveranderingen van de afzonderlijke vezels eruit zien. Essentieel

daarbij is de (driedimensionale) uitwaaiering van elektrische stromen in het medium rond de zenuwvezels (*volumegeleiding*). De vezelaktiepotentialen verschillen in vorm en snelheid, afhankelijk van de dikte van de vezel. De samengestelde aktiepotentiaal wordt in het model berekend als een lineaire sommatie van alle afzonderlijke vezelaktiepotentialen.

In hoofdstuk 1 worden de achtergronden van de manier van rekenen, de gebruikte meetprocedure en de relatie met morfologische gegevens van een zenuw kort belicht. De mathematische beschrijving van het gebruikte model vindt men in hoofdstuk 2. Daar wordt tevens aannemelijk gemaakt dat de meest eenvoudige aanname die met betrekking tot de volumegeleiding denkbaar is, verworpen moet worden. De structuur van het extracellulaire medium is namelijk *niet* homogeen en isotroop: er is vooral in de zenuwbundel een duidelijk verschil tussen de elektrische geleidbaarheid in de vezelrichting en loodrecht daarop.

Hoofdstuk 3 begint met een beschrijving van het model in minder formele termen. Verder wordt in dat hoofdstuk het resultaat van een elementair experiment gegeven, namelijk de meting van samengestelde aktiepotentialen bij verschillende afstanden tussen stimulatie- en meetplaats. Beschrijving van de uitkomsten van deze experimenten met het model blijkt alleen dan goede resultaten op te leveren wanneer een *niet-lineaire*, S-vormige, relatie tussen vezeldiameter en geleidingssnelheid wordt aangenomen. De uitkomsten blijken voor deze relatie zeer gevoelig te zijn.

De invloed van de *temperatuur* op zenuwgeleiding is nogal ingrijpend. In hoofdstuk 4 wordt een serie experimenten beschreven waarbij samengestelde aktiepotentialen zijn afgeleid bij proefpersonen in een temperatuurgebied van 20-39°C. Beschrijving van deze experimenten met modelberekeningen is mogelijk met een goede nauwkeurigheid. De resultaten bevestigen de veronderstelling dat de invloed van de temperatuur op individuele vezels, zoals die uit de literatuur bekend zijn, het gedrag van de samengestelde aktiepotentiaal kan worden verklaard. Aanpassing van de modeluitkomsten aan de metingen leidt tot parameterschattingen met betrekking tot een aantal cruciale fenomenen op het niveau van individuele vezels. Dit resultaat stemt hoopvol met betrekking tot de mogelijkheden van een zogenaamde *inverse* modelbenadering, dat wil zeggen het schatten van de parameters van onderliggende fenomenen uit de metingen.

Hoofdstuk 5 handelt over zenuwgeleiding in de *refraktaire periode*. Modelberekeningen geven ook wat dit aspect van de zenuwgeleiding betreft een goed beeld van de relatie tussen het 'microniveau' van de aktiepotentialen

van individuele vezels en het 'macroniveau' van de samengestelde aktiepotentiaal. Klinisch gezien zijn de uitkomsten van hoofdstuk 5 waarschijnlijk het meest relevant, vooral omdat de duur van de refraktaire periode als diagnostisch criterium in de literatuur al veel aandacht gehad heeft.

Hoofdstuk 6 is een uitgebreide samenvatting van de belangrijke aspecten die bij de modellering van samengestelde aktiepotentialen een rol spelen.

Hoofdstuk 7 geeft tenslotte puntsgewijs de belangrijkste resultaten in de volgorde waarin deze in het proefschrift voorkomen.

CURRICULUM VITAE

Dick Stegeman werd geboren op 9 maart 1951 te Enschede. In 1968 deed hij eindexamen hbs-b aan de Gemeentelijke HBS te Hengelo (Ov.). In dat jaar liet hij zich inschrijven als student aan de Technische Hogeschool Twente te Enschede. Daar haalde hij het baccalaureaatsexamen elektrotechniek in januari 1973 na een onderzoek bij de vakgroep Bio-informatica onder leiding van mevr. dr. W. Wallinga-de Jonge. Gezocht werd naar een beschrijving van de niet-lineariteit in de krachtrespons van de soleusspier bij de rat. Tijdens de doktoraalfase van de studie verrichtte hij onderzoek bij dezelfde vakgroep onder leiding van dr.ir. K.L. Boon en dr.ir. P.A.M. Griep naar de achtergronden van het willekeurig elektromyogram zoals dat klinisch wordt gemeten. Het ingenieursdiploma werd gehaald in juni 1976. Na een aantal maanden research-assistent-schap kwam hij op 1 januari 1977 voor de duur van 4 jaar in dienst van de K.U. Nijmegen bij het laboratorium voor Medische Fysica en Biofysica. Daar werd in een samenwerkingsproject met de afdeling Klinische Neurofysiologie van het Instituut voor Neurologie het onderzoek gedaan waarvan dit proefschrift de neerslag vormt. Sinds februari 1981 is hij bij Medische Fysica en Biofysica werkzaam in het kader van een samenwerkingsproject met de KNO-kliniek met als onderwerp de visueel gestuurde oogbewegingen bij proefpersonen en patiënten.

I

Gezien het quasi-statische karakter van volumegeleiding van elektrofyysiologische stromen in biologische weefsels is de snelheid van die geleiding quasi oneindig.

II

Het sprongsgewijze karakter van voortgeleiding langs gemyeliniseerde zenuwvezels komt niet naar voren in metingen aan de buitenkant van de zenuw als geheel. Veronachtzaming van deze onderdrukking kan tot duidelijk foute conclusies leiden.

Lorente de No, R. en Honrubia, V. Continuous conduction of action potentials by peripheral myelinated nerve fibers. Science, 1963, 140: 383.

III

Voor kennis van de humane neurofyysiologie is er te weinig gepubliceerd over metingen aan individuele zenuwvezels van warmbloedigen bij lichaamstemperatuur.

IV

Het schatten van kansdichtheidsfuncties via operaties in het frequentiedomein wordt bemoeilijkt door het ontbreken van bruikbare voorwaarden voor het niet-negatief zijn van de Fouriergetransformeerde van een functie.

V

Een westerse bezoeker die zich in de Duitse Demokratische Republiek voortdurend geobserveerd voelt, overschat de aandacht die men in de DDR voor een individu heeft.

VI

Het is niet verantwoord veel waarde te hechten aan de uitkomsten van een procedure die een invers probleem oplost, wanneer het bijbehorende voorwaartse probleem nog maar gedeeltelijk begrepen is.

VII

Het nemen van een biopsie van de *N. suralis* dient voorafgegaan te worden door een zorgvuldig uitgevoerd elektrofysiologisch onderzoek aan die zenuw.

VIII

Een 'vrije' pers die zich om financiële redenen op een bepaald publiek moet richten, draagt niet bij aan de opinievorming.

IX

De veronderstelling dat elektrofysiologische processen op elk tijdstip met gesloten kringstromen beschreven kunnen worden laat niet toe dat een actie-potentiaal ontstaat en weer verdwijnt. Waargenomen extracellulaire potentiaalveranderingen bij het verdwijnen van actiepotentialen aan het eind van spiervezels ondersteunen deze bewering.

Kosarov, D. en Gydikov, A. The influence of various factors on the shape of the myopotentials in using monopolar electrodes. *Electromyogr. clin. Neurophysiol.*, 1973, 13: 319-343.

X

Veranderingen in geleidbaarheid onder invloed van de temperatuur hebben alleen dan invloed op de overdracht van een intracellulair naar een extracellulair potentiaalveld indien de betrokken media niet alle dezelfde temperatuurcoëfficiënt hebben.

Tasaki, I. The excitatory and recovery processes in the nerve fibre as modified by temperature changes. *Biochim., Biophys. acta*, 1949, 3: 498-509.

XI

In de discussie moet er rekening gehouden worden met het feit dat de door de Amerikaanse regering in het vooruitzicht gestelde onderhandelingen over wapencontrole net zo goed het breken van het verzet tegen de wapenwedloop als de wapencontrole zelf tot doel kunnen hebben.

